THE OHIO STATE UNIVERSITY

Improved Computer Simulation of the TCAS III Circular Array Mounted on an Aircraft

R.G. Rojas, Y.C. Chen, W.D. Burnside

The Ohio State University
ElectroScience Laboratory
Department of Electrical Engineering
Columbus, Ohio 43212

Technical Report 716199-12
Grant No. NSG 1498
March 1989

National Aeronautics and Space Administration Center
Langley Research Center
Hampton, VA 23665

NOTICES

When Government drawings, specifications, or other data are used for any purpose other than in connection with a definitely related Government procurement operation, the United States Government thereby incurs no responsibility nor any obligation whatsoever, and the fact that the Government may have formulated, furnished, or in any way supplied the said drawings, specifications, or other data, is not to be regarded by implication or otherwise as in any manner licensing the holder or any other person or corporation, or conveying any rights or permission to manufacture, use, or sell any patented invention that may in any way be related thereto.

TABLE OF CONTENTS

APPENDICES

LIST OF TABLES

LIST OF FIGURES

CHAPTER I

INTRODUCTION

The development of the Traffic advisory and Collision Avoidance System (TCAS) was initiated by the FAA in the early 1970's. The function of this system is to help aircraft pilots avoid collisions caused the by extremely burdened air traffic [17]. Its function is not only to provide the pilots enough information about nearby aircraft but also to give them some advice on how to avoid collisions. Presently, there are three generations of the TCAS system, each providing more features.

Basically, the principles of the operation of these systems have remained unchanged. A receiver on an TCAS-equipped aircraft listens to the signals emitted by radar transponders on other aircraft in response to interrogation signals emitted from the TCAS-equipped aircraft. The TCAS system can then determine the altitude, velocity, distance and direction of nearby transponder-equipped aircraft by interpreting the transponder return and measuring the time delay of the response.

This system was first demonstrated in the early 1970's; however, the performance was not ideal because of the interference caused by overlapping signals from multiple aircraft. After modifications including directional antennas and variable-strength interrogation signals, the system seems to work adequately at the present time.

The first system, known as TCAS I, can not give pilots advice on what maneuvers to take to avoid a collision even if they know that another aircraft is approaching from a known direction. The second system, known as TCAS II, includes a conflict resolution logic subsystem which can tell pilots to climb, dive or maintain the same altitude to avoid a collision. This easy to use system has a CRT display showing nearby aircraft. Actually, it has passed the experimental period and is in the pre-production phase at the present time.

Although TCAS II can be used in the real world with adequate results, airplane pilots prefer a new TCAS system, referred to as TCAS III (or enhanced TCAS II), which can give them advice to turn right or left as well as to climb or dive. Since it can display the whole traffic situation and give maneuvering instructions, it is the most powerful aid to avoid a mid-air collision. However, it is still in the experimental stage and far from real-world implementation.

In this study, the TCAS system is investigated in terms of the enhanced TCAS II system. With the help of a digital computer, a theoretical analysis of this system is performed to obtain a model that can be used to save time and money with reasonable and accurate results instead of numerous and costly measurements. The steps followed to build a successful computer model for the enhanced TCAS II antenna and how to simulate this system when it is installed on a Boeing 727 are described. In addition, several algorithms are developed here to evaluate the performance of the TCAS system. Note that the algorithms developed are very general and can be applied to many similar systems.

This report is divided into five chapters. Chapter II describes how to utilize the moment method to build a computer model for an antenna array, such as the enhanced TCAS II antenna system considered here. With this antenna model, Chapter III describes how to install it on a Boeing 727 with the help of the OSU Aircraft Code [2]. The OSU Aircraft Code, which is a computer code used to analyze the radiation patterns of antennas mounted on an aircraft or any similar geometry, is based on the Uniform Geometrical Theory of Diffraction (UTD) [3]. Combining the results of the OSU Aircraft Code and some additional algorithms, error curves due to structural scattering are also generated and interpreted. In Chapter IV, the results obtained in all the previous chapters are combined, and with some additional information, the tracking of an aircraft by a TCAS III-equipped airplane is evaluated using computer simulation. Actually the tracking can be examined graphically using a color workstation. Finally, some concluding remarks are given, and areas of further research are discussed in Chapter V.

CHAPTER II

DEVELOPMENT OF AN IMPROVED MODEL FOR THE ENHANCED TCAS II ARRAY BY THE MOMENT METHOD

A. CONFIGURATION OF THE ENHANCED TCAS II

The enhanced TCAS II interrogator consists of a pair of eight-element, 10.5-inch diameter, electronically-steerable circular arrays, which continuously scan the sky surrounding the protected aircraft. One array is mounted on the top of the aircraft and the other on the bottom. The two antenna arrays can provide a nearly complete spherical coverage.

The steering electronics of the TCAS system can transmit a sum and difference beam to any one of 64 beam directions at 1030 MHz to interrogate targets located within a 22.5 degree azimuth sector around boresight. The interrogator transmits a pair of pulses in time sequence, one via the sum beam and the other via the difference beam. The transponder equipped on the target aircraft then compares the amplitudes of the two pulses and it will reply to the interrogation only when the pulse via the sum beam is stronger than the other via the difference beam. The transponder replies a series of encoded pulses which are received simultaneously by the sum and difference beams at 1090 MHz. The time interval from transmission and reception is used to measure the relative distance between the two aircraft. The altitude and related information of the target aircraft is decoded from the received pulses. In addition, the interrogator receiving system

utilizes its sum and difference beam returns to compute the target bearing by use of a monopulse angle-measurement technique. This is done using an eight-element array with a central transponder element. This transponder receives interogations from other TCAS systems at 1030 MHz and replies at 1090 MHz. A combination of the calculated target's bearing, measured range and altitude information allows the system to 3-D track the target aircraft. The TCAS will then use the roll, pitch and heading of the TCAS-equipped aircraft to transform the target coordinates from a TCAS-fixed coordinate system to an airplane-fixed coordinate system [14,16].

Each antenna array, shown in Figure 2.1, consists of eight top-loaded monopoles on a 10.5-inch diameter circle and a transponder in the center. Each monopole consists of a 0.75-inch thin wire and a top-mounted circular disc. The transponder has a similar structure as the

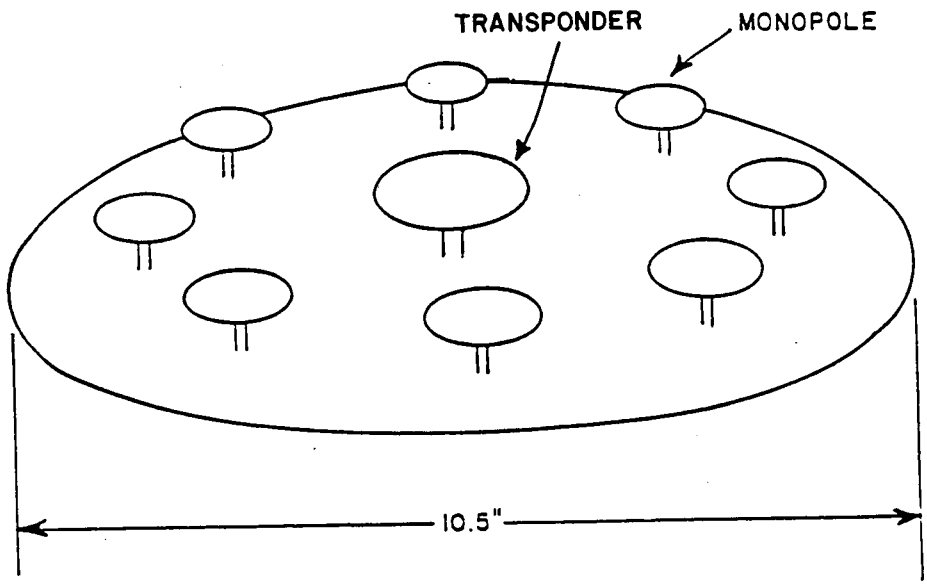

Figure 2.1. Enhanced TCAS II antenna array [1].

monopole except a larger diameter and circular disc. The detailed dimensions of the two antennas are shown in Figure 2.2. Note that all the microstrip matching networks are printed on a single 0.03" thick, Teflon-fiberglass disc. Also a low dielectric constant foam material, which is high temperature resistant, is epoxy bonded to the microstrip foil to form a rigid core and a rain-erosion coated fiberglass radome encloses the whole assembly [14]. The material of these antennas is copper, whose conductivity is 5.8×10^7 si. In addition, note that each antenna is conjugate matched to obtain maximum power transfer.

B. THE OLD TWO-MONOPOLE MODEL FOR THE TCAS III

When the OSU Aircraft Code [2] is used to analyze the radiation patterns of an antenna array mounted on an aircraft, the antenna model should already include coupling effects because this code does not consider this important effect. Therefore, the coupling effects should be considered before the Aircraft Code is used. Since the coupling comes from the interaction between these array elements, it turns out that the pattern of a single monopole of the TCAS III array radiating in the presence of the other monopoles, which are terminated in a matched load, can be simulated by the radiation pattern of a set of monopoles where it is assumed that there is no mutual coupling between these latter monopoles.

The original model of the TCAS III array including the coupling effects was suggested by Bendix. It uses only a pair of monopoles with appropriate weights to simulate each monopole in this antenna array, except for the transponder. Figures 2.3 and 2.4 show the geometry of

this model for each monopole and the whole antenna array, respectively. For detailed information, please refer to Reference [1]. A very important assumption was made to construct the model depicted in Figure 2.4. The phase center of each element of the TCAS array was assumed to be located at the position of the element itself. By means of a more sophisticated analysis, it will be shown that this assumption is not quite correct. However, as shown in Section G of this chapter, it turns

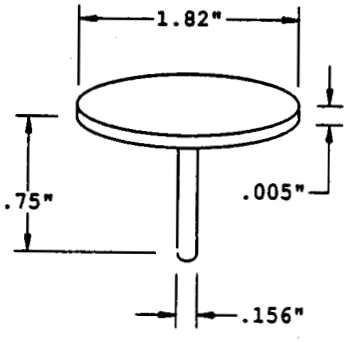

MONOPOLE

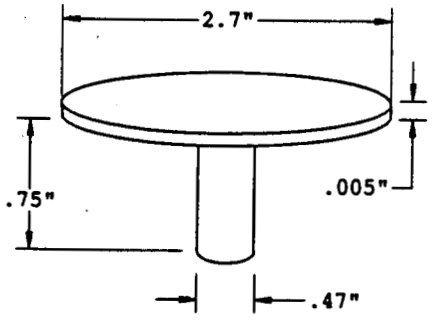

TRANSPONDER

Figure 2.2. The dimensions of the monopole and the transponder of the TCAS III array.

out that the error curves generated with this model are accurate in the forward region of the airplane; i.e., $-90° \leq \phi \leq 90°$.

The simple model depicted in Figure 2.3 is constructed based on the measured data from Bendix. The weights of the two monopoles were adjusted such that the front-to-back ratio of its radiation pattern is close to 16 dB as indicated in the measured data supplied by Bendix. Figure 2.5 is the measured pattern, including azimuth and elevation patterns of elements 2, 8 and the transponder of the TCAS III system, mounted on a 6-foot curved ground plane with a curvature similar to that of the Boeing 727. Figure 2.6 depicts the radiation pattern of the element 8 array mounted on a Boeing 727 at an elevation angle of 10° based on the old two-monopole model and the corresponding measured pattern. The agreement between the measured and calculated patterns is reasonable, but a more accurate model will give much better agreement as shown later.

Thus, a moment method analysis was done to obtain an improved antenna model. The detailed procedures followed to construct the model will be discussed in the next section. The moment method code used here is the ESP III Code (Electromagnetic Surface Patch Code) developed by Dr. E.H. Newman at OSU [6,7]. The ESP Code is a user-oriented code which can treat geometries including thin wires, polygonal plates and their interconnections. It also computes many useful quantities, such as current distribution, input impedance, radiation efficiency, mutual coupling, far-zone pattern and radar cross section. It's a powerful and easy to use computer code.

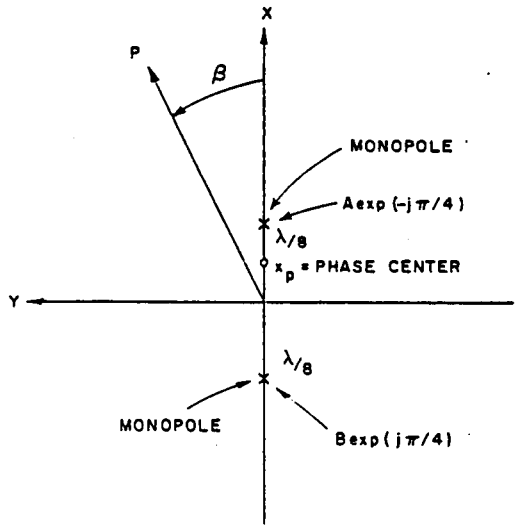

Figure 2.3. Geometry of a monopole pair for the two-monopole model [1].

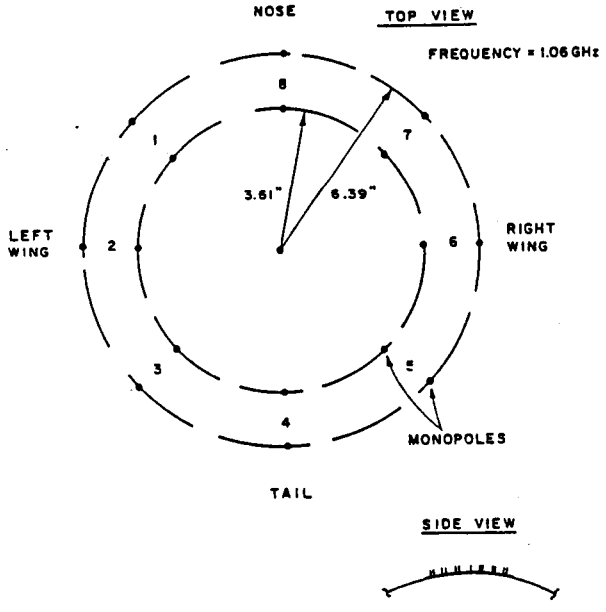

Figure 2.4. Geometry of the TCAS III circular array for the old two-monopole model [1].

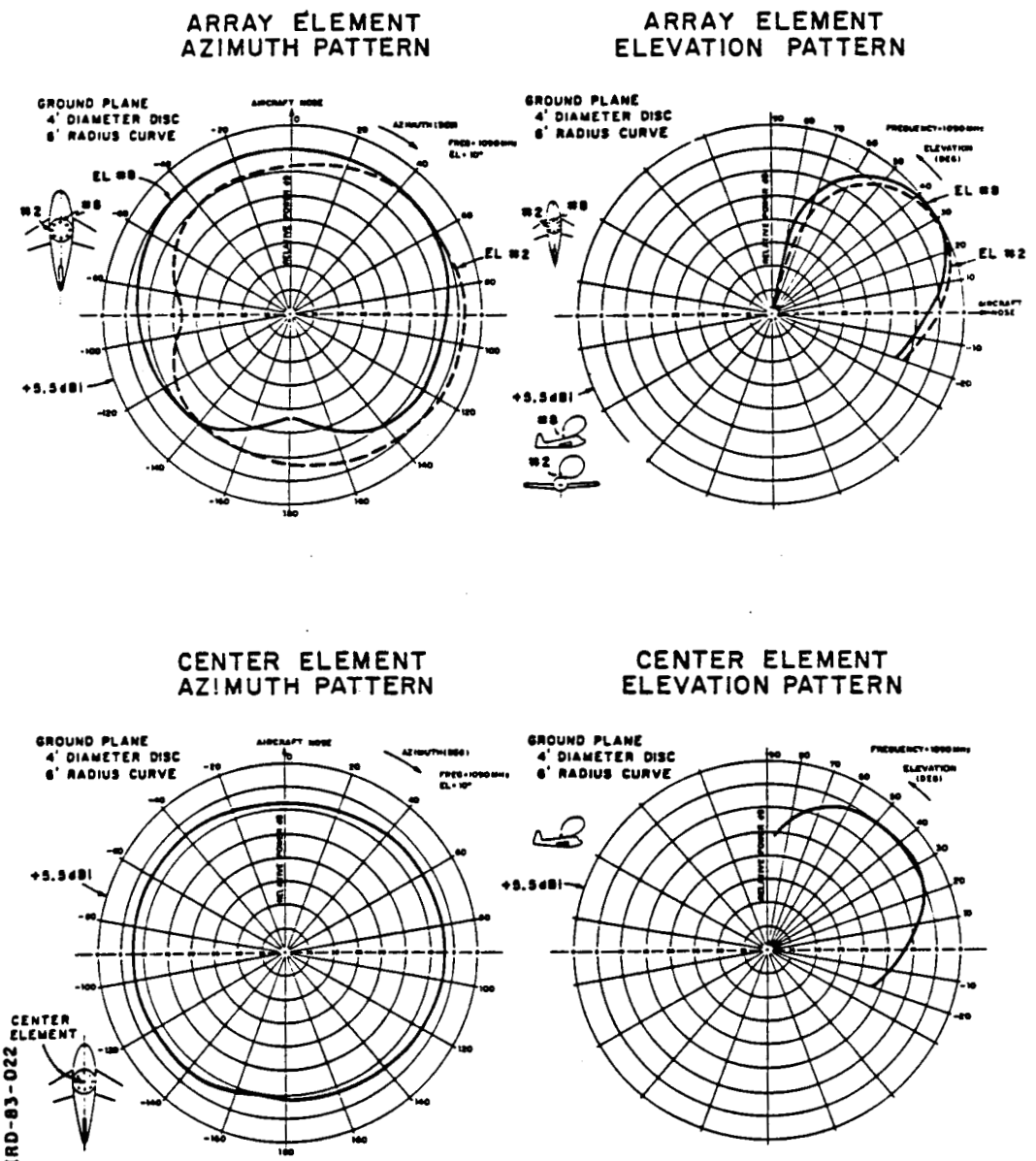

Figure 2.5. Measured patterns of elements 2, 8 and transponder (center element) of the TCAS III on a curved ground plane with the same curvature of the Boeing 727 [16].

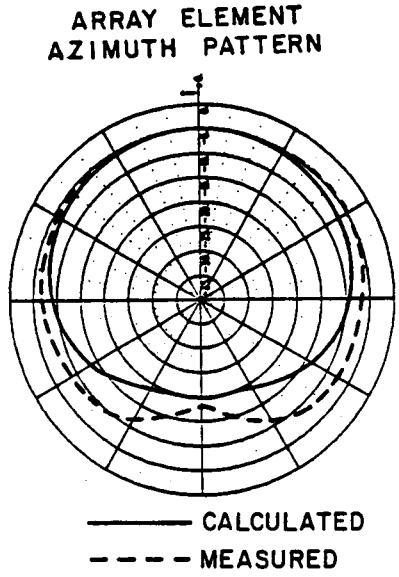

(a) Azimuth pattern at an elevation angle of 10°

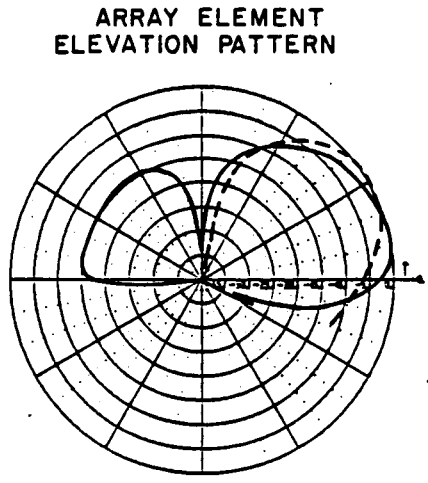

(b) Elevation pattern

Figure 2.6. The radiation patterns of element 8 in the old two-monopole model on the fuselage of a Boeing 727.

C. IMPROVED MODEL FOR THE TCAS III ARRAY

One of the reasons the moment method was used here was to analyze the coupling effects analytically. When one element is excited in this array in the presence of the other array-elements, which are terminated in a conjugate matched load, the other elements will have induced currents due to mutual coupling and these currents in turn will induce currents on the other elements. Therefore, the radiation pattern of the excited element in the TCAS array should be a combination of the radiated fields from all these currents. In order to find all the induced currents, the complete geometry of the TCAS III array is input to the moment method code. The induced currents on any element can then be found. Hence, to calculate the radiation pattern of each element of the TCAS III array with the Aircraft Code, the total induced currents obtained with the moment method should be used. Note that these elements are now radiating without mutual coupling since the coupling effects are included in the induced currents found using the moment method.

Thus, the first step in this analysis is to prepare the geometry of this antenna array for the ESP III Code including the conductivity of the monopoles which are made of copper wires. An octagonal plate is used to simulate the top loaded circular disc with the same area. Also, because of the limitation of the ESP III Code, where only one kind of radius of the thin wires is allowed: the radius of the transponder is forced to be the same as the other monopoles. The antennas are placed on a flat, infinite ground plane because the ESP III Code can't model the curved plane as the fuselage of the Boeing 727. By image theory,

the ground plane can then be taken out by replacing the monopole with dipoles of twice the length. Since each element of the array is conjugate matched, the input impedance of each element should be found first so that the appropriate loads can be attached to the terminals of each monopole.

Figure 2.7 shows the geometry of the monopole and the transponder. Placing a unit voltage source in the middle of the dipole under study, the ESP III Code can then be run. The input impedances are

$$Z_{in} = 23.906 + j159.389 \ (\Omega)$$

for the transponder, and

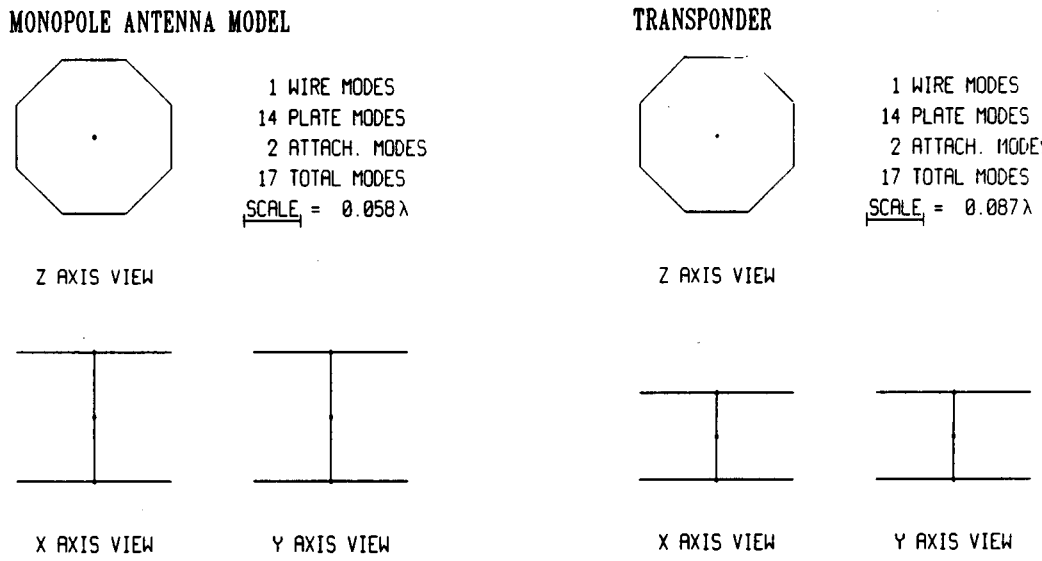

Figure 2.7. The input geometries of the monopole and transponder for the moment method.

$$Z_{in} = 20.208 + j142.639 \ (\Omega)$$

for the monopole. Of course, the input impedances of the original monopoles are only one half of the above values which were calculated for dipoles of twice the length of the monopoles. The detailed input data is listed in Appendix A.

Once the input impedances are found, the conjugate load can then be attached to each element in this array. Note that the frequency used is 1060 MHz, which is the average value of 1030 MHz and 1090 MHz. Because of the symmetry of the circular array, it is only necessary to excite one element. Here, element 8 is excited and then the radiation patterns and the induced currents on the other elements are found by executing the ESP III Code. The detailed input data is also shown in Appendix A.

Figure 2.8 shows the geometry of the TCAS III array used for the moment method analysis and the azimuth radiation pattern at an elevation angle of 10°. Comparing the pattern of Figure 2.8 with that of the measured data of Figure 2.5, the basic shapes are similar; however, the front-to-back ratio is 22 dB; whereas, the measured result gives 16 dB. Because of lack of additional information about this antenna array and the limitations of the ESP Code, it is difficult to build a model which is closer to the real physical structure. There are two main reasons that the calculated radiation pattern can not match the measured pattern perfectly. First, the code allows only one radius of the thin wires so the model of the transponder can't be implemented correctly. According to [12], the use of a larger-diameter center element is partially an

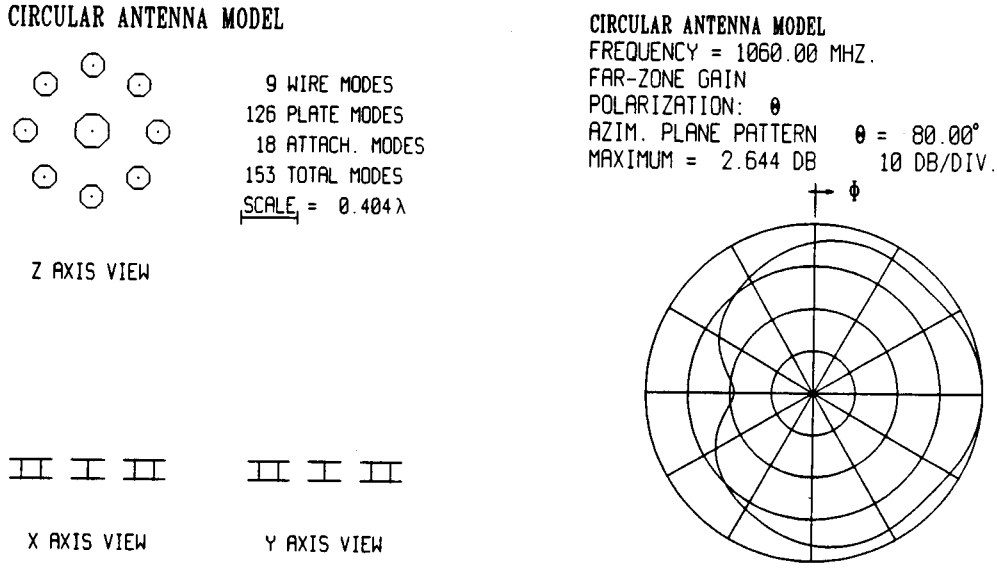

Figure 2.8. The input geometry of the TCAS III for the moment method and its azimuth radiation pattern.

attempt to improve the outer element front-to-back ratio by absorbing energy over a large physical area. Another reason is that the measured data comes from the TCAS III system mounted on a 6-foot curved plane with the curvature of the Boeing 727, but the result from the ESP Code is based on a flat plane because of the limitation of this code. Referring to the research of [3], the patterns on a ground plane, a curved ground plane and the fuselage of an aircraft will have only small difference. In conclusion, the results obtained with the moment method code are used later since these patterns are still acceptable and are an improvement over previous results.

Table 2.1 lists the induced currents when only element 8 is excited. When the Aircraft Code is used, element 8 can then be replaced by the 9 monopoles with the current distribution as shown in Table 2.1. Since the antenna array is symmetric, the model for the other elements is the same. Of course, this ignores the fact that principal radii of curvature of the Boeing 727 are not the same at the location when the TCAS array is mounted. Note that the circular disks mounted on the monopoles of the original TCAS array can not be included in the Aircraft Code.

The procedure followed to obtain a model for the TCAS III array is general so that it can apply to any similar system and configuration. If a more powerful moment method code is used and more detailed information about the array system is known, one can obtain an even better model to simulate the TCAS III array.

Table 2.1

Induced Current of Each Element in this Circular Antenna Array When Element 8 is Excited

MONOPOLE POSITION	INDUCED CURRENT	
	RELATIVE MAGNITUDE	PHASE (DEGREES)
Transponder	0.198	102
Element #1	0.379	103
#2	0.113	-143
#3	0.081	- 93
#4	0.058	- 88
#5	0.078	- 97
#6	0.109	-142
#7	0.402	101
#8	0.812	- 19

Once the Aircraft Code is run with the input of Table 2.1, it can generate radiation patterns in any desired conical cut around the airplane. Figures 2.9(a) and (b) are the radiation patterns of element 8 of the TCAS array which uses 9 monopoles to simulate an element radiation in the presence of the other elements in the azimuth plane and the elevation plane, respectively. The elevation angle is still 10°. Comparing them with the measured results, the azimuth plane pattern has the same shape as the measured result, but a different front-to-back ratio. The elevation plane pattern also has the same shape as the corresponding measured result, except that the maximum occurs at a different elevation angle. As shown later, these results are accurate enough for the applications considered here. It is important to mention that the agreement between the calculated and measured data can be improved even further if the currents of Table 2.1 are slightly modified. This will not be tried for the nine-element model, but it will be done for the four-element model considered next.

D. GENERATION OF A FOUR-MONOPOLE MODEL

In order to reduce computer time, it is important to study whether it is possible to reduce the number of elements in our model and still obtain accurate results. Take element 8 as an example; the induced currents on elements 2, 3, 4, 5 and 6 (see Table 2.1) can be taken out since their induced currents are small in relation to the others. The currents of the remaining monopoles can then be adjusted such that the front-to-back ratio of the resulting pattern is about 17 dB and the front-to-side ratio about 6 dB. The azimuth pattern will be closer to

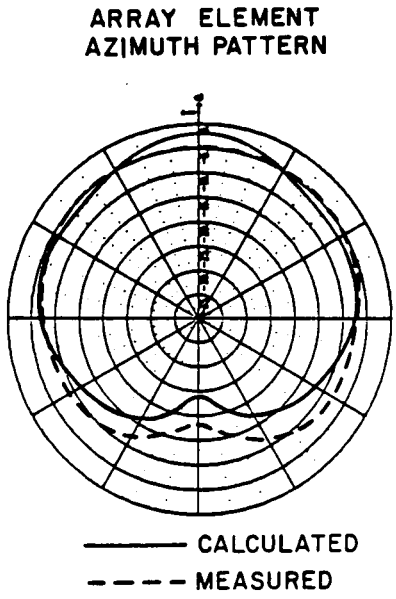

(a) Azimuth pattern at an elevation angle of 10°

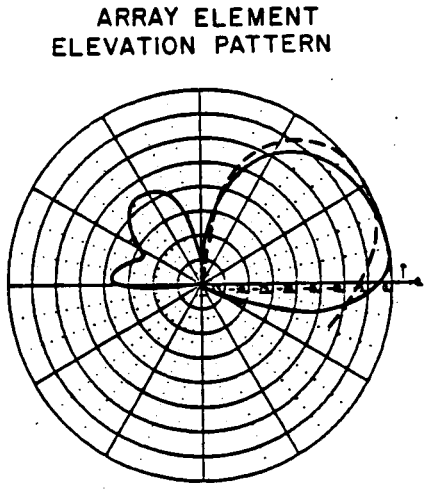

(b) Elevation pattern

Figure 2.9. The radiation patterns of element 8 in the nine-monopole model mounted on the fuselage of a Boeing 727.

Table 2.2

Induced Current of the Monopoles in the Four-Monopole Model used to Replace Element 8

MONOPOLE POSITION	INDUCED CURRENT	
	RELATIVE MAGNITUDE	PHASE (DEGREES)
Transponder	0.3564	102
Element #1	0.4169	103
#7	0.4422	101
#8	0.812	- 19

the measured pattern than that of the nine-monopole model. The list of the induced currents for the remaining four monopoles is shown in Table 2.2.

Figures 2.10(a) and (b) show the radiation patterns in the azimuth and elevation planes, respectively, for element 8 in this four-monopole model. The agreement between the calculated and measured patterns is very good. The four-monopole model is more accurate than the old two-monopole model and less expensive than the nine-monopole model.

E. PHASE CENTER ADJUSTMENT

The far-zone field radiated by any antenna can be written as

$$\vec{E} = \left\{ \hat{\phi}\, E_{\phi}(\theta,\phi) e^{j\psi_{\phi}(\theta,\phi)} + \hat{\theta}\, E_{\theta}(\theta,\phi) e^{j\psi_{\theta}(\theta,\phi)} \right\} \cdot \frac{e^{-jkr}}{r} \qquad (2.1)$$

where k is the free-space wave number, $\hat{\phi}$ and $\hat{\theta}$ are the usual phi and theta unit vectors, respectively, of a spherical coordinate system, and $E(\theta,\phi)$ and $\psi(\theta,\phi)$ are the magnitude and phase, respectively. In most

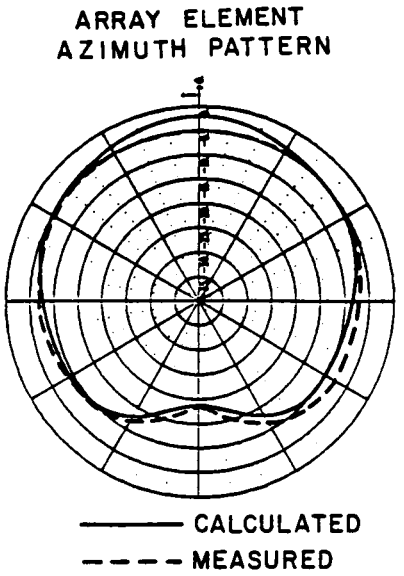

(a) Azimuth pattern at an elevation angle of 10°

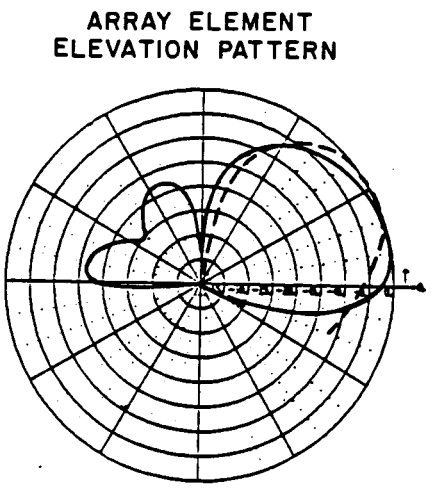

(b) Elevation pattern

Figure 2.10. The radiation patterns of element 8 in the four-monopole model on the fuselage of a Boeing 727.

applications of antennas, especially when arrays of antennas are used, it is important to assign a reference point, which is called the phase center [18] of the antenna, such that $\psi(\theta,\phi)$ is independent of θ and ϕ (and r is kept constant) for a given frequency. In other words, when the radiation fields are referenced to the phase center, the fields will appear as spherical waves with ideal spherical wavefronts or equiphase surface just as a point source but with a variable amplitude pattern. However, for most antennas used in practical applications, a single phase center valid for all θ and ϕ can not be found. Usually a reference point whose $\psi(\theta,\phi)$ is constant over an angular sector, especially over the main beam, can be found from measurements [18].

In the previous section, the magnitude of calculated radiation patterns for a single element of the TCAS array have been verified with measured data. However, to obtain the sum and difference beam patterns, the radiation patterns of each element of the TCAS array have to be added. Thus, before all these radiation patterns are superimposed, it is necessary to determine the phase center of the models considered in Sections B-D and also the phase center of each element of the actual TCAS III array.

In previous reports [1,3-5], it was assumed that the phase center for each monopole antenna in the actual TCAS array was at the position of the monopole itself. This assumption is correct when the mutual coupling effects in the array are insignificant. However, if the excitation of one element induces currents in the other elements, then the radiation field for each element is generated by the combination of all 9 elements and the phase center will shift. Unfortunately, during

this study, we did not have measured phase centers for the TCAS array elements. Therefore, the phase center for each element of the actual TCAS array was obtained by means of a moment method analysis.

It is mentioned above that in general there is no single phase center for all values of θ and ϕ. For a specific value of θ, the reference point which has the smallest variation when the phase function $\psi(\theta,\phi)$ is calculated for $0° \leq \phi \leq 360°$, is chosen as the phase center. Although the phase center will change with θ, only $\theta=80°$ or an elevation angle of 10° is investigated here, since this is the region of interest in the study of the TCAS array.

Figure 2.11(a) is the phase plot of the radiation pattern of one element of the TCAS III array obtained by the moment method with the reference point at the antenna itself. The curve is flat enough, especially in the region $-30° \leq \phi \leq 30°$; however, it can not be considered to be the phase center before it is verified to be the best choice. If there exists a better reference point, it should be located on the line connecting the element itself and the array center because of the symmetric structure of the array. Figure 2.12 shows how to shift the observation point to get a new phase plot without rerunning the ESP Code. After changing the reference point a few times, a reference point with the least variation of phase is found as shown in Figure 2.11(b). The reference point is located 5.86" from the array center, on the line joining the array center and the element under study. Note that the phase center is only 0.61" away from the monopole.

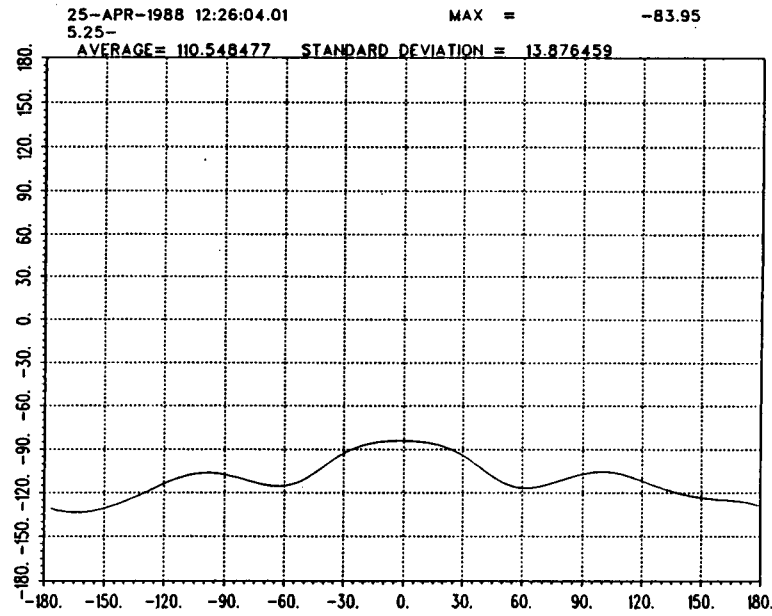

(a) Reference point: 5.25" from the center (antenna position)

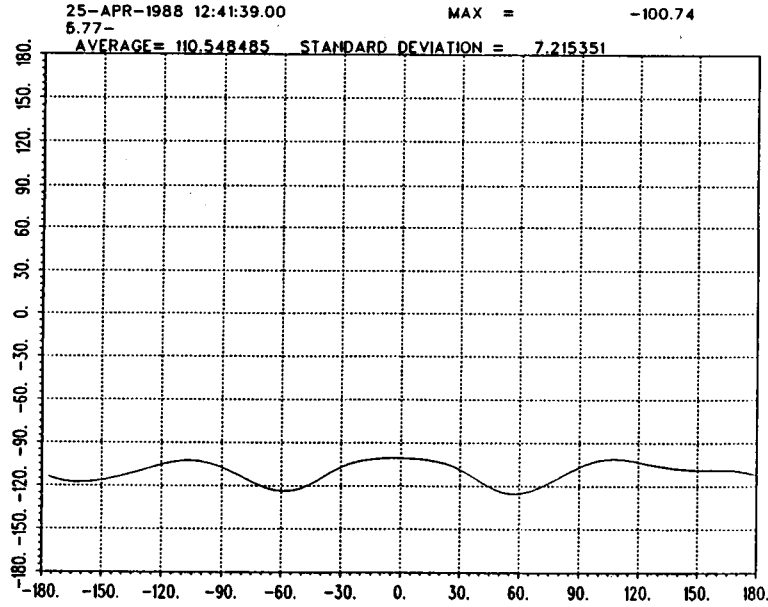

(b) Reference point: 5.86" from the center

Figure 2.11. Phase plots of a single element from the moment method.

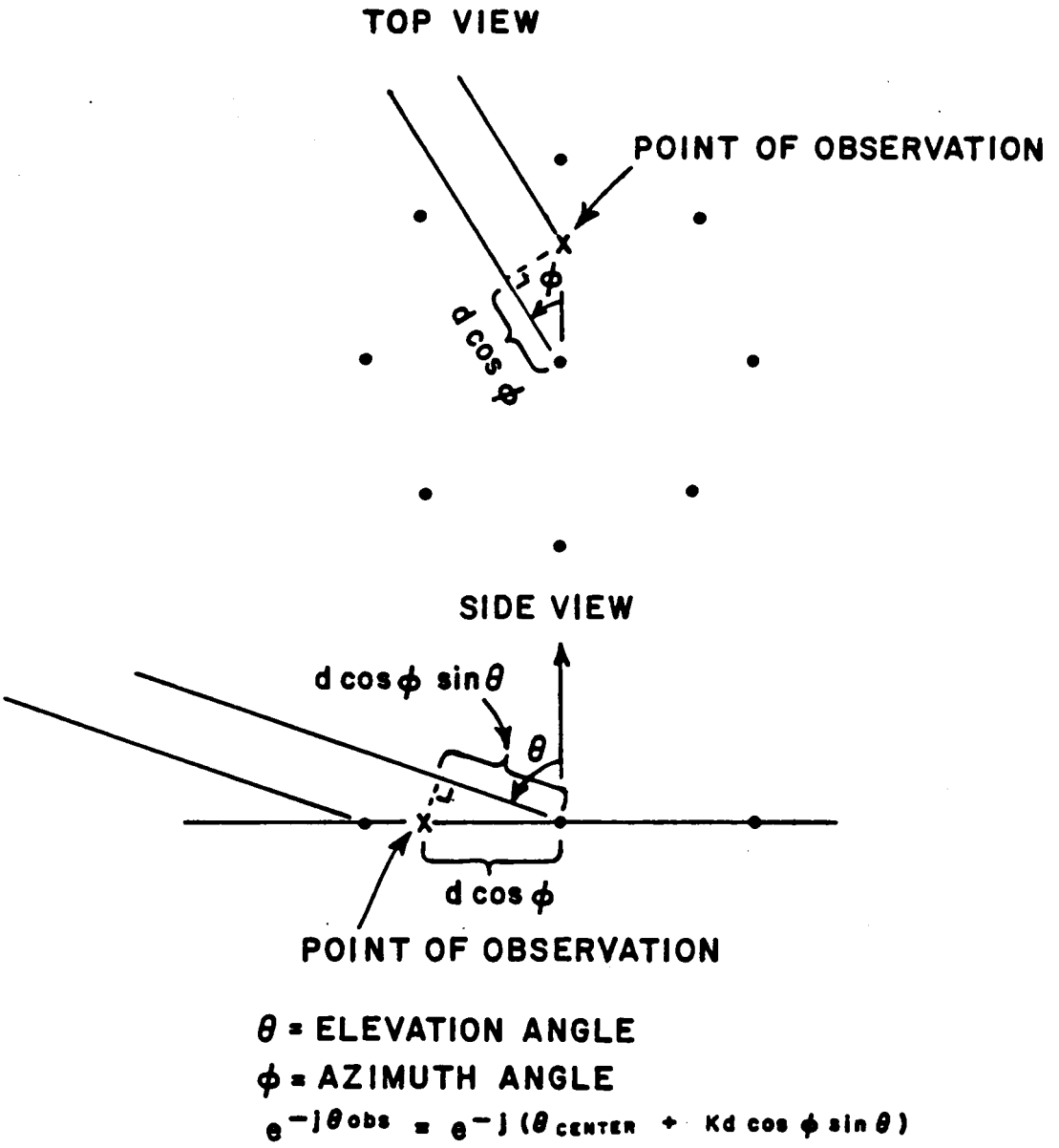

Figure 2.12. The change of the phase term when the observation point is changed.

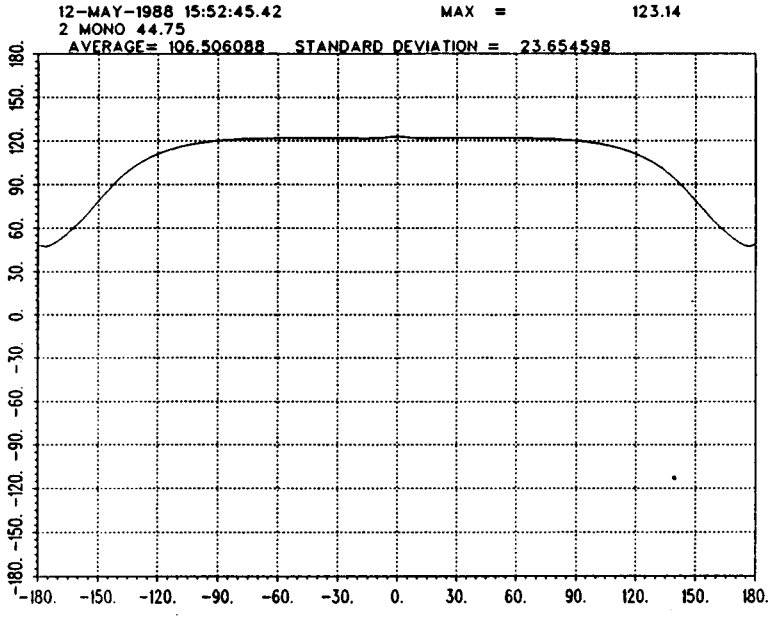

Figure 2.13. Phase plot of the two-monopole model with the reference point at its phase center.

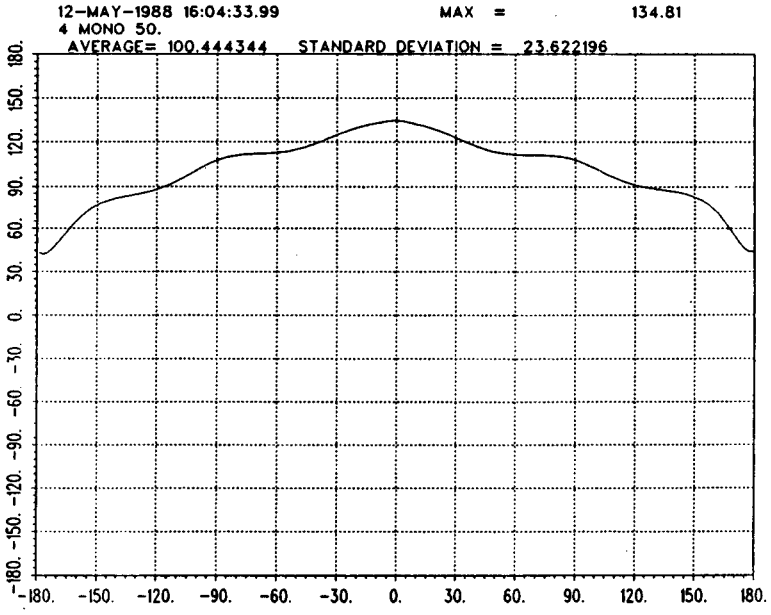

Figure 2.14. Phase plot of the four-monopole model with the reference point located 5.25" from the center.

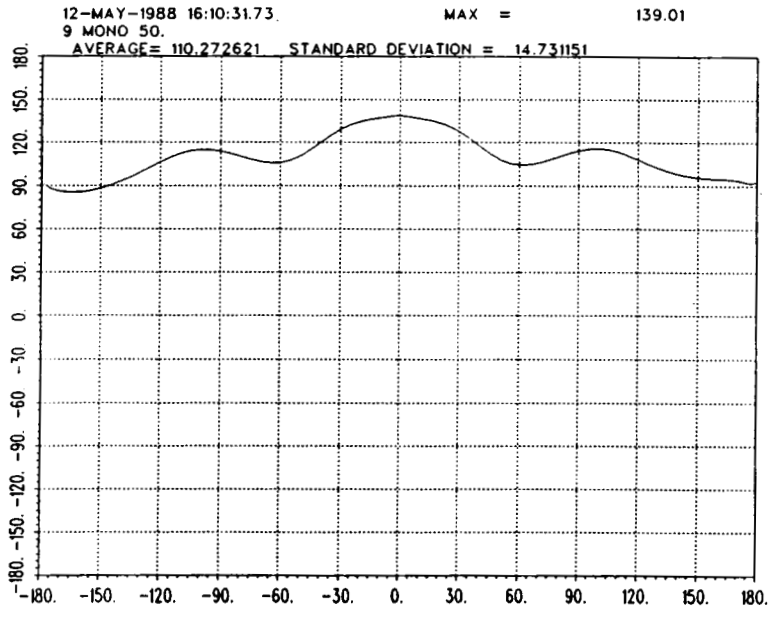

Figure 2.15. Phase plot of a single element in the nine-monopole model with the reference point at 5.25" from the center.

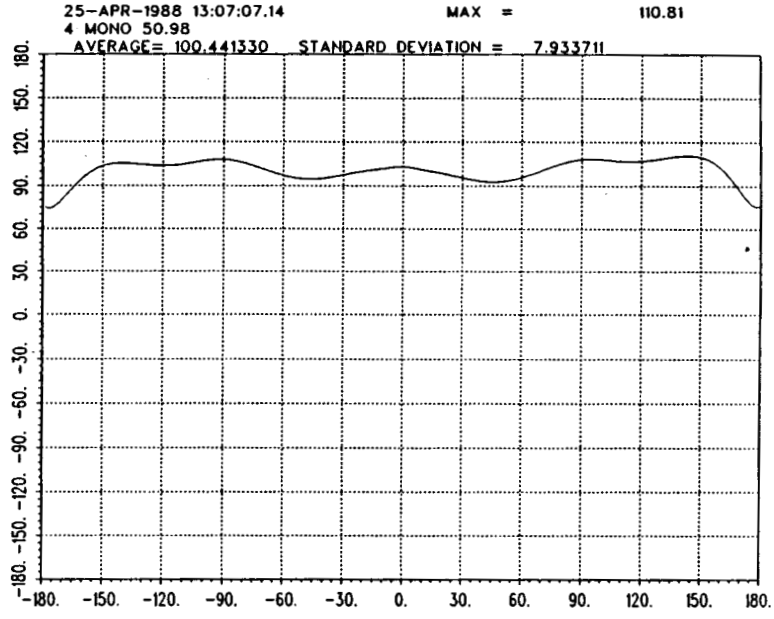

Figure 2.16. Phase plot of a single element in the four-monopole model with the reference point at 6.23" from the center.

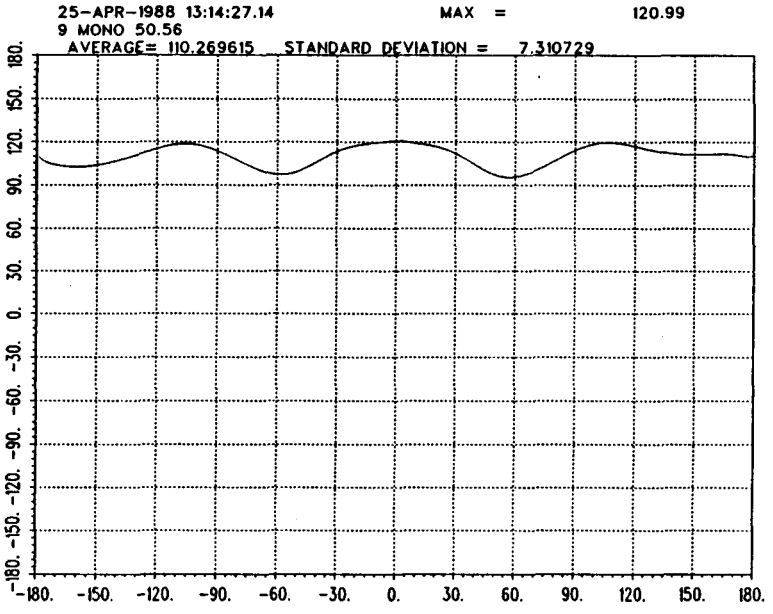

Figure 2.17. Phase plot of a single element in the nine-monopole model with the reference point at 5.81" from the center.

Once the phase center of each element of the TCAS array is calculated by means of the moment method, the next step is to calculate the phase center of the various models considered in Sections B-D, namely, the two-, four- and nine-element models. The phase center of the two-element model is easily calculated [1], and it is located at a distance of $\lambda/8$ from the outer monopole as shown in Figure 2.3. Figure 2.13 depicts the phase plot of the two-monopole model. The phase centers of the four- and nine-element models are harder to calculate. As in the moment method analysis, the phase center of the four- and nine-element models is located on the line joining element 8 and the center element. The initial guess is to assume that the phase center is located at the same position as element 8. Figures 2.14 and 2.15

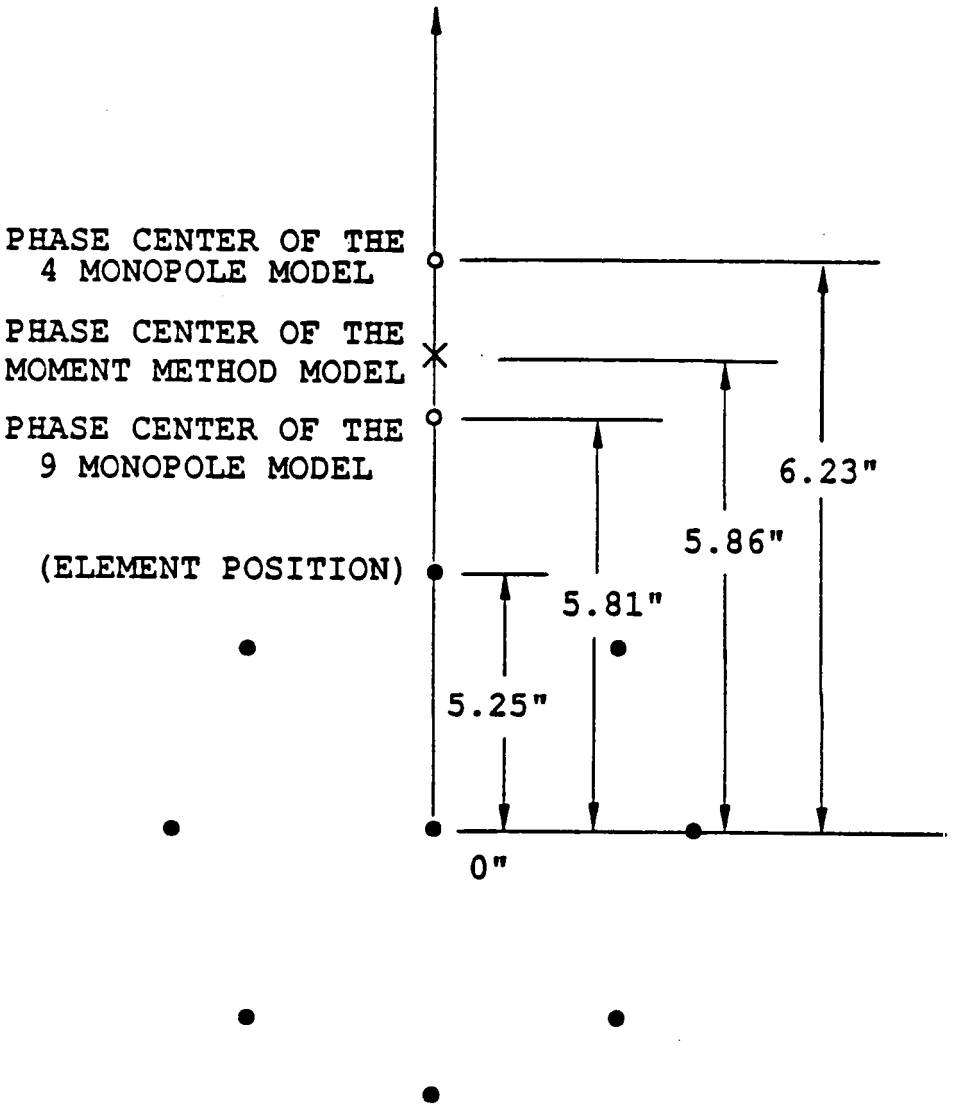

Figure 2.18. A summary of the phase center of single element (top) from each model.

show the phase plots of the four- and nine-monopole models, respectively. By moving the reference point towards the center element, the phase center of these two models can be found. The phase center of the four-monopole model is located at 6.23" from the center

and that of the nine-monopole model is located at 5.81" from the center. Their phase plots referenced to their phase centers are shown in Figures 2.16 and 2.17, respectively. A summary of these results is depicted in Figure 2.18.

The phase center of the nine-monopole model is only 0.05" from that of the moment method analysis which is assumed to be the closest to the exact result. Ideally, they will overlap together; however, for the same reasons listed in the previous section, the results are not exactly the same. The phase center of the four-monopole model is a little farther away from the moment method result. Since 5 elements were taken out and the weights of the currents in the remaining elements have been modified, the shift in the position of the phase center was expected.

Now that the phase centers of the two-, four-, and nine-element models have been found, the sum and difference beams can be obtained by properly adding the radiation patterns of all the elements of the TCAS array after adjusting their phase centers to the proper position.

F. VERIFICATION OF THE SUM AND DIFFERENCE BEAM PATTERNS

As mentioned before, the antenna array will radiate and receive sum and difference beam patterns to calculate the bearing of nearby aircraft. The basic concepts of the sum and difference beams can be found in [1,3]. This section uses the results obtained in Section B-D to obtain sum and difference patterns.

Figure 2.19 shows the measured sum and difference beam patterns for three different bearings. The measurement was made with a TCAS III

array mounted on a curved plane with the same curvature as that of a Boeing 727. According to the original design, the sum and difference patterns must be independent of the bearing angle near boresight direction. The measurements show some change in the sum and difference beams; however, the change is small and it is confined to the backlobes. The change is due to the curvature of the curved ground plane.

Figures 2.20, 2.21 and 2.22 show the sum and difference beam patterns for three different bearings and five elevation angles as in Figure 2.19, using the two-, four- and nine-monopole models, respectively. To avoid any confusion, the two-monopole case discussed here will be referred to as the new two-monopole model where the phase center of each element of the actual TCAS array is assumed to be located 5.86" from the center. The difference beam patterns of the three models are similar to the measured patterns, especially for the nine-monopole model. However, the sum beam patterns are not as close in the backlobe region. The agreement improves for larger elevation angles, and as expected, the nine- and four-monopole models give better results than the two-monopole model.

The weights used to generate the sum and difference beam patterns were obtained from Bendix. It might be possible to adjust these weights to obtain a better agreement between the measured and calculated sum beams in the backlobe region. However, the region of interest is in the main beam where there is good agreement. Thus, the weights provided by Bendix were not adjusted. Recall that there are 64

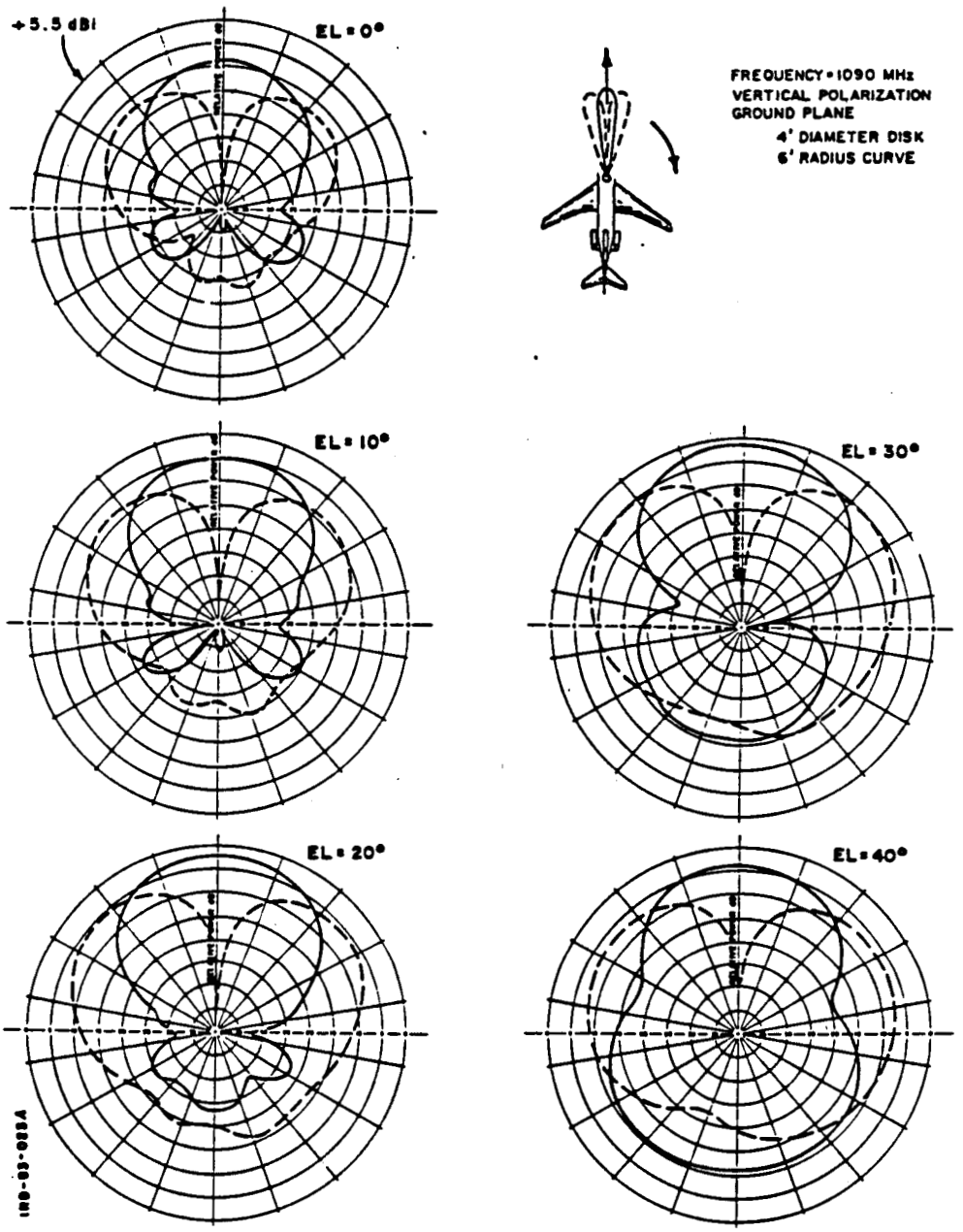

(a) Boresight = 0° AZ

Figure 2.19. The measured sum and difference beam patterns on the fuselage of a Boeing 727 [16].

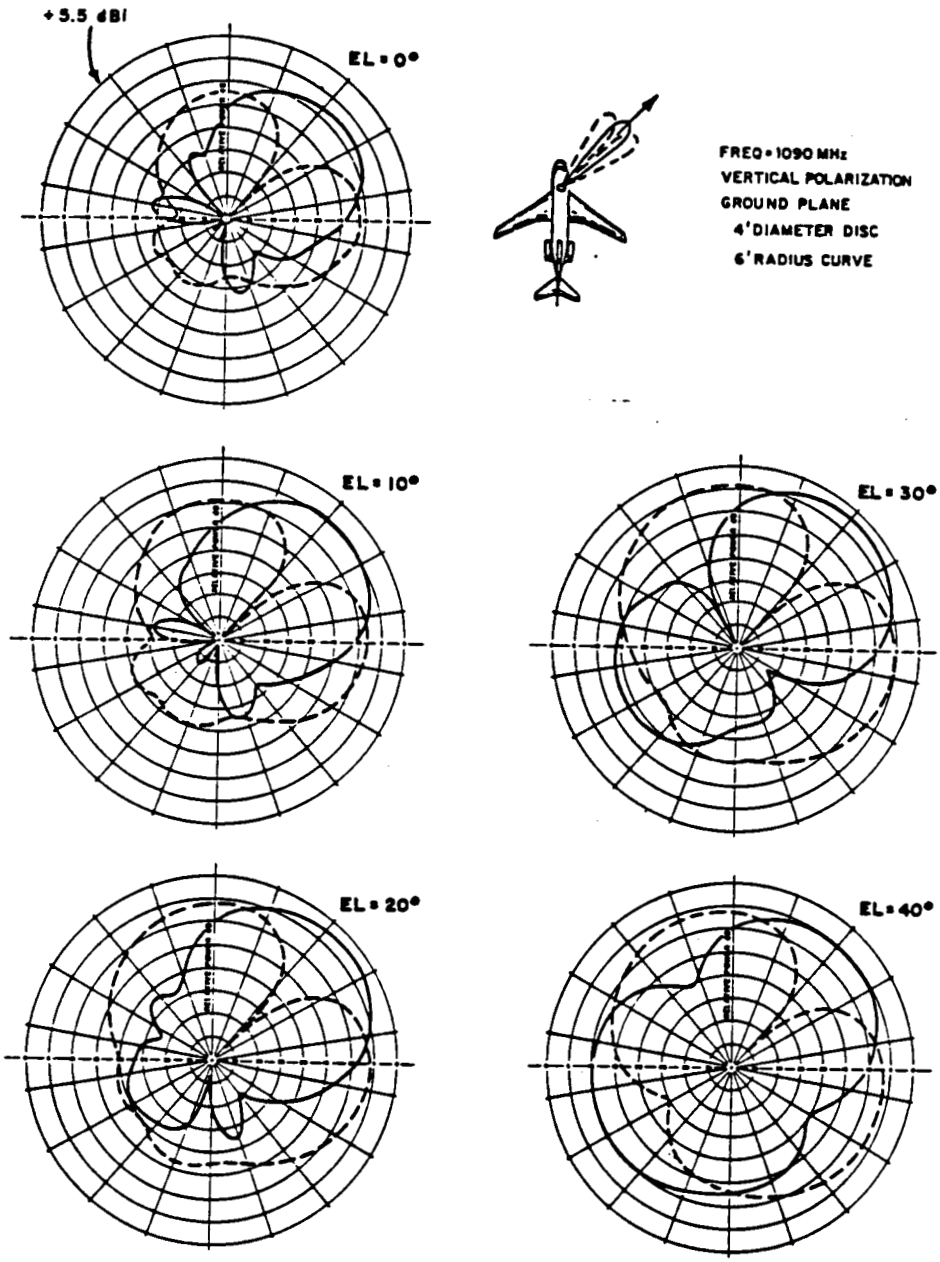

(b) Boresight = 315° AZ

Figure 2.19. Continued.

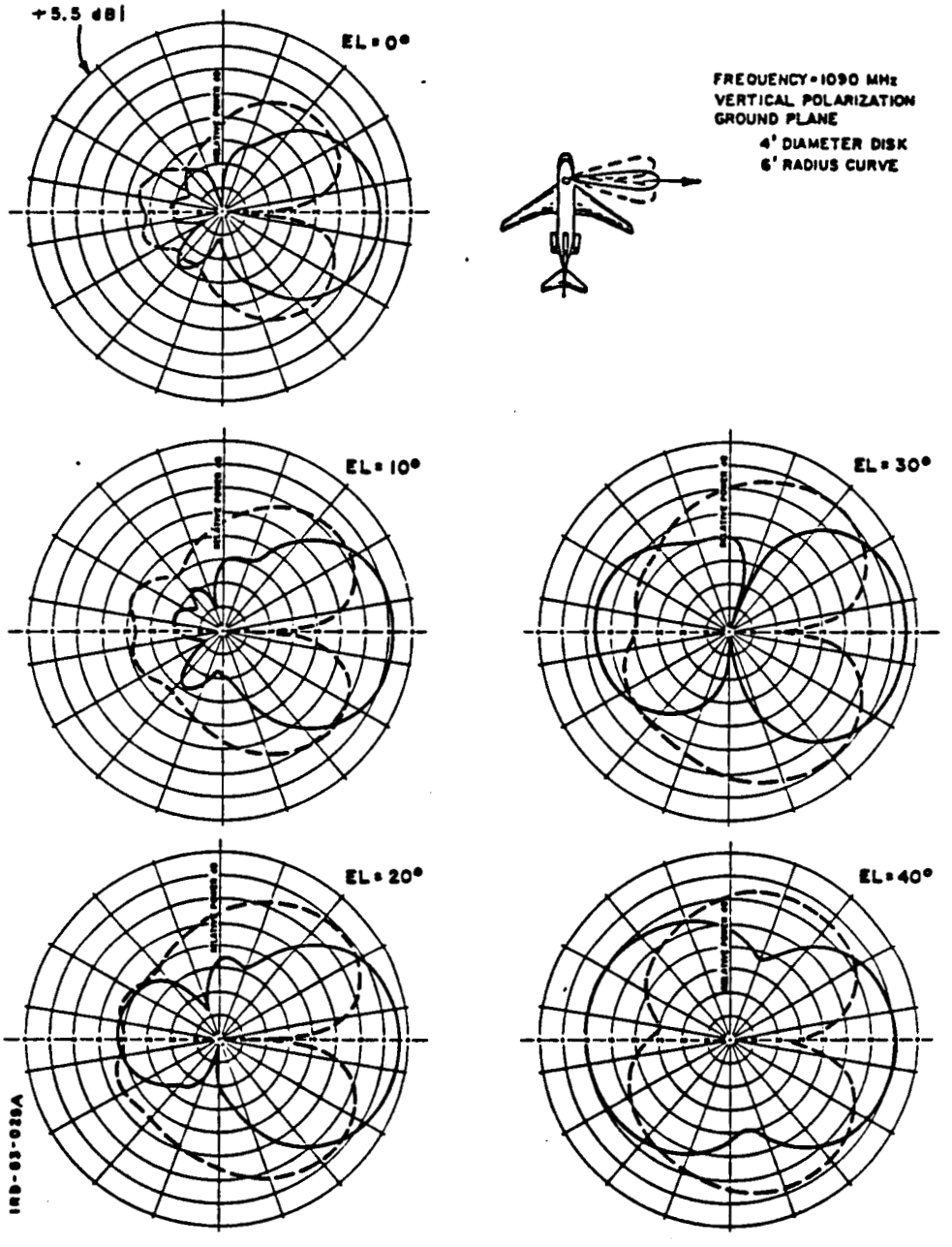

(c) Boresight = 270° AZ

Figure 2.19. Continued.

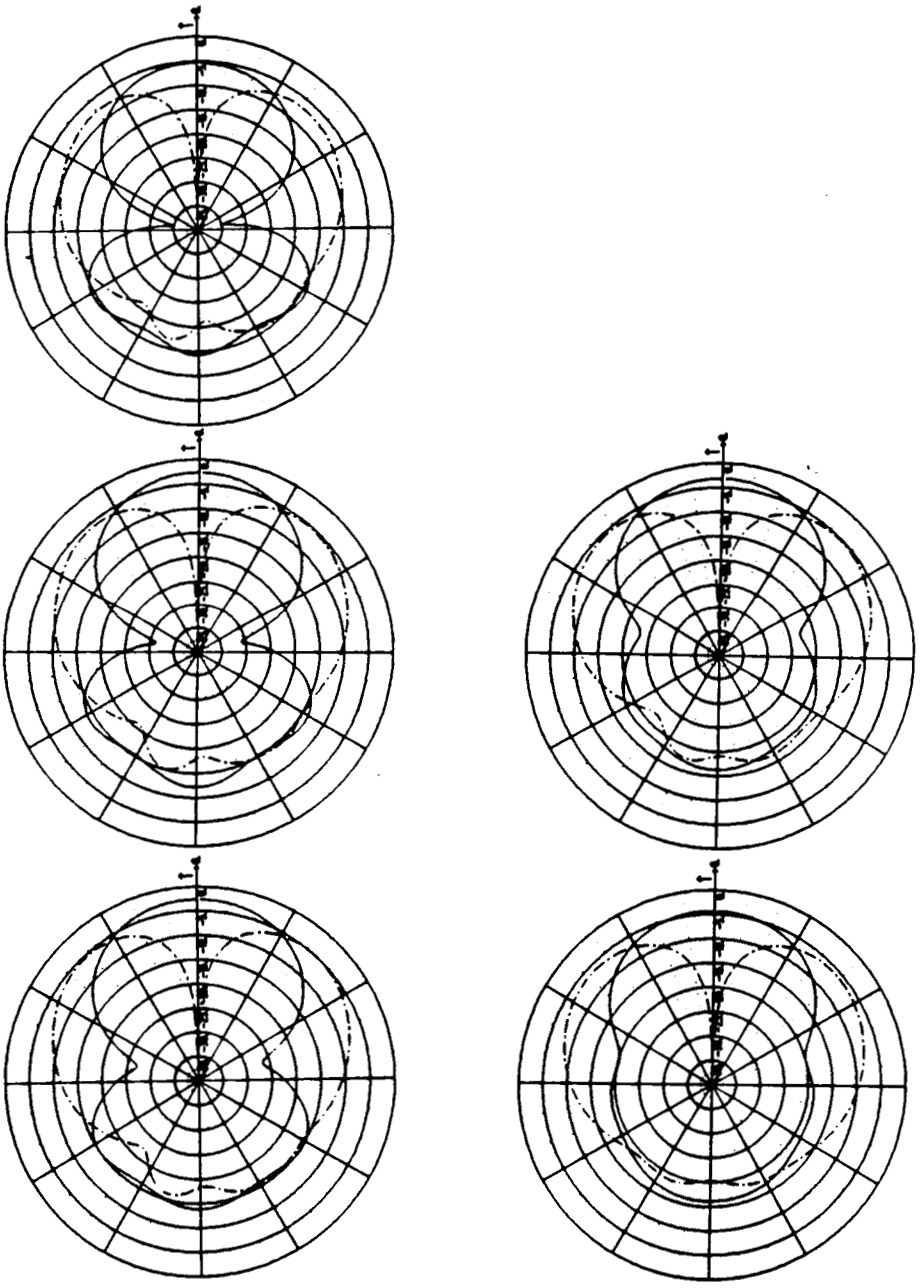

(a) Boresight = 0° AZ

Figure 2.20. The sum and difference beam patterns using the two-monopole model mounted on the fuselage of a Boeing 727.

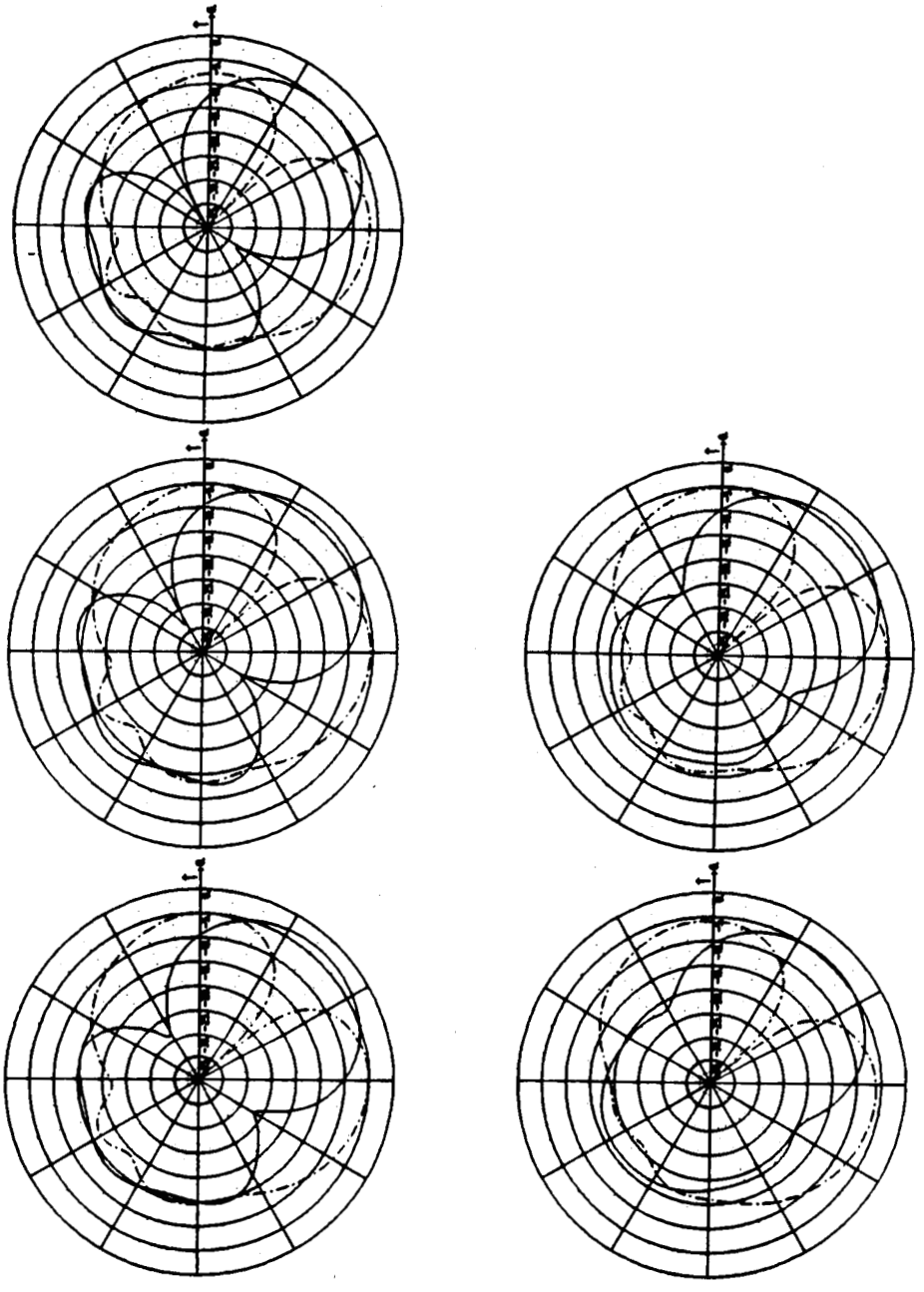

(b) Boresight = 315° AZ

Figure 2.20. Continued.

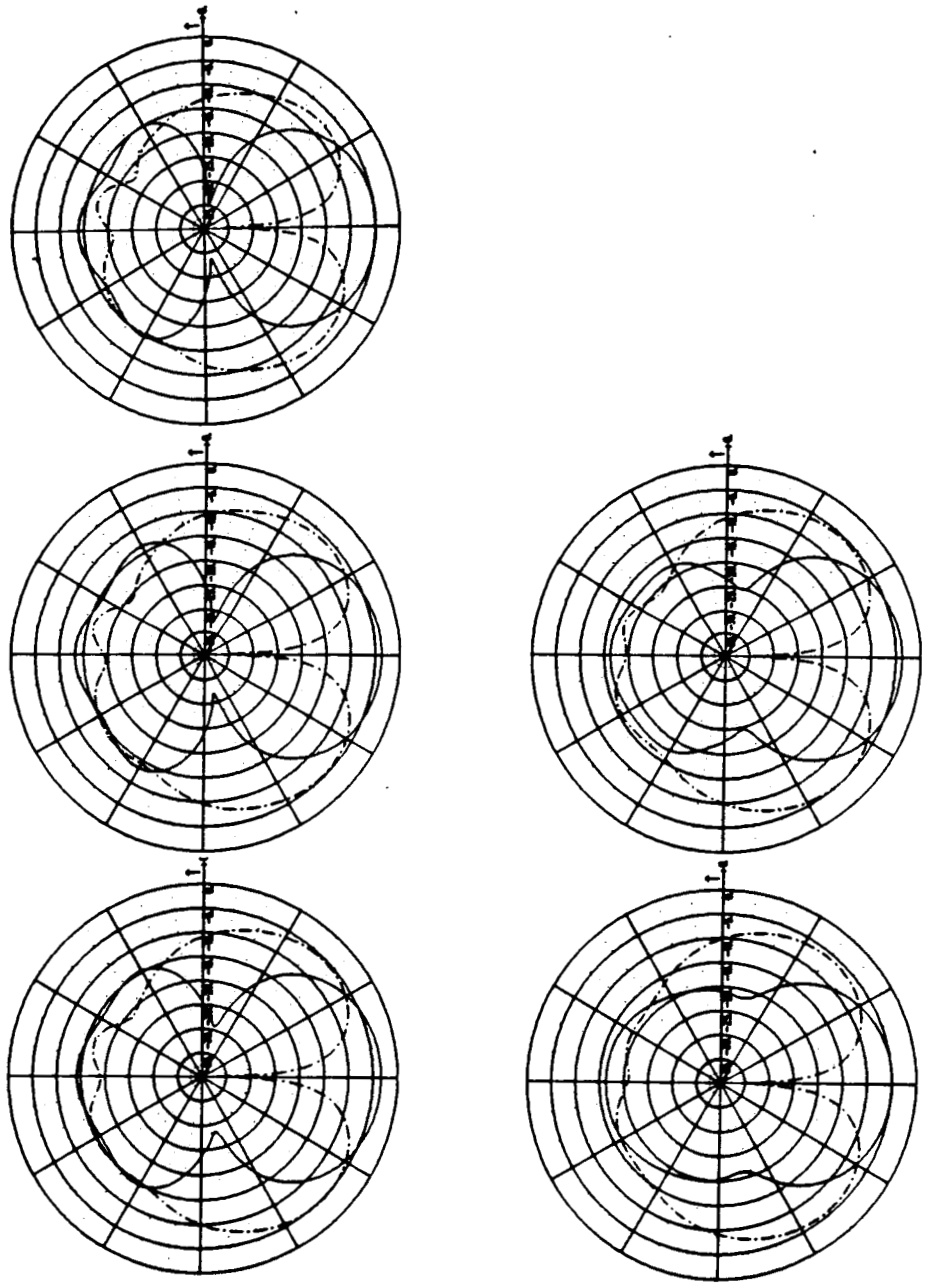

(c) Boresight = 270° AZ

Figure 2.20. Continued.

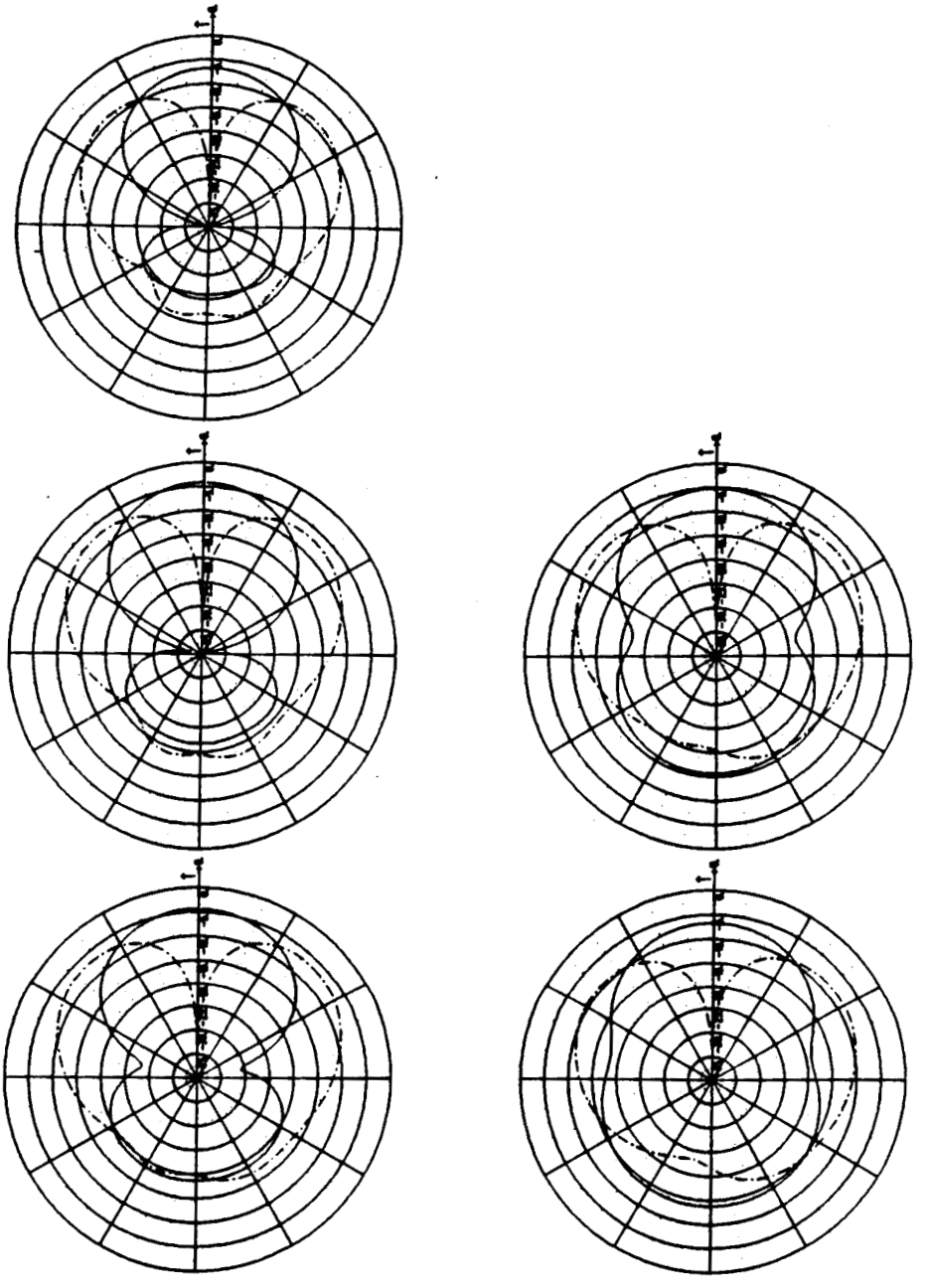

(a) Boresight = 0° AZ

Figure 2.21. The sum and difference beam patterns using the four-monopole model mounted on the fuselage of a Boeing 727.

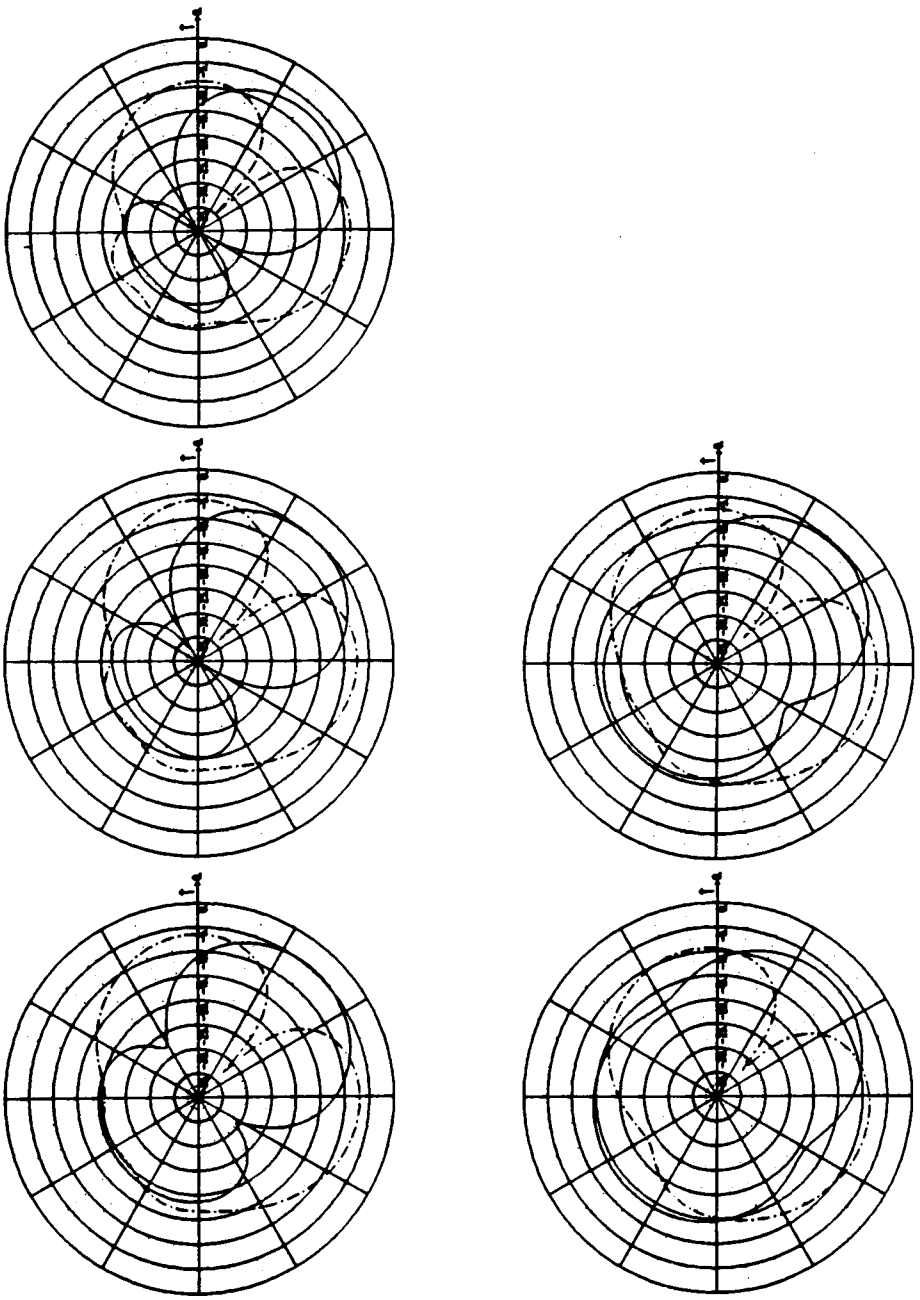

(b) Boresight = 315° AZ

Figure 2.21. Continued.

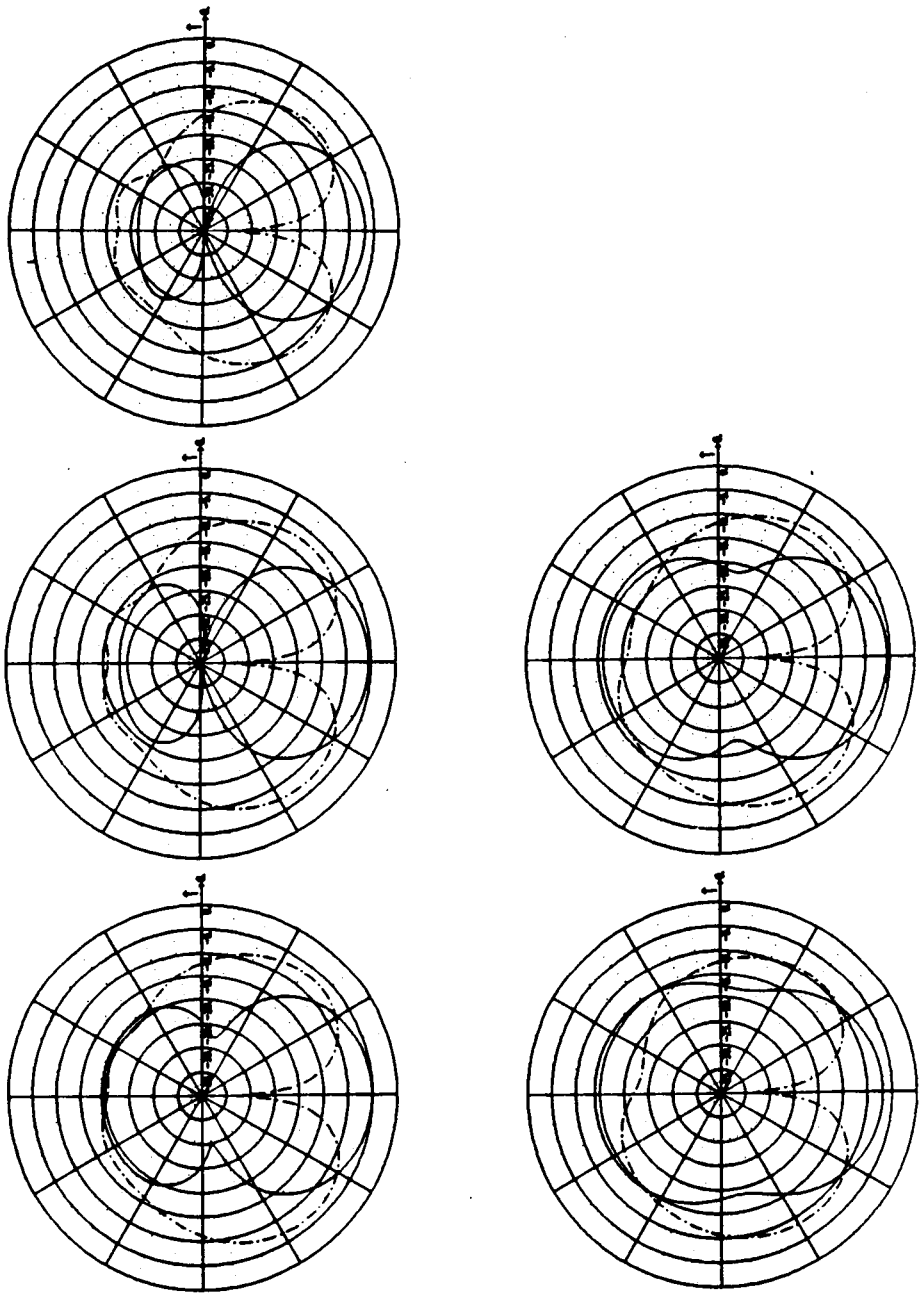

(c) Boresight = 270° AZ

Figure 2.21. Continued.

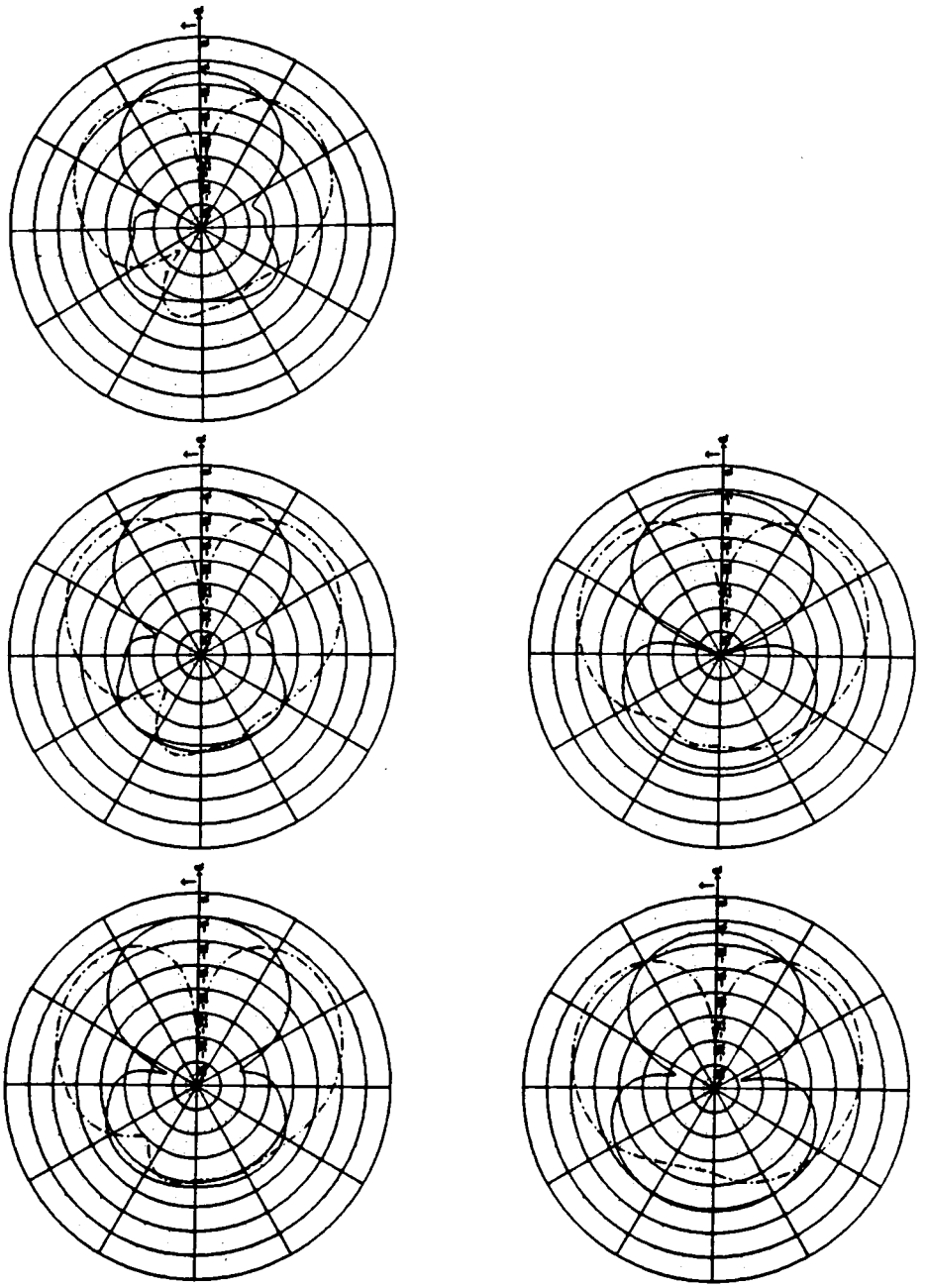

(a) Boresight = 0° AZ

Figure 2.22. The sum and difference beam patterns using the nine-monopole model mounted on the fuselage of a Boeing 727.

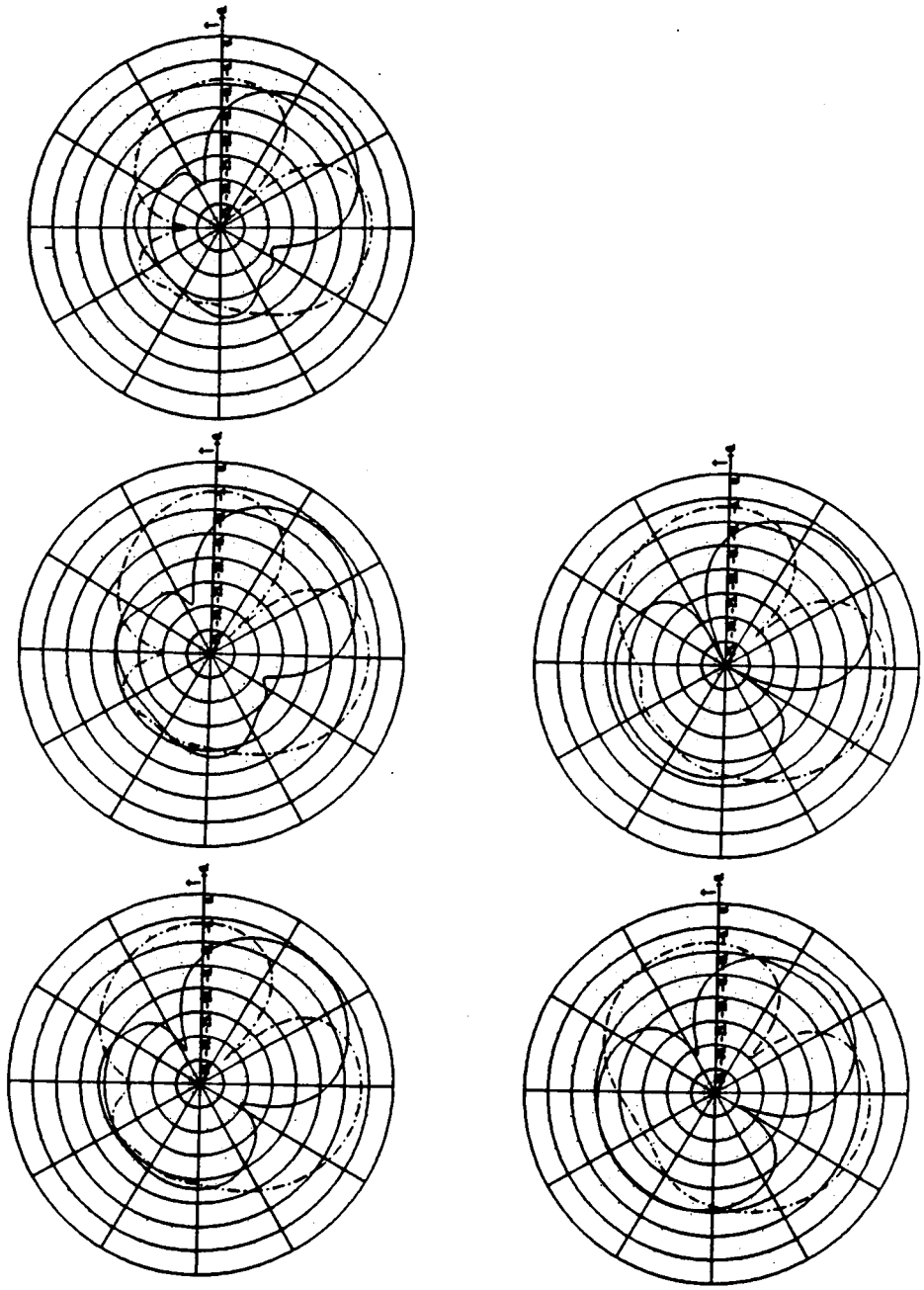

(b) Boresight = 315° AZ

Figure 2.22. Continued.

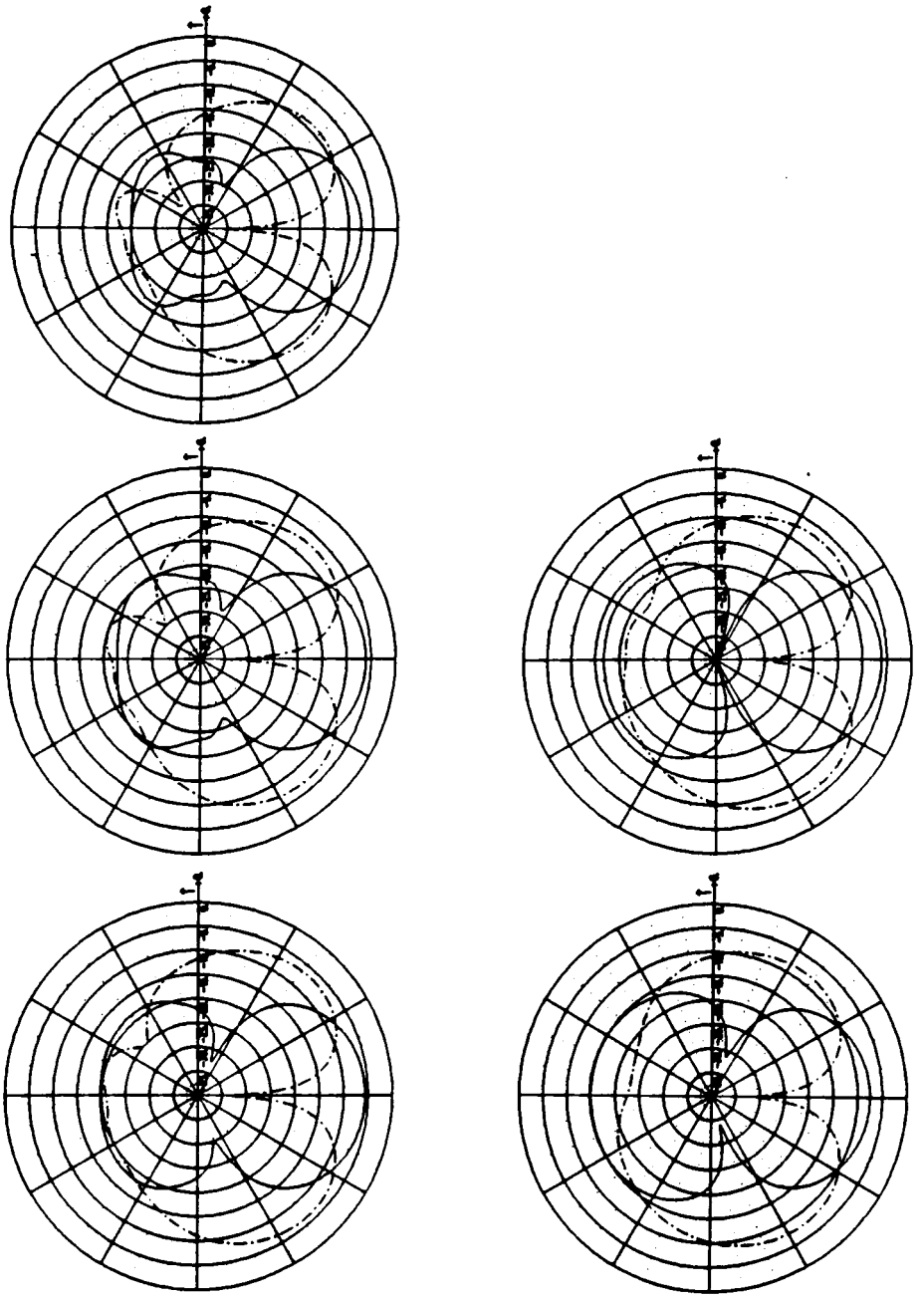

(c) Boresight = 270° AZ

Figure 2.22. Continued.

different beam positions, and therefore, only the area in the neighborhood of the null of the difference beam is important.

Once the sum and difference beams are generated, the next step is to calculate the monopulse curves. A detailed explanation of how to calculate a monopulse is given in [1], [3] and [4].

G. SCATTERING ERROR CURVES

The purpose of generating the monopulse curves is to obtain the bearing of an airplane in the vicinity of the TCAS-equipped aircraft. As discussed in [4] and [14], the system is calibrated by generating a lookup table which takes into account only the fuselage of the airplane and ignores the scattering by the wings, tail, engines, etc. With the algorithms developed so far, it is possible to generate in the computer the lookup table and the monopulse curves which take into account structural scattering.

The procedure followed to generate these curves is discussed in Appendix B. In these curves, the scattering effect from the structure of aircraft is estimated by the detected bearing errors of the target. The bearing error is the difference between the system estimated bearing and the actual aircraft bearing. It is normally plotted relative to the actual bearing. This bearing error depends on not only the configuration of the TCAS system and the aircraft but also the current azimuth and elevation angle of the target. In this section, the scattering error curves obtained with the 3 antenna models developed in the previous sections will be discussed. The TCAS III array is assumed to be top-mounted (off-center) on a Boeing 727. The

input data used for these three models can be found in Appendix A. Figure 2.23 shows the error curve generated with the old two-monopole model (see Figure 2.4). Recall that in this model, the phase center of each element of the actual TCAS array is assumed to be located at the element itself. This model predicts large scattering errors in the aft region of the airplane. The interpretation of this error is discussed in [3], [4] and [5]. Figure 2.24 shows the error curve generated with the new two-monopole model. The error curves in Figures 2.23 and 2.24 are very similar, especially in the region $-120° \leq \phi \leq 120°$. Figures 2.25 and 2.26 depict the scattering error curves using the four-monopole and nine-monopole models, respectively. These two error curves agree very well, especially in the region $-120° \leq \phi \leq 120°$.

Note that all 4 models discussed here produce very similar error curves in the front region $-90° \leq \phi \leq 90°$. The largest difference is in the aft region where the new and old two-monopole models predict larger errors than the four- and nine-monopole models. Because the four- and nine-monopole models are considered more accurate, their corresponding error curves are also considered more realistic. However, since the region of interest is in the forward region, all the models discussed here generate similar results. Therefore, computer time can be saved by using the two-monopole or four-monopole models. As mentioned before, the models generated here can be improved by adjusting the weights of the elements of the TCAS III array to obtain better agreement between the measured and calculated sum and difference beams.

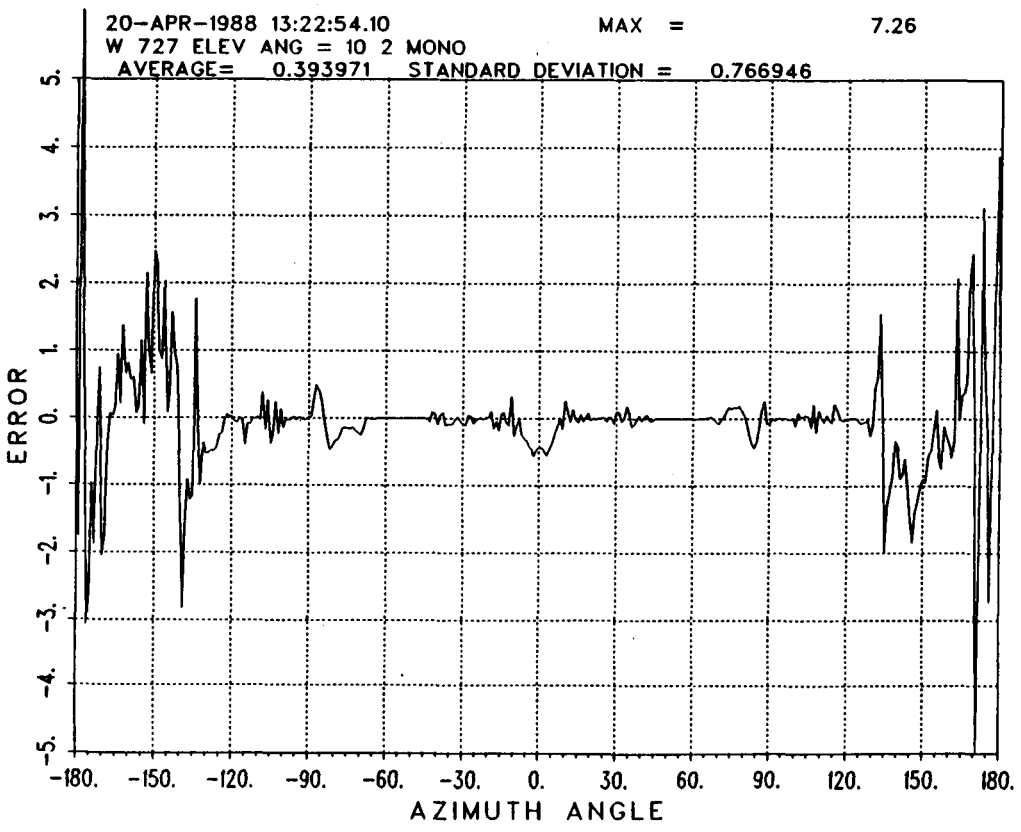

Figure 2.23. The scattering error curve of the Boeing 727 with the top-mounted off-centered TCAS III using the old two-monopole model.

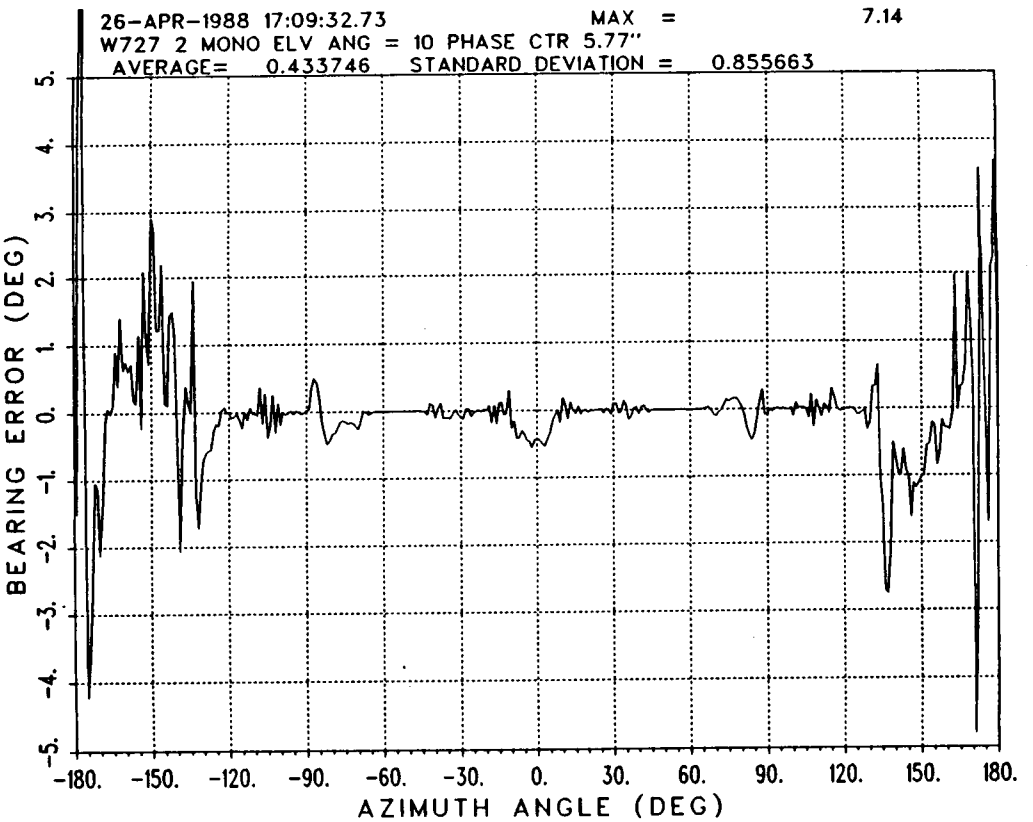

Figure 2.24. The scattering error curve of the Boeing 727 with the top-mounted off-centered TCAS III using the new two-monopole model.

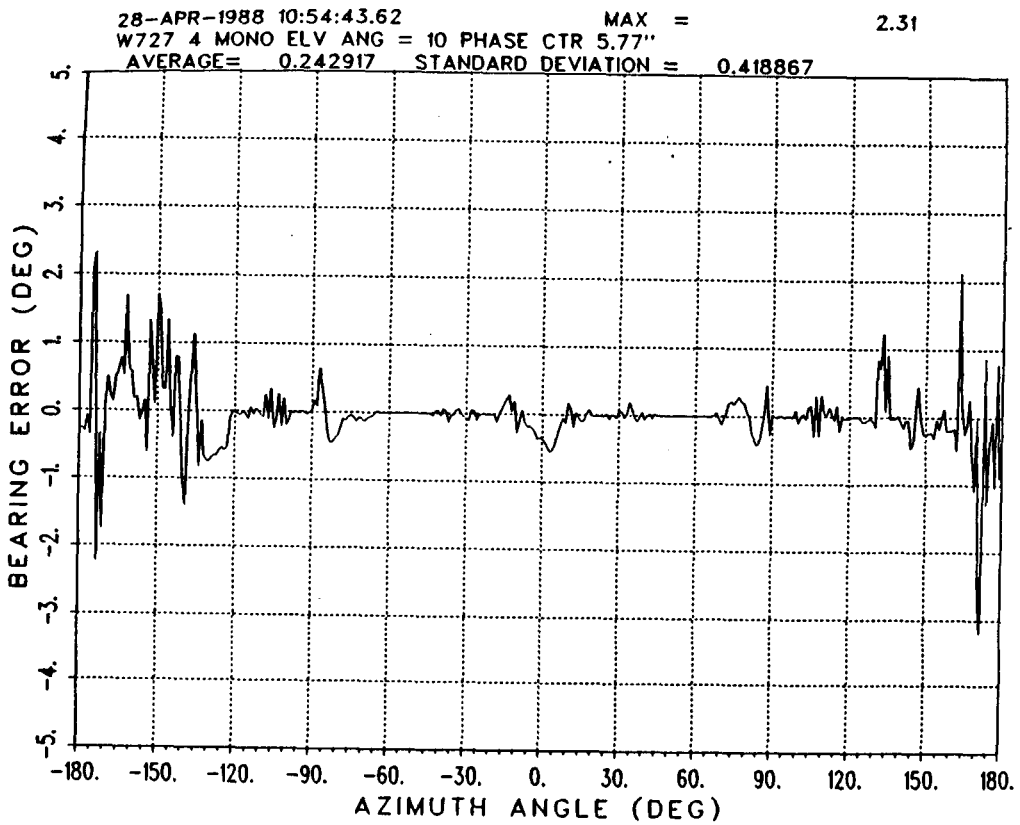

Figure 2.25. The scattering error curve of the Boeing 727 with the top-mounted off-centered TCAS III using the four-monopole model.

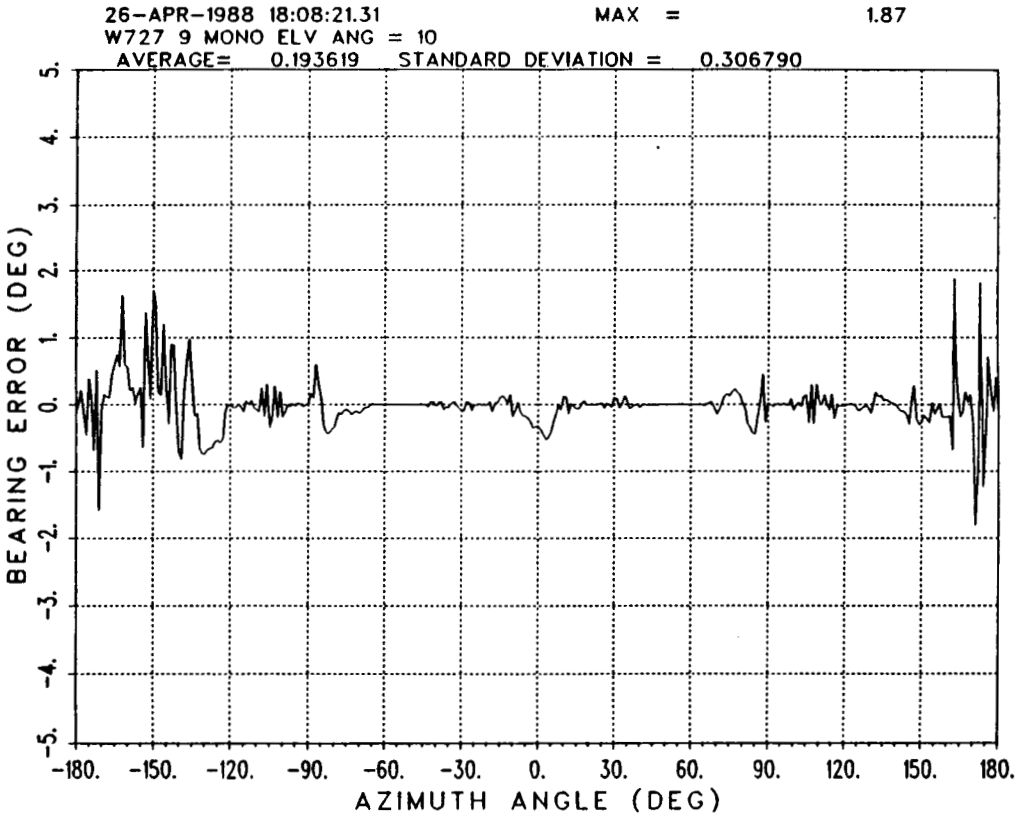

Figure 2.26. The scattering error curve of the Boeing 727 with the top-mounted off-centered TCAS III using the nine-monopole model.

CHAPTER III

COMPUTER-SIMULATED MODEL FOR A TCAS-EQUIPPED BOEING 727

A. INTRODUCTION

In this chapter, the computer models for the structure of the Boeing 727 as well as the TCAS III system which is mounted on it are discussed. Also, scattering error curves with different elevation angles are generated and then discussed. In addition, the best position of the TCAS array on an aircraft is suggested.

B. BOEING 727

Figure 3.1 shows three-dimensional (3-D) views of a Boeing 727. Figure 3.2 depicts more detailed graphs for the fuselage of the Boeing 727. Since there are two TCAS III arrays mounted on the fuselage of the Boeing 727 aircraft, one on the top and the other on the bottom, the models of the aircraft structure should be considered separately for each TCAS III array. Also, because of the results of Chapter II, where it is shown that the old two-monopole model is good enough for the front region, this model will be used for the analysis in this chapter.

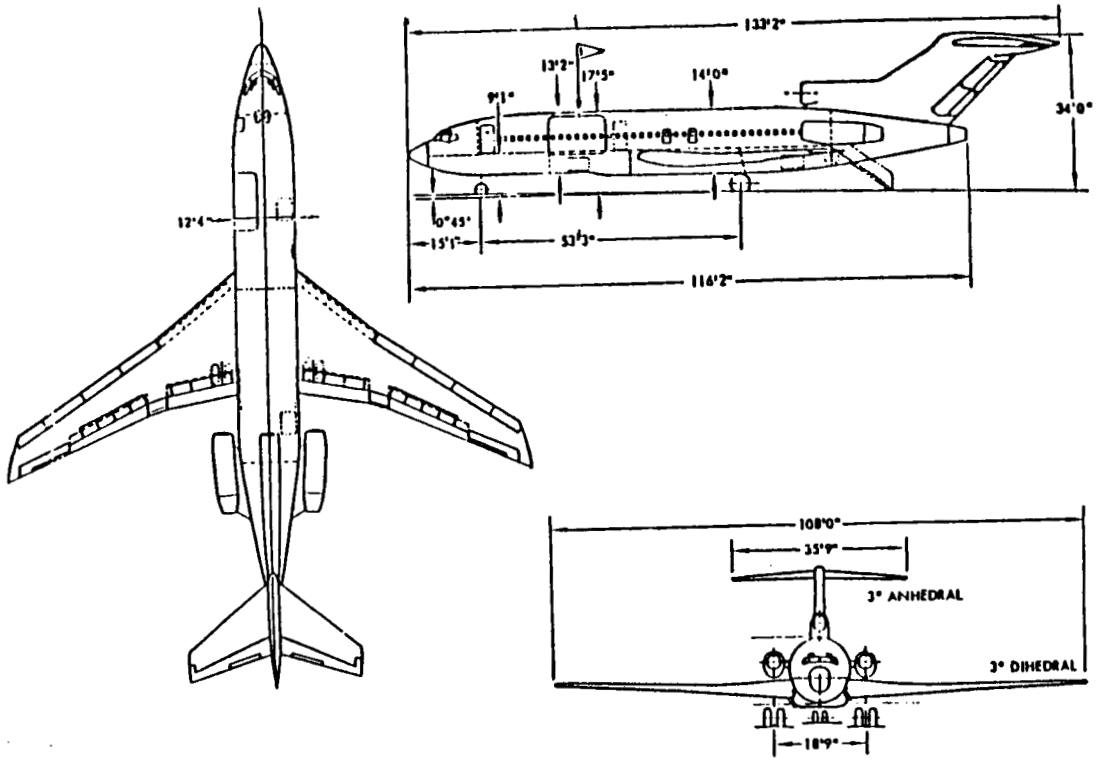

Figure 3.1. Principal dimensions of the Boeing 727 [19].

ORIGINAL PAGE IS
OF POOR QUALITY

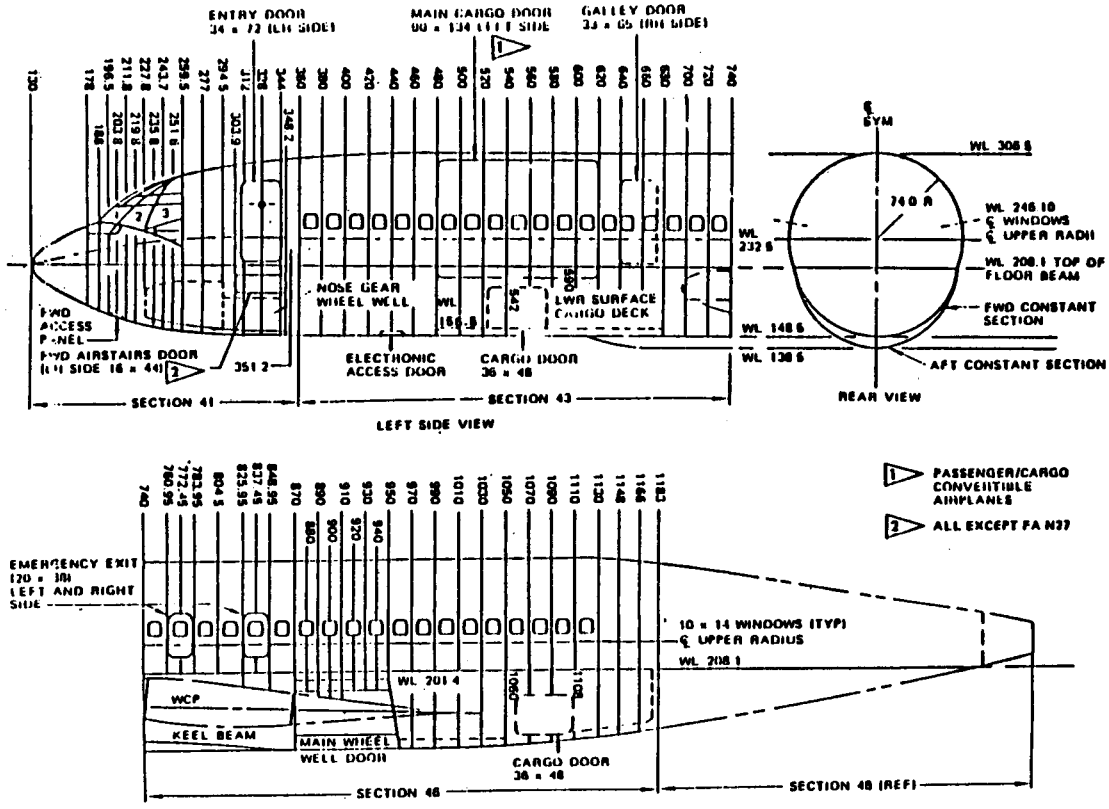

Figure 3.2. Forward body station diagram of the Boeing 727 [19].

C. COMPUTER-SIMULATED MODEL FOR THE TOP-MOUNTED TCAS III

From Figure 3.2, it is clear the cross section of the Boeing 727 is not purely elliptical. The parameters for the FG: command in the Aircraft Code [4], which models the fuselage with a composite ellipsoid can not be easily determined. Since the curvature of the fuselage near the antenna location is very important for the GTD calculation, the curvature in the upper region is more important than in the lower region for the top-mounted antenna. Therefore, the input parameters are chosen as close to the upper curvature as possible. Actually, the upper section is a half circle; therefore, a circular cross section in the x-y plane (see Figure 3.3) is assumed for the fuselage of the top-mounted Boeing 727.

Once the fuselage is determined, the plates of the Boeing 727 can then be attached. Table 3.1(a) shows the plates that must be used for the Boeing 727 model as suggested by the FAA [19]; 21 plates are to be attached to the fuselage of the Boeing 727 for the top-mounted TCAS III array. The more plates are added, the more CPU time is spent; therefore, the model should be simplified to save CPU time. Some plates which are not as important are taken out, and some plates can be combined to form a larger and simpler one. In addition, two plates, the right engine pylon and the left engine pylon, which are important but not recommended by the FAA, are added here. The final model includes 17 plates.

The final task is to place the TCAS III antenna array on the Boeing 727. The TCAS III array is flush-mounted on the top of the fuselage at 380" from the nose and 4.75 inches off-centered. The 3-D

Table 3.1

Attached Plates for the Boeing 727 Model as Suggested by the FAA [19]

(a) for top antenna model

Item	# Plates	Plate names
Right wing (upper surface)	2	P1, P2
Right engine nacelle (top)	3	P4, P5, P6
Right horizontal stabilizer	3	P9, P10, P11
Vertical stabilizer	3	P12, P13, P14
Center engine intake	5	P15, P16, P17, P18, P19
Center engine pylon	2	P20, P21
Left horizontal stabilizer	3	P22, P23, P24
Left engine nacelle (top)	3	P25, P26, P27
Left wing (upper surface)	2	P31, P32

(b) for bottom antenna model

Item	# Plates	Plate names
Right wing (lower surface)	2	P39, P40
Right engine nacelle (bottom)	3	P4, P7, P8
Right horizontal stabilizer	3	P9, P10, P11
Left horizontal stabilizer	3	P22, P23, P24
Left engine nacelle (bottom)	3	P25, P28, P29
Left wing (lower surface)	2	P41, P42
Fuselage surface (bottom)	7	P33, P34, P35, P36, P37, P38, P39

Table 3.2

Input Data of the Boeing 727 with top-mounted TCAS III for the Aircraft Code

```
UN:INCHES
3
FQ:1.06 GHZ
1,1.06,1.
FG:BOEING 727 WITH TOP-MOUNTED ANTENNA
74.,74.,1064.,330.
T
0.,0.,50.
PD:
90.,0.,80.
0,360,1
T,1000000.
BO:
T
PP:POLAR PLOT IN DB
F
1,2.,3
PG:LEFT WING
6,T
-24.,78.,249.
-24.,277.,411.
-24.,625.,636.
-24.,652.,750.
-24.,250.,587.
-24.,76.,558.
PG:RIGHT WING
6,T
-24.,-76.,558.
-24.,-250.,587.
-24.,-652.,750.
-24.,-625.,636.
-24.,-277.,411.
-24.,-78.,249.
PG:RIGHT VERTICAL STABILIZER
4,T
65.,0.,719.
252.,0.,996.
252.,-15.,1257.
65.,-15.,980.
PG:LEFT VERTICAL STABILIZER
4,T
65.,15.,980.
252.,15.,1257.
252.,0.,996.
65.,0.,719.
PG:LEFT HORIZONTAL STABILIZER
4,F
```

Table 3.2 - Continued

```
239.,14.,1188.
239.,210.,1243.
239.,210.,1172.
239.,14.,1016.
PG:RIGHT HORIZONTAL STABILIZER
4,F
239.,-14.,1016.
239.,-210.,1172.
239.,-210.,1243.
239.,-14.,1188.
PG:CENTER ENGINE FRONT
4,T
75.,22.,652.5
145.,22.,652.5
145.,-22.,652.5
75.,-22.,652.5
PG:CENTER ENGINE LEFT
4,T
70.,22.,710.
145.,22.,815.
145.,22.,652.5
75.,22.,652.5
PG: CENTER ENGINE RIGHT
4,T
75.,-22.,652.5
145.,-22.,652.5
145.,-22.,815.
70.,-22.,710.
PG:RIGHT ENGINE TOP
4,F
63.,-80.,646.
63.,-80.,837.
63.,-140.,837.
63.,-140.,646.
PG:RIGHT ENGINE FRONT
4,F
63.,-80.,646.
63.,-140.,646.
0.,-140.,646.
0.,-80.,646.
PG:RIGHT ENGINE SIDE
4,F
63.,-80.,646.
0.,-80.,646.
0.,-80.,837.
63.,-80.,837.
PG:RIGHT PYLON
4,T
12.5,-60.,854.
12.5,-81.,827.
```

Table 3.2 - Continued

```
12.5,-81.,682.
12.5,-65.,682.
PG:LEFT PYLON
4,T
12.5,65.,682.
12.5,81.,682.
12.5,81.,827.
12.5,60.,854.
PG:LEFT ENGINE TOP
4,F
63.,80.,646.
63.,140.,646.
63.,140.,837.
63.,80.,837.
PG:LEFT ENGINE FRONT
4,F
63.,80.,646.
0.,80.,646.
0.,140.,646.
63.,140.,646.
PG:LEFT ENGINE SIDE
4,F
63.,80.,646.
63.,80.,837.
0.,80.,837.
0.,80.,646.
SG:ELEMENT 1
-0.753,46.288
2
1.14,-45.
0.,0.,0.,2.78,3
1.,-45.
1.64,135.
0.,0.,0.,2.78,3
0.698,45.
EX:
SG:ELEMENT 2
0.363,50.
2
1.14,0.
0.,0.,0.,2.78,3
1.,-45.
1.64,180.
0.,0.,0.,2.78,3
0.698,45.
EX:
SG:ELEMENT 3
-0.754,53.712
2
1.14,45.
```

Table 3.2 - Continued

```
0.,0.,0.,2.78,3
1.,-45.
1.64,225.
0.,0.,0.,2.78,3
0.698,45.
EX:
SG:ELEMENT 4
-3.450,55.25
2
1.14,90.
0.,0.,0.,2.78,3
1.,-45.
1.64,270.
0.,0.,0.,2.78,3
0.698,45.
EX:
SG:ELEMENT 5
-6.145,53.712
2
1.14,135.
0.,0.,0.,2.78,3
1.,-45.
1.64,-45.
0.,0.,0.,2.78,3
0.698,45.
EX:
SG:ELEMENT 6
-7.261,50.
2
1.14,180.
0.,0.,0.,2.78,3
1.,-45.
1.64,0.
0.,0.,0.,2.78,3
0.698,45.
EX:
SG:ELEMENT 7
-6.143,46.288
2
1.14,225.
0.,0.,0.,2.78,3
1.,-45.
1.64,45.
0.,0.,0.,2.78,3
0.698,45.
EX:
SG:ELEMENT 8
-3.448,44.75
2
1.14,270.
```

Table 3.2 - Continued

```
0.,0.,0.,2.78,3
1.,-45.
1.64,90.
0.,0.,0.,2.78,3
0.698,45.
EX:
```

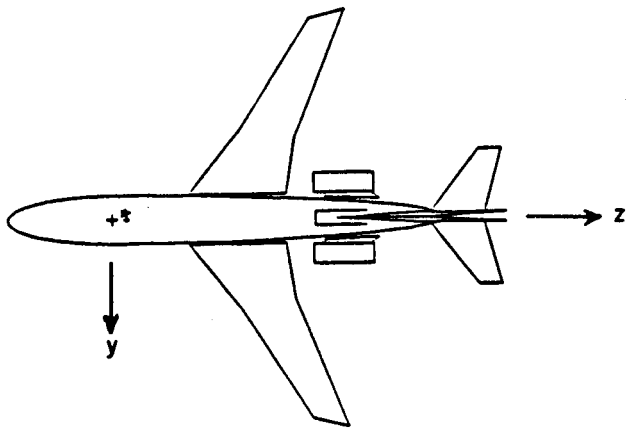

X-AXIS

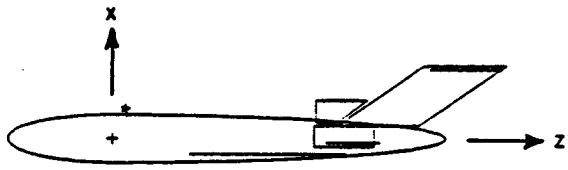

Y-AXIS

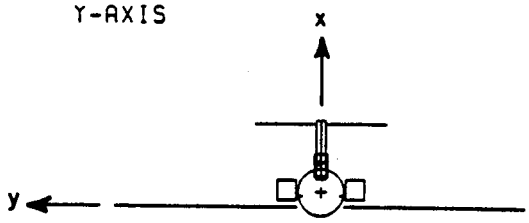

Z-AXIS

Figure 3.3. 3-D views of the Boeing 727 model for top-mounted TCAS III.

views of the complete model is shown in Figure 3.3, and the complete input data for the Aircraft Code are shown in Table 3.2.

D. COMPUTER-SIMULATED MODEL FOR THE BOTTOM-MOUNTED TCAS III

The curvature of the composite ellipsoid of the computer model for the Boeing 727 for the bottom-mounted TCAS III array should be determined by the curvature of the lower fuselage. From Figure 3.2, the lower fuselage of the Boeing 727 consists of two sections, the FWD section and AFT section. The FWD section is implemented by a composite ellipsoid of the same curvature in the x-y plane and the AFT section is implemented by several plates attached to the lower fuselage. The curvature of the FWD section is chosen as 60" (x axis) and 70" (y axis).

The plates used to represent the fuselage for the bottom-mounted antenna as recommended by the FAA are shown in Table 3.1(b). There are a total of 23 plates. After simplifying, only 16 plates are needed, including 7 plates to simulate the AFT section. The position of the bottom TCAS III system is on the opposite side of the top TCAS III system, which is off-centered, too.

The 3-D views of the complete model is shown in Figure 3.4. The input data for the Aircraft Code is shown in Table 3.3. It should be noted that for convenience in using the Aircraft Code, the bottom antenna is on the top of the graph and the whole aircraft is turned over. However, the convention for the elevation and azimuth angles is still that for the top-mounted antenna coordinate system shown in Figure 3.3.

Table 3.3

Input Data of the Boeing 727 with bottom-mounted TCAS III for the Aircraft Code

```
UN:INCHES
3
FQ:1.06 GHZ
1,1.06,1.
FG:BOEING 727 WITH BOTTOM ANTENNA
60.,70.,1064.,330.
T
0.,0.,50.
PD:
90.,0.,80.
0,360,1
T,1000000.
BO:
T
PP:POLAR PLOT IN DB
F
1,2.,3
PG:LEFT WING
6,T
26.,78.,249.
26.,277.,411.
26.,625.,636.
26.,652.,750.
26.,298.,600.
26.,76.,558.
PG:RIGHT WING
6,T
26.,-76.,558.
26.,-298.,600.
26.,-652.,750.
26.,-625.,636.
26.,-277.,411.
26.,-78.,249.
PG:FUSELAGE FRONT UPPER PLATE
4,T
26.,45.,190.
37.,65.,150.
37.,-65.,150.
26.,-45.,190.
PG:FUSELAGE FRONT LOWER PLATE
4,F
37.,65.,150.
72.,45.,190.
72.,-45.,190.
37.,-65.,150.
PG:FUSELAGE RIGHT UPPER PLATE
4,T
```

Table 3.3 - Continued

```
26.,45.,190.
37.,65.,150.
37.,65.,587.
26.,45.,641.
PG:FUSELAGE RIGHT LOWER PLATE
3,F
37.,65.,150.
72.,45.,190.
37.,65.,587.
PG:FUSELAGE LEFT UPPER PLATE
4,T
26.,-45.,641.
37.,-65.,587.
37.,-65.,150.
26.,-45.,190.
PG:FUSELAGE LEFT LOWER PLATE
3,F
37.,-65.,150.
37.,-65.,587.
72.,-45.,190.
PG:FUSELAGE BOTTOM PLATE
4,F
72.,45.,190.
72.,-45.,190.
37.,-65.,587.
37.,65.,587.
PG:LEFT ENGINE BOTTOM
4,F
0.,80.,646.
0.,140.,646.
0.,140.,837.
0.,80.,837.
PG:LEFT ENGINE FRONT
4,F
0.,80.,646.
-63.,80.,646.
-63.,140.,646.
0.,140.,646.
PG:LEFT ENGINE SIDE
4,F
0.,80.,646.
0.,80.,837.
-63.,80.,837.
-63.,80.,646.
PG:RIGHT ENGINE BOTTOM
4,F
0.,-80.,646.
0.,-80.,837.
0.,-140.,837.
0.,-140.,646.
```

Table 3.3 - Continued

```
PG:RIGHT ENGINE FRONT
4,F
0.,-80.,646.
0.,-140.,646.
-63.,-140.,646.
-63.,-80.,646.
PG:RIGHT ENGINE SIDE
4,F
0.,-80.,646.
-63.,-80.,646.
-63.,-80.,837.
0.,-80.,837.
PG:HORIZONTAL STABILIZER
6,F
-239.,0.,1004.8
-239.,210.,1172.
-239.,210.,1243.
-239.,0.,1184.
-239.,-210.,1243.
-239.,-210.,1172.
SG:ELEMENT 1
-0.753,46.288
2
1.14,-45.
0.,0.,0.,2.78,3
1.,-45.
1.64,135.
0.,0.,0.,2.78,3
0.698,45.
EX:
SG:ELEMENT 2
0.363,50.
2
1.14,0.
0.,0.,0.,2.78,3
1.,-45.
1.64,180.
0.,0.,0.,2.78,3
0.698,45.
EX:
SG:ELEMENT 3
-0.754,53.712
2
1.14,45.
0.,0.,0.,2.78,3
1.,-45.
1.64,225.
0.,0.,0.,2.78,3
0.698,45.
EX:
```

Table 3.3 - Continued

```
SG:ELEMENT 4
-3.450,55.25
2
1.14,90.
0.,0.,0.,2.78,3
1.,-45.
1.64,270.
0.,0.,0.,2.78,3
0.698,45.
EX:
SG:ELEMENT 5
-6.145,53.712
2
1.14,135.
0.,0.,0.,2.78,3
1.,-45.
1.64,-45.
0.,0.,0.,2.78,3
0.698,45.
EX:
SG:ELEMENT 6
-7.261,50.
2
1.14,180.
0.,0.,0.,2.78,3
1.,-45.
1.64,0.
0.,0.,0.,2.78,3
0.698,45.
EX:
SG:ELEMENT 7
-6.143,46.288
2
1.14,225.
0.,0.,0.,2.78,3
1.,-45.
1.64,45.
0.,0.,0.,2.78,3
0.698,45.
EX:
SG:ELEMENT 8
-3.448,44.75
2
1.14,270.
0.,0.,0.,2.78,3
1.,-45.
1.64,90.
0.,0.,0.,2.78,3
0.698,45.
EX:
```

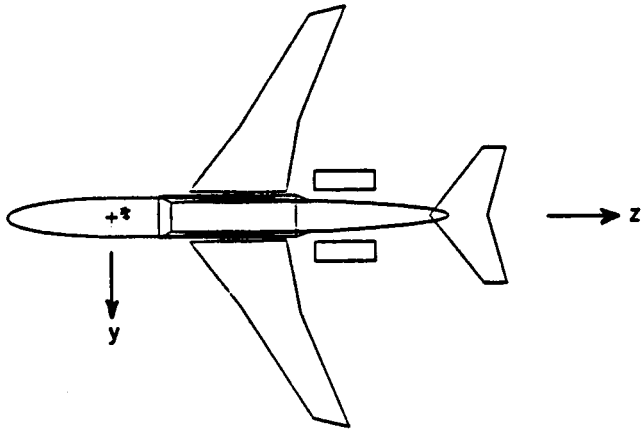

X-AXIS

Y-AXIS

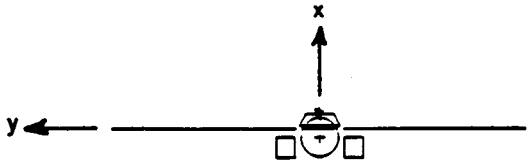

Z-AXIS

Figure 3.4. 3-D views of the Boeing 727 model for bottom-mounted TCAS III system.

E. SCATTERING ERROR CURVES OF THE BOEING 727

The steps followed to generate the scattering error curves are given in Appendix B and will not be repeated here. It is enough to mention that the lookup table [4] generated for the top-mounted array corresponds to an elevation angle of 10°. On the other hand, the lookup table for the bottom-mounted array corresponds to an elevation angle of -10°.

The calculated bearing error curves are very useful in evaluating the performance of the TCAS system. The errors being investigated here are due to scattering by the structure of the airplane; i.e., wings, tail, and engines. The error curves can also be used to determine the optimum location of the TCAS array. Time and money can be saved if all the analyses described here is done before a TCAS system is installed and tested.

Several error curves for the top- and bottom-mounted TCAS array with different elevation angles are generated here. Figure 3.5 shows some error curves for the top-mounted array for several typical elevation angles. Figure 3.6 also shows some curves for the bottom-mounted array for several elevation angles. From these error curves, several conclusions may be drawn:

(1) As expected, the top-mounted array is only good for positive elevation angles. It is easy to see that the radiated fields will be blocked by the Boeing 727's fuselage and wings for negative elevation angles. For the same reasons, the bottom TCAS III system is only good for negative elevation angles.

(2) From Figure 3.5, the errors at an elevation angle of 45° are larger than those at 10°. This result seems unreasonable; however, it is important to keep in mind that the lookup table was obtained for an elevation angle of 10°. Thus, the larger errors predicted at 45° may be due to the fact that the patterns of the elements of the TCAS array (monopoles) are not constant as a function of the elevation angle.

(3) As mentioned in the previous chapter, the two-monopole model generates error curves that are only good in the region 90° to -90°. The large errors predicted in the back of the aircraft are probably exaggerated.

(4) The position of the bottom antenna might not be the ideal location. The fields radiated by the TCAS array in the aft direction are blocked by the AFT structure of the Boeing 727's fuselage (see Figure 3.2). Thus, the bottom-mounted antenna may need to be placed at the lowest position of the fuselage to obtain a better line of sight in the aft direction.

F. THE OPTIMUM POSITION OF THE TOP-MOUNTED TCAS III ON THE BOEING 737

The scattering error curves can also be used to determine the optimum position of the TCAS array on an aircraft. An example that is considered here is the determination of the optimum position of a top-mounted array on a Boeing 737 aircraft. According to [5], the diffraction from the vertical stabilizer produces serious scattering

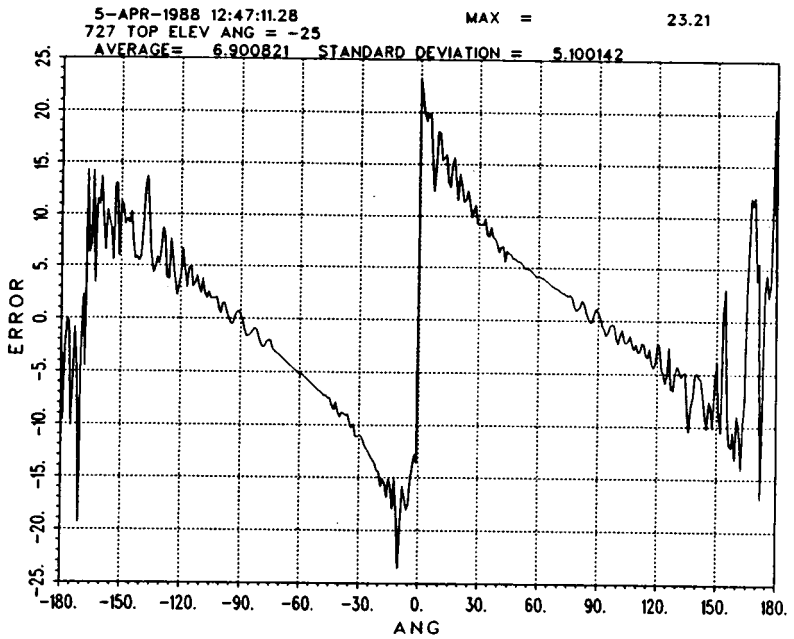

(a) Elevation angle = -25°

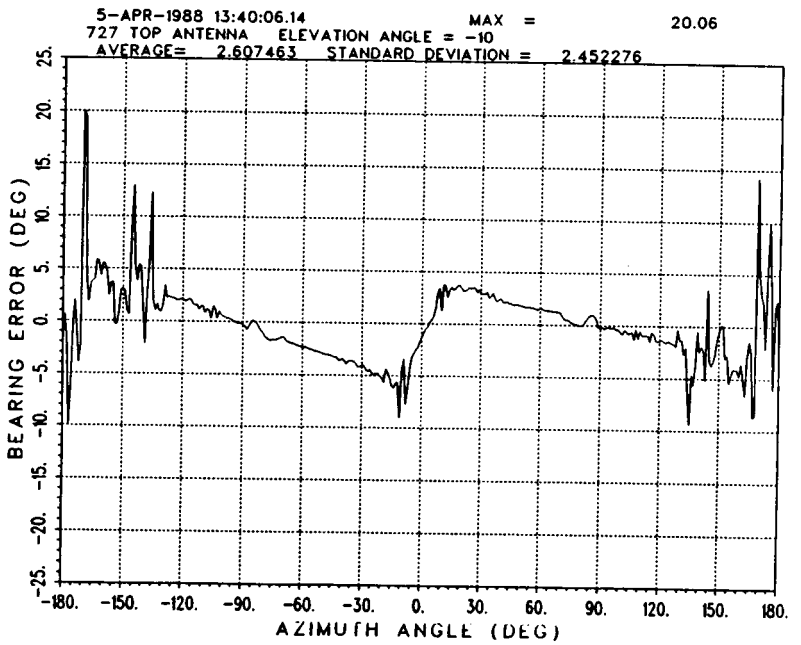

(b) Elevation angle = -10°

Figure 3.5. Error curves for the top-mounted TCAS array for several elevation angles.

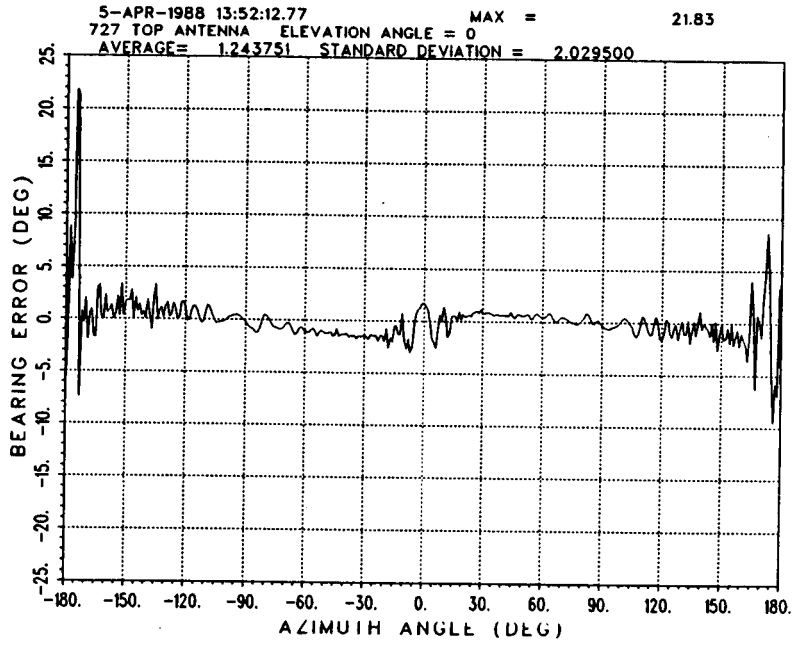

(c) Elevation angle = 0°

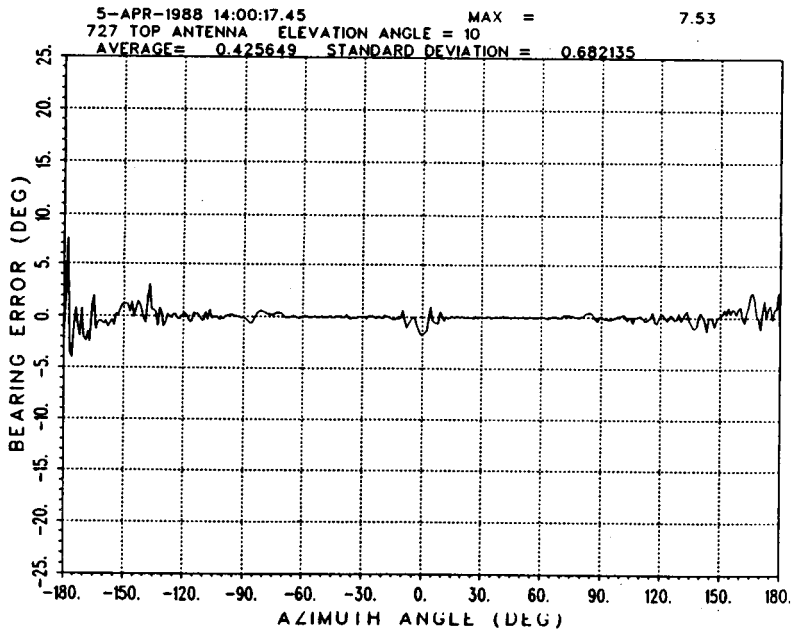

(d) Elevation angle = 10°

Figure 3.5. Continued.

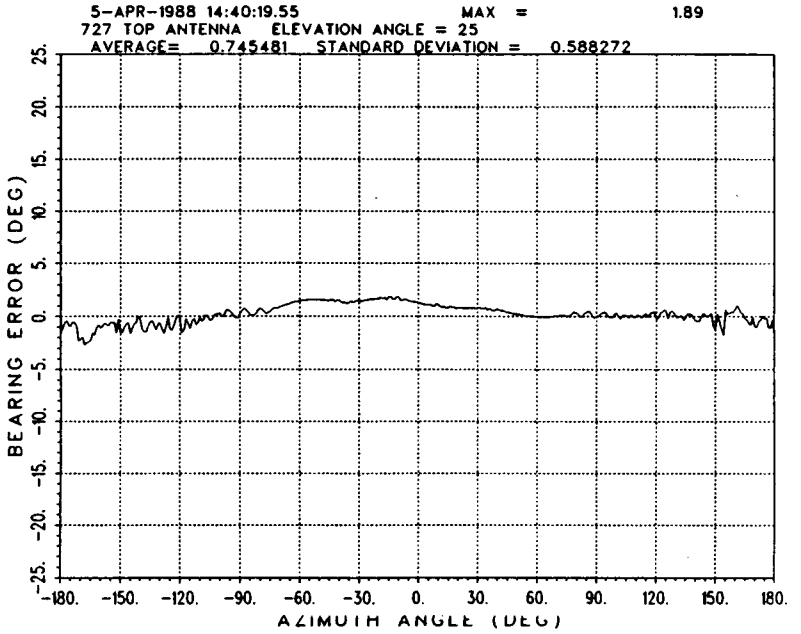

(e) Elevation angle = 25°

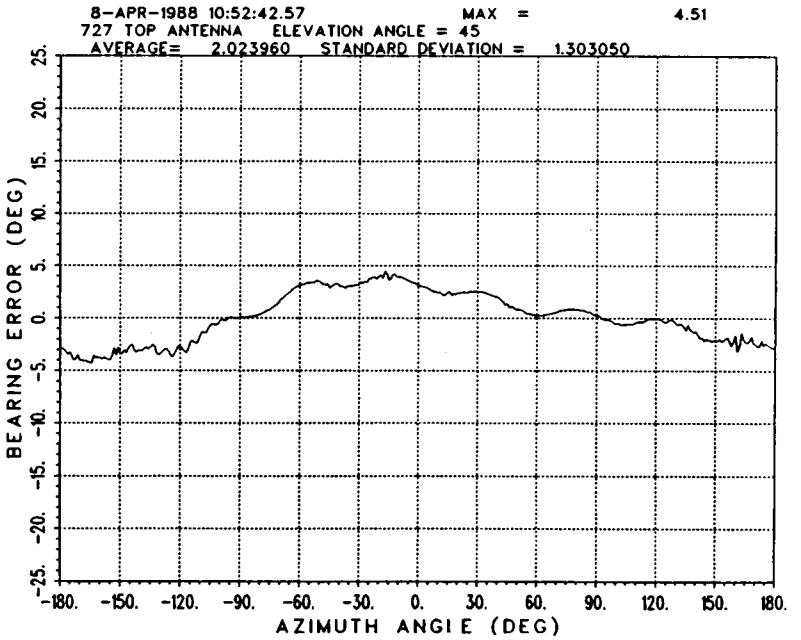

(f) Elevation angle = 45°

Figure 3.5. Continued.

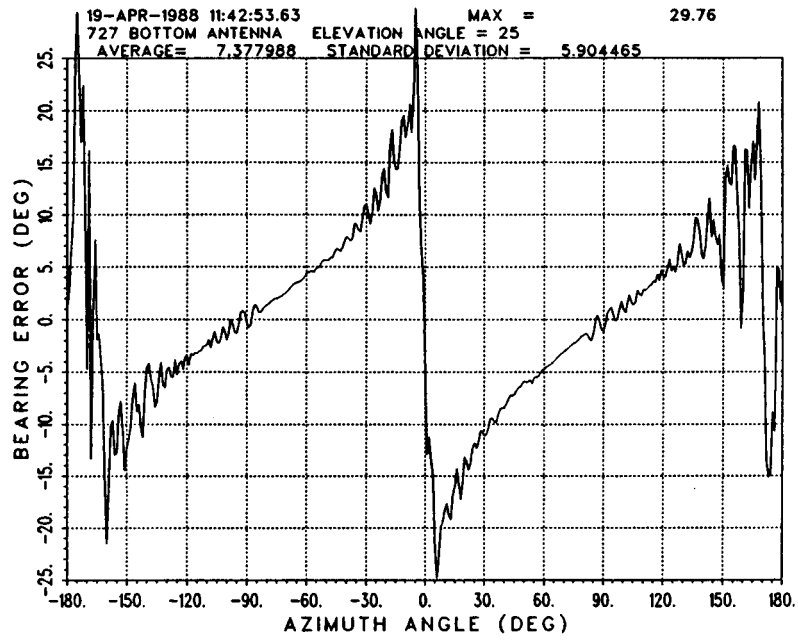

(a) Elevation angle = 25°

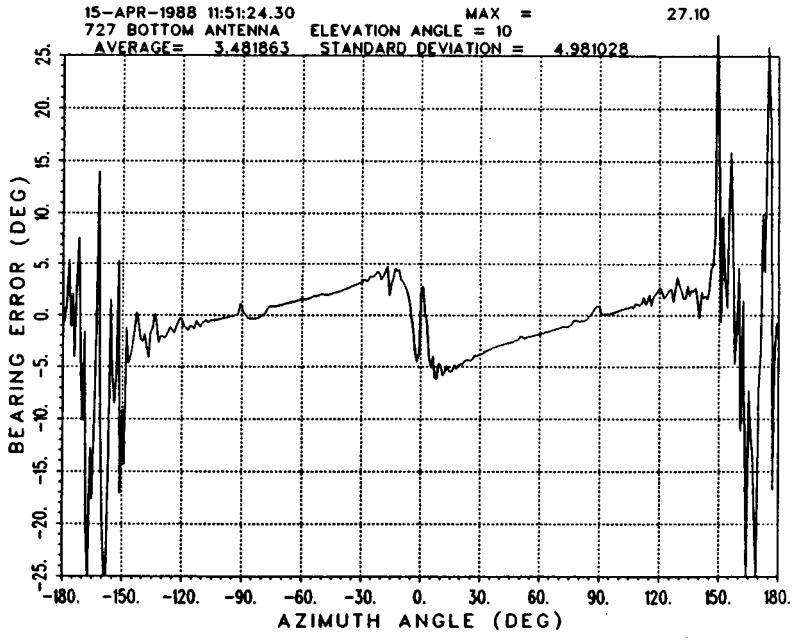

(b) Elevation angle = 10°

Figure 3.6. Error curves for bottom-mounted TCAS array for several elevation angles.

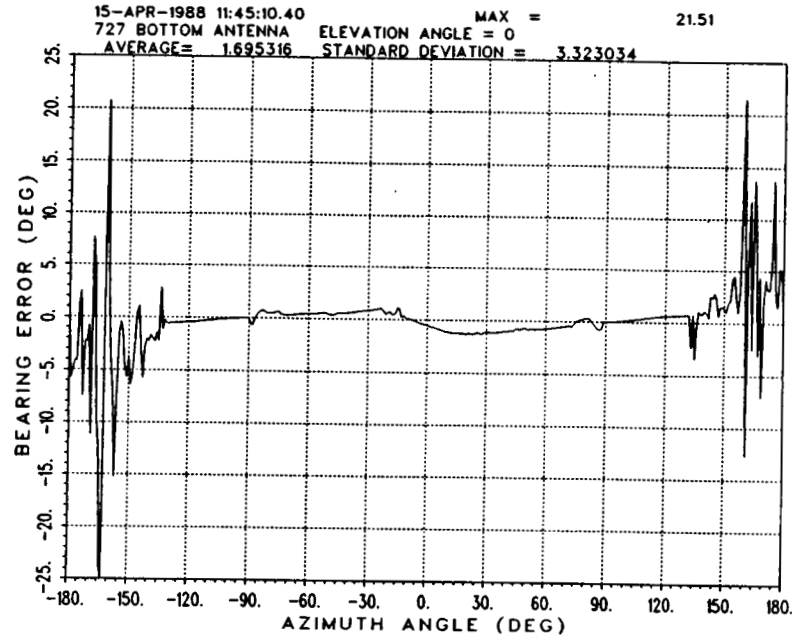

(c) Elevation angle = 0°

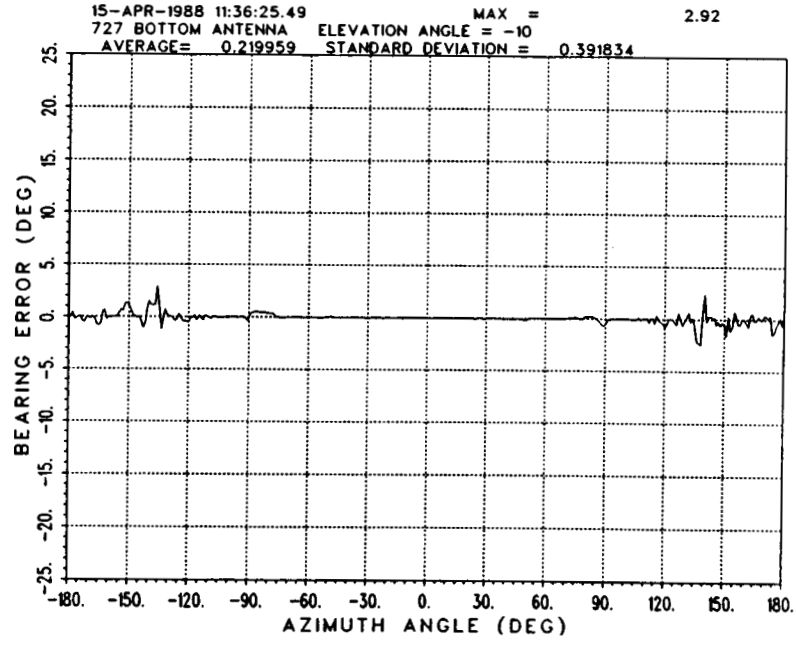

(d) Elevation angle = -10°

Figure 3.6. Continued.

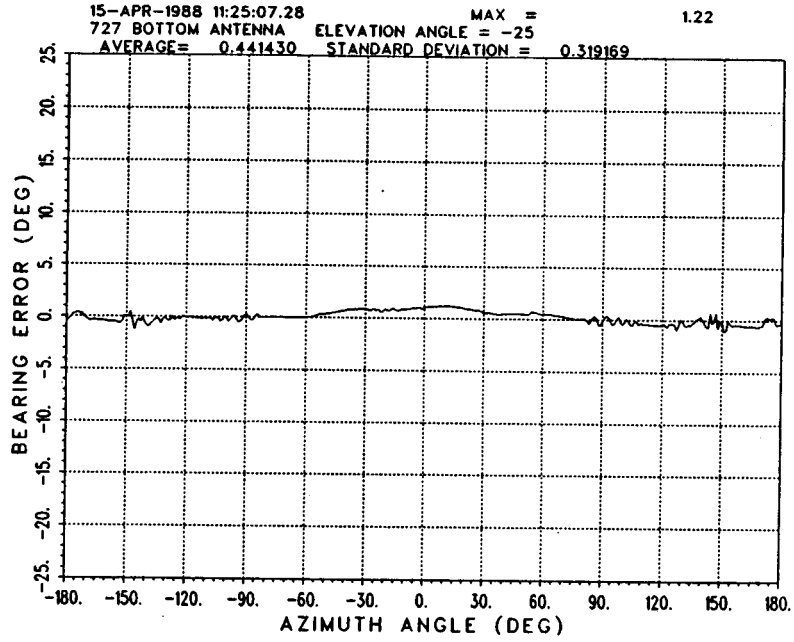

(e) Elevation angle = -25°

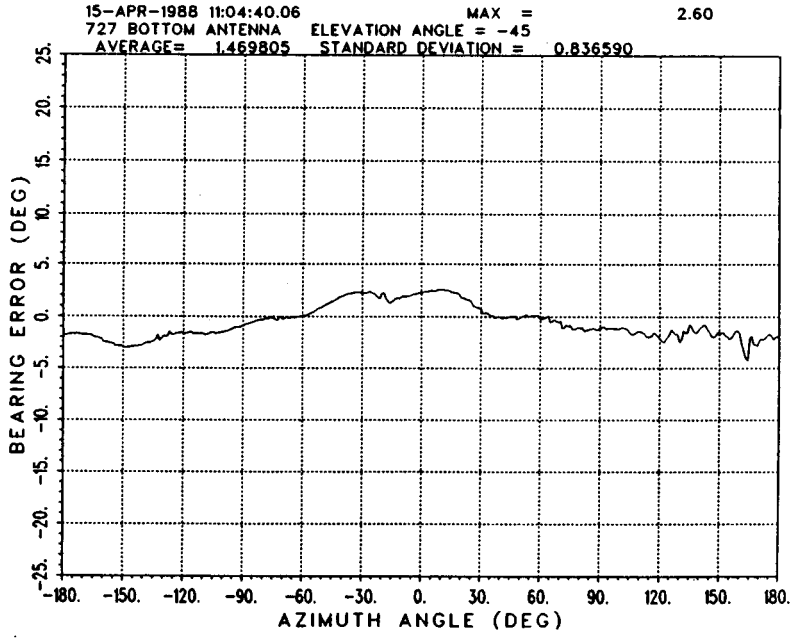

(f) Elevation angle = -45°

Figure 3.6. Continued.

errors which adversely affect the performance of the TCAS system. By studying the sum and difference beams and the monopulse curves of the five different antenna positions depicted in Figure 3.7, it is determined in [5] that the best position of the TCAS array is as close to the nose of the aircraft as possible. In this section, the scattering error curves will be used to find the optimum array location.

Figure 3.8 shows scattering error curves of the Boeing 737 corresponding to antenna position A to E with elevation angles of 0° and 10°. When the elevation angle is 10°, position E which is the closest to the nose gives the smallest average error and standard deviation. However, when the elevation angle is 0°, position D rather than E has the best result. It appears that for an elevation angle of 0°, the fuselage-blockage is more pronounced at position E than D when the beams are directed toward or near the tail of the aircraft. Therefore, the optimum position of the TCAS III array will change slightly with the elevation angle. Thus, one should choose the position which has the best average performance in all elevation angles. Therefore, the position which is close to the nose of the aircraft but still on the flat region of the fuselage would be a good choice. In this case, position D appears to be better than position E for the overall performance of the TCAS system.

An added benefit of mounting the array near the nose of the Boeing 737 aircraft is that the fuselage blockage is reduced for angles of elevation below the horizon in the forward direction. Note that the same analysis can be done to find the optimum position of the TCAS III array on the Boeing 727.

Antenna Location	Z coordinate (inches)	
A	310	
B	190	
C	70	; current TCAS position
D	- 50	for Boeing 737 model
E	-170	
NOSE	-308.56	

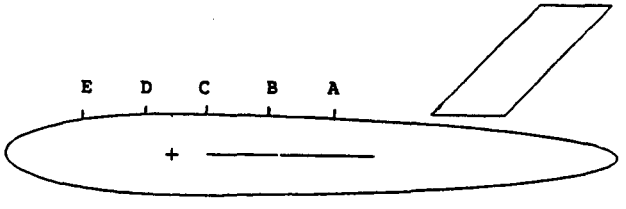

Figure 3.7. Five different array locations on the Boeing 737 computer model [5].

Table 3.4

Input Data of the Boeing 737 with Top-mounted TCAS III for Aircraft Code

```
UN:INCHES
3
FQ: 1.06 GHZ
1,1.06,1.
FG: BOEING 737
77.,74.,830.,308.56
T
0.,0.,70.
PG: RIGHT WING
4,T
1.,75.,67.952
1.,536.93,316.14
1.,536.93,379.86
1.,75.,240.26
PG: LEFT WING
4,T
1.,-75.,240.26
1.,-536.93,379.86
1.,-536.93,316.14
1.,-75.,67.952
PG: TAIL
4,T
77.,8.25,618.55
284.147,8.25,819.056
284.147,0.,683.696
77.,0.,483.19
PG: TAIL
4,T
77.,0.,483.19
284.147,0.,683.696
284.147,-8.25,819.056
77.,-8.25,618.55
BO:
T
PP: POLAR PLOT IN DB
F
1,1.5,3
PD: AZIMUTH PLANE
90.,0.,80.
0,360,1
T,1000000.
SG:ELEMENT 1
2.771,66.288
2
1.14,-45.
0.,0.,0.,2.78,3
1.,-45.
```

Table 3.4 - Continued

```
1.64,135.
0.,0.,0.,2.78,3
0.698,45.
EX:
SG:ELEMENT 2
3.921,70.
2
1.14,0.
0.,0.,0.,2.78,3
1.,-45.
1.64,180.
0.,0.,0.,2.78,3
0.698,45.
EX:
SG:ELEMENT 3
2.773,73.712
2
1.14,45.
0.,0.,0.,2.78,3
1.,-45.
1.64,225.
0.,0.,0.,2.78,3
0.698,45.
EX:
SG:ELEMENT 4
0.,75.25
2
1.14,90.
0.,0.,0.,2.78,3
1.,-45.
1.64,270.
0.,0.,0.,2.78,3
0.698,45.
EX:
SG:ELEMENT 5
-2.773,73.712
2
1.14,135.
0.,0.,0.,2.78,3
1.,-45.
1.64,-45.
0.,0.,0.,2.78,3
0.698,45.
EX:
SG:ELEMENT 6
-3.921,70.
2
1.14,180.
0.,0.,0.,2.78,3
1.,-45.
```

Table 3.4 - Continued

```
1.64,0.
0.,0.,0.,2.78,3
0.698,45.
EX:
SG:ELEMENT 7
-2.762,66.288
2
1.14,225.
0.,0.,0.,2.78,3
1.,-45.
1.64,45.
0.,0.,0.,2.78,3
0.698,45.
EX:
SG:ELEMENT 8
0.,64.75
2
1.14,270.
0.,0.,0.,2.78,3
1.,-45.
1.64,90.
0.,0.,0.,2.78,3
0.698,45.
EX:
```

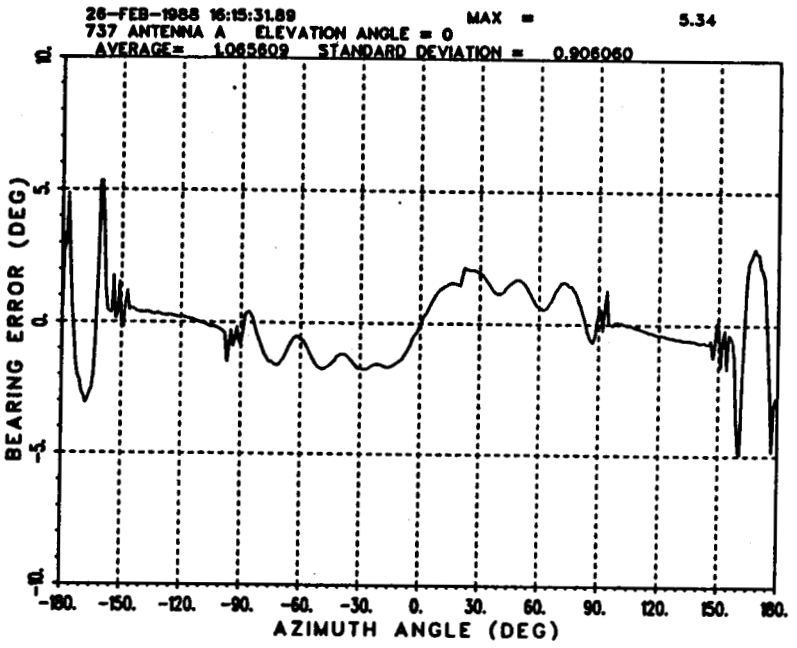

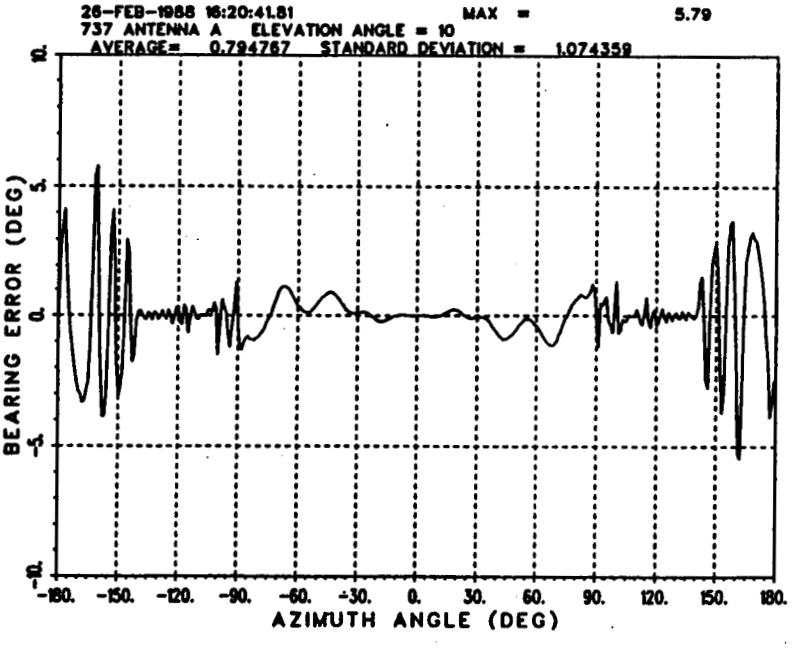

(a) Antenna position A with elevation angles of 0° and 10°

Figure 3.8. Scattering error curves of the Boeing 737.

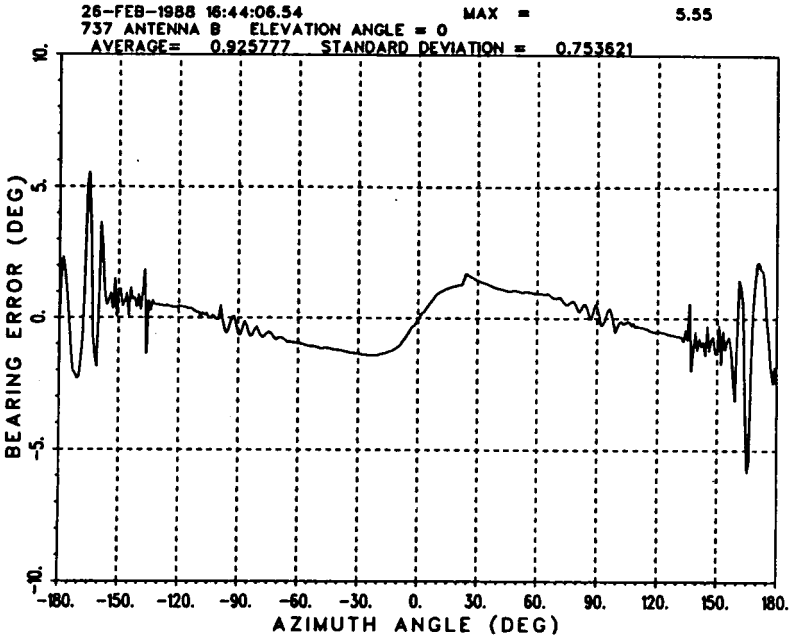

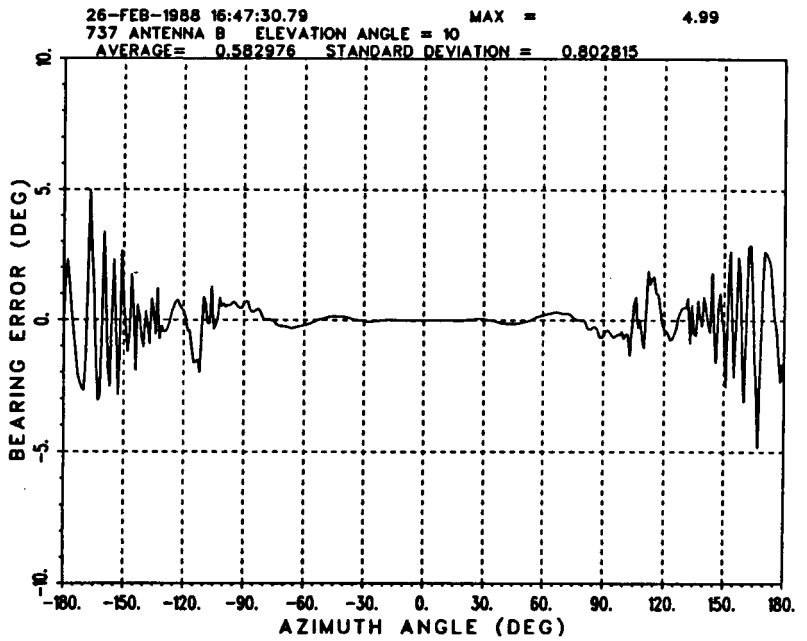

(b) Antenna position B with elevation angles of 0° and 10°

Figure 3.8. Continued.

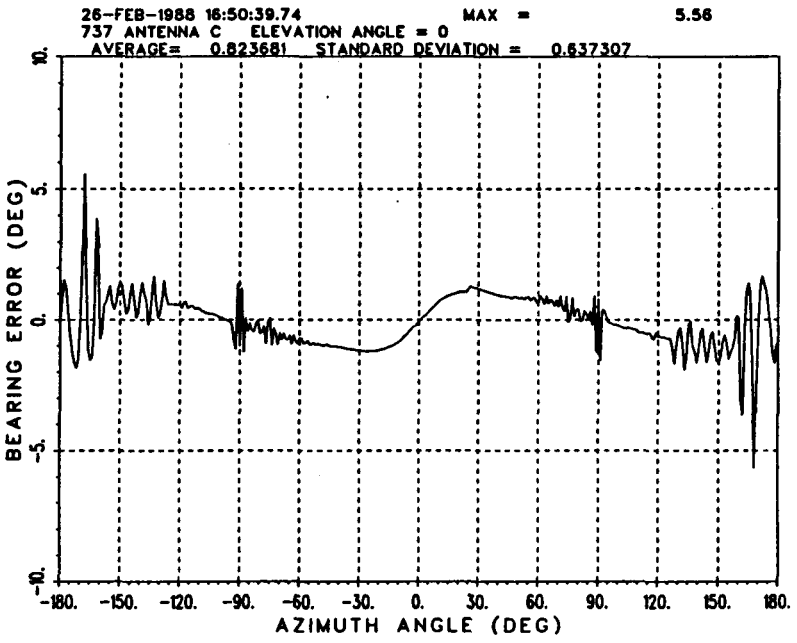

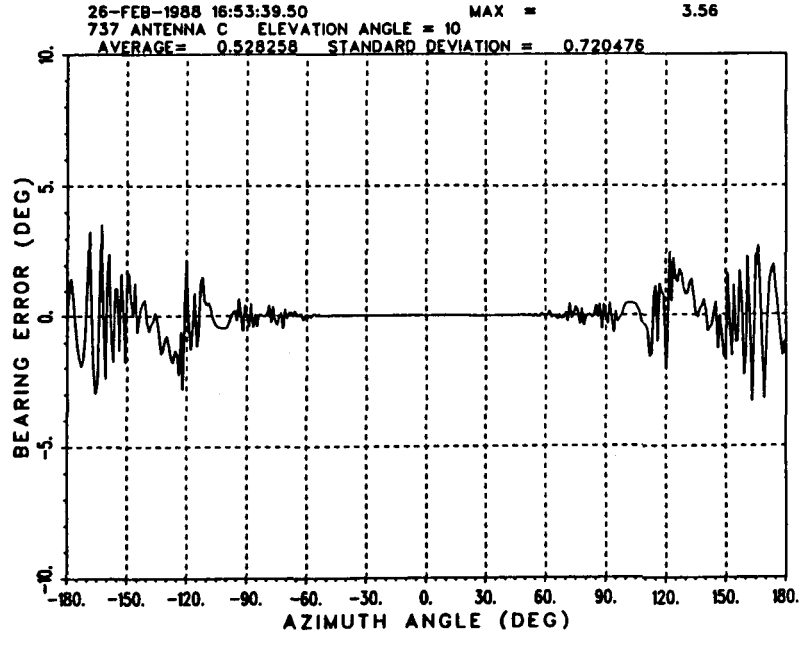

(c) Antenna position C with elevation angles of 0° and 10°

Figure 3.8. Continued.

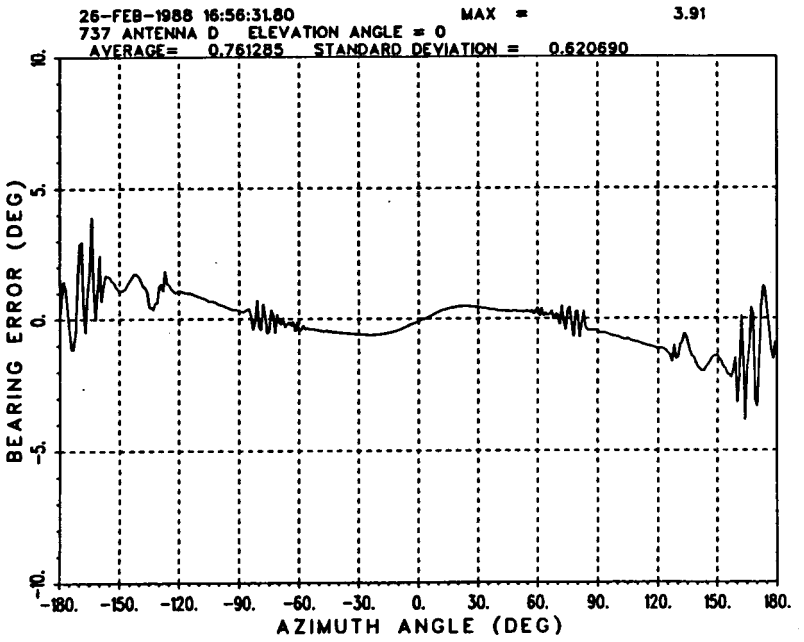

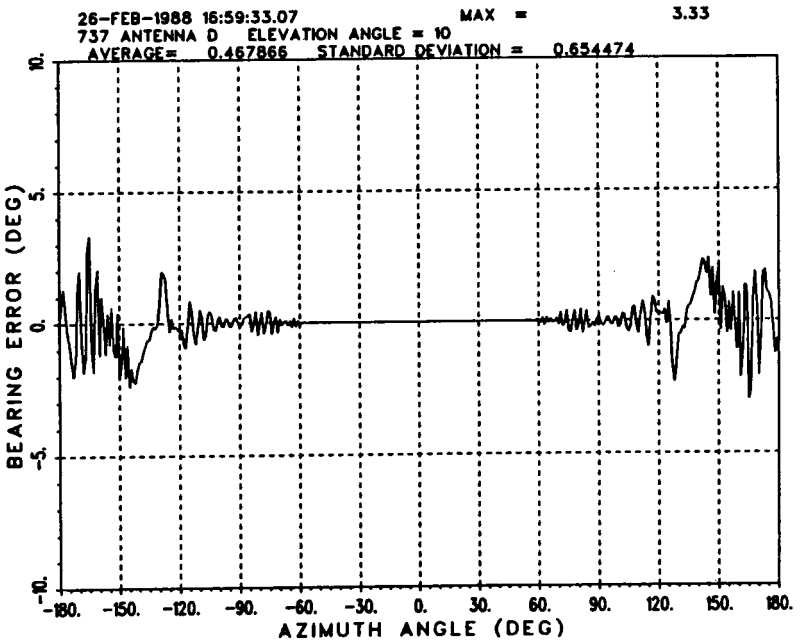

(d) Antenna position D with elevation angles of 0° and 10°

Figure 3.8. Continued.

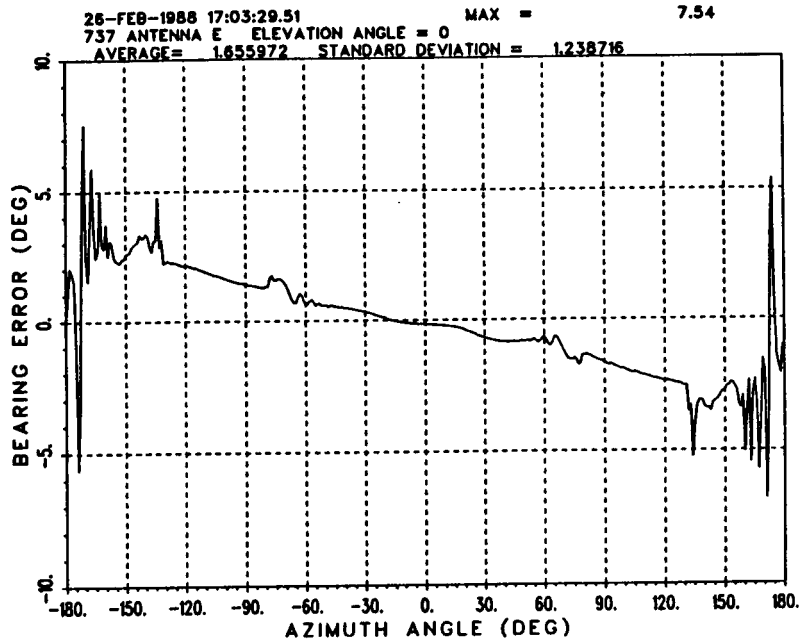

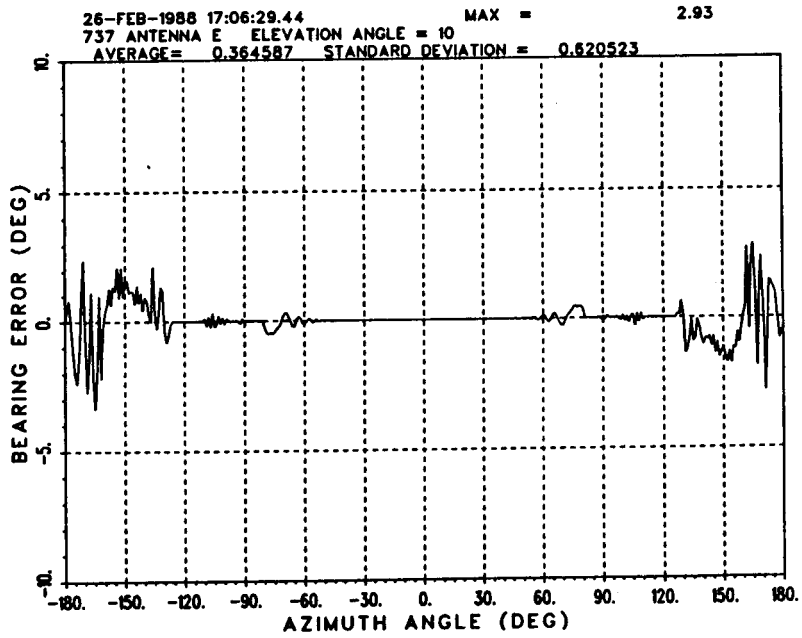

(e) Antenna position E with elevation angles of 0° and 10°

Figure 3.8. Continued.

CHAPTER IV

SIMULATION OF AN ENCOUNTER BETWEEN A TCAS-EQUIPPED BOEING 727 AND ANOTHER AIRPLANE

A. INTRODUCTION

Another application of the scattering error curves generated in the previous chapter is discussed here. This chapter describes the computer simulation of an encounter between a TCAS III-equipped Boeing 727 and an airplane (equipped with a transponder) in its vicinity. This airplane is sometimes referred to as the intruder. The details of this program are discussed in [4] for an encounter of a Boeing 737 instead of a Boeing 727. The algorithm discussed here is an improved version of the one discussed in [4]. The main improvement is the careful calculation of an escape path followed by the TCAS III-equipped airplane. The simulation is done for top- and bottom-mounted TCAS III arrays. Note that in this simulation, the flight paths of the two airplanes in the earth-fixed coordinate have constant altitude, including the escape path.

B. COORDINATE SYSTEMS

The calculation of the position, velocity, height, etc., of the two airplanes being studied requires the use of the three coordinate systems shown in Figure 4.1. The first coordinate system is referred to as the earth-fixed coordinate system. This system is fixed on the earth and

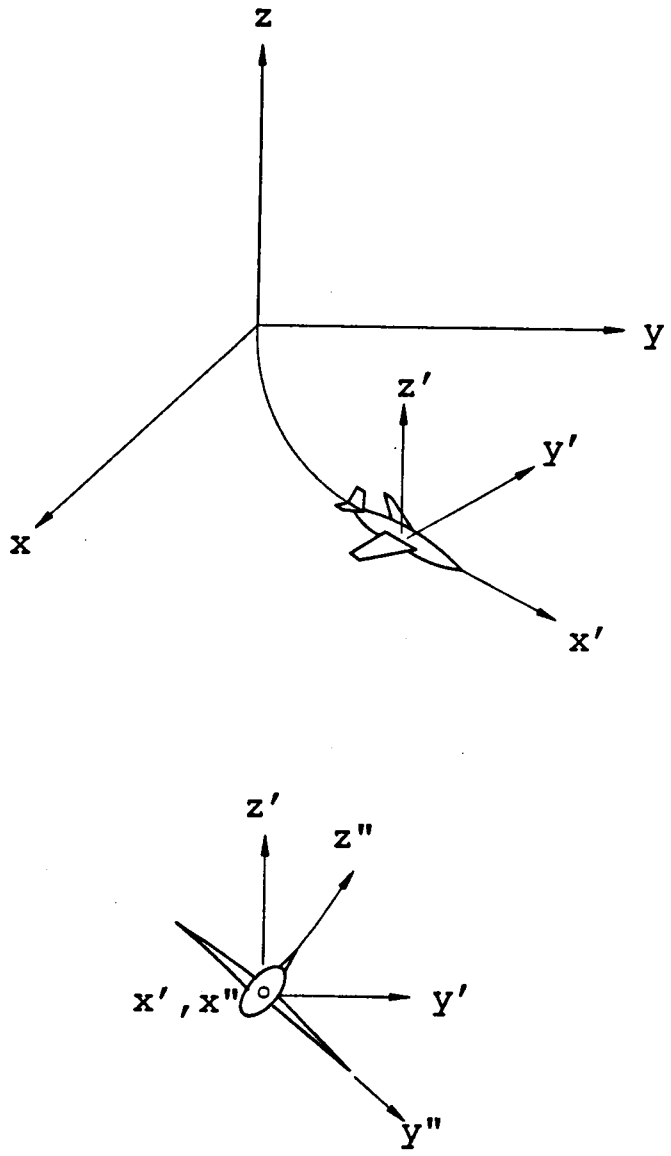

x,y,z : earth-fixed coordinate system
x',y',z' : airplane-fixed coordinate system
x",y",z" : TCAS-fixed coordinate system

Figure 4.1. Three coordinate systems.

is independent of the aircraft. The second coordinate system is referred to as the airplane-fixed coordinate system. The origin of this coordinate system is fixed on the airplane at the position where the TCAS array is located. The x axis is fixed in the direction of the flight path of the aircraft and the z-axis is kept the same as the earth-fixed coordinate system; then the y axis can be determined since x and z are known. The last coordinate system is referred to as the TCAS-fixed coordinate system. The difference between the airplane- and TCAS-fixed coordinates is that the z axis of the latter is fixed on the TCAS III array. In other words, when the aircraft rolls, the z axis of the TCAS-fixed coordinate system will also roll. The transformations between these coordinate systems will be discussed in more detail in the following sections and in Appendices C and E.

C. SIMULATION ALGORITHM

Figure 4.2 is a flow chart showing the steps of the computer simulation of the encounter between a TCAS-equipped airplane and a intruder-equipped with a transponder. Before starting the simulation, the scattering error curves should be generated in advance. For the Boeing 727, there are 142 error curves, 71 for the top-mounted TCAS III array for elevation angles -25° to 45° in steps of one degree and 71 for the bottom-mounted TCAS III array for elevation angles -45° to 25°, also in steps of one degree. For both cases, the azimuth angle is from 0 to 360 in steps of one degree. The accuracy of the simulation can be improved by calculating a larger number of error curves.

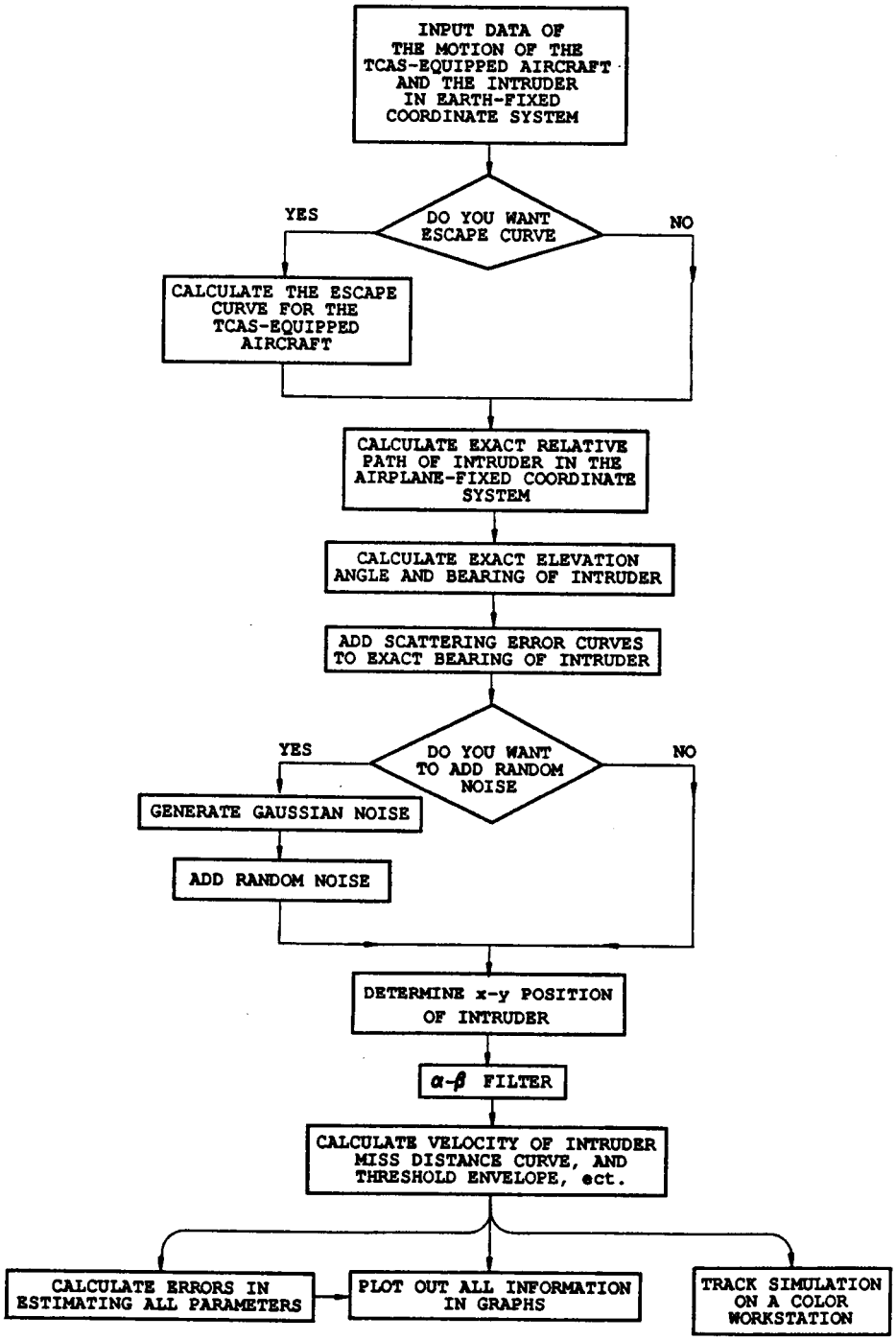

Figure 4.2. Flow chart of tracking simulation.

As shown in Figure 4.2, the parameters which describe the exact paths of the two aircraft in the earth-fixed coordinates should be input. After a series of coordinate transformations, the relative path of the intruder can then be calculated. Furthermore, if it is desired, an escape path can also be input in the earth-fixed coordinate system. As explained later, the escape can be specified by two parameters. An algorithm will then calculate the path of the intruder in the airplane-fixed coordinate system, taking into account the escape path followed by the TCAS-equipped airplane.

Since this simulation concentrates on studying the errors of the TCAS III system in calculating the bearing of the intruder due to structural scattering, the scattering error curves are added to the exact bearing of the intruder in the TCAS-fixed coordinate system. As discussed in [4], the sources of error are divided into two groups to simplify this simulation. One source of error is structural scattering which is taken into account with the error curves. The second source of error is a combination of hardware-related errors, thermal noise and errors introduced by the inertial navigation system [11]. In this algorithm, the second source of error is simulated by a Gaussian noise generator with zero mean and a standard deviation given in Equation (4.7). After adding these two sources of error; the position of the intruder in the TCAS-fixed coordinate system, which is referred to as the detected position, can be determined. This position is then input to the alpha-beta filter [4] to calculate the horizontal miss distance, time to closest point of approach (time to CPA), speed, etc. [4]. The α-β parameters used for the alpha-beta filter are the same as those used

in [4]; namely, α=0.25 and β=0.066 with a sampling time interval of 1 second. Note that the whole simulation can be displayed on a color workstation using the Graphical Kernel System (GKS). The color display shows the exact and detected location of the intruder and various parameters which is updated every second.

D. RELATIVE PATH CALCULATION

The next step according to Figure 4.2 is to calculate the relative path of the intruder in the airplane-fixed coordinate system. For simplicity, it is assumed that the aircraft with the TCAS III system is initially flying in the x direction of the earth-fixed coordinate. Since the input parameters are given in the earth-fixed coordinate system, the calculation of the relative path and velocity of the intruder in the airplane-fixed coordinate system involves the transformation between the earth-fixed and airplane-fixed coordinate systems. Appendix C describes a general algorithm to accomplish this transformation. It is assumed that the flight paths of the two airplanes are constant altitude paths in the earth-fixed coordinate system.

As long as the TCAS-equipped airplane flies in a straight-line path and does not rotate around the x-axis, the airplane-fixed and TCAS-fixed coordinate systems are the same. However, if the TCAS-equipped airplane starts to follow an escape path to avoid a mid-air collision, these two coordinate systems are no longer the same due to the rotation of the aircraft around the x-axis as depicted in Figure 4.1. Unlike the coordinate transformation discussed in Appendix C, the transformation

between the airplane- and TCAS-fixed coordinate systems is very simple. It is shown in Appendix C.

E. ESCAPE CURVE CALCULATION

When an aircraft, which is initially flying in a straight line, starts to turn to the right or left, it will roll its fuselage and introduce a centrifugal force [8]. During a steady coordinate turn maintaining constant altitude, the lift tends to produce a horizontal component of force equal to the centrifugal force of the turn and a vertical component of force equal to the weight of the airplane, such that there is no acceleration in the vertical directions as depicted in Figure 4.3.

From Figure 4.3, one finds that

$$w = L \cdot \cos\phi$$

$$m \cdot \frac{V^2}{r} = L \cdot \sin\phi = w \tan\phi = mg \tan\phi$$

and

$$r = \frac{V^2}{g \cdot \tan\phi} \qquad (4.1)$$

where r is the turn radius, L is the lift, V is the speed, ϕ is the bank angle, g is the gravitational constant, and M and W are the mass and weight of the airplane, respectively. Also, the normal acceleration is given by

$$a_n = \frac{V^2}{r} = g \cdot \tan\phi \ . \qquad (4.2)$$

C-2

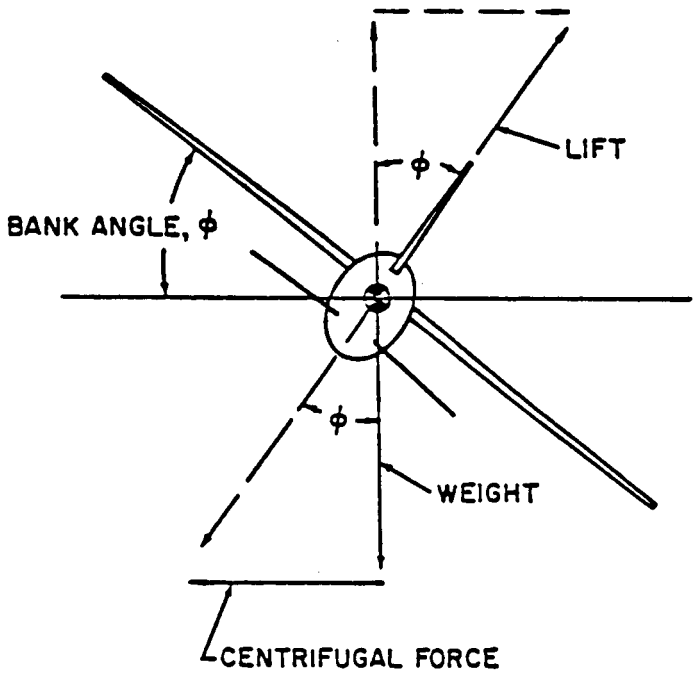

Figure 4.3. Turn flight of an aircraft [8].

If a function which describes the changes of bank angle with time is given, the normal acceleration can be obtained from (4.2). Appendix D discusses a numerical solution which calculates the escape path when a_n is given. A closed form solution is very difficult to obtain and in general does not exist.

Figure 4.4 shows a typical case of the change of the bank angle with respect to time. It is almost linear except at the top area and bottom of the curve. In this simulation, it is assumed that both aircraft always keep a constant speed, and when the TCAS-equipped airplane turns, the bank angle will change linearly with respect to time

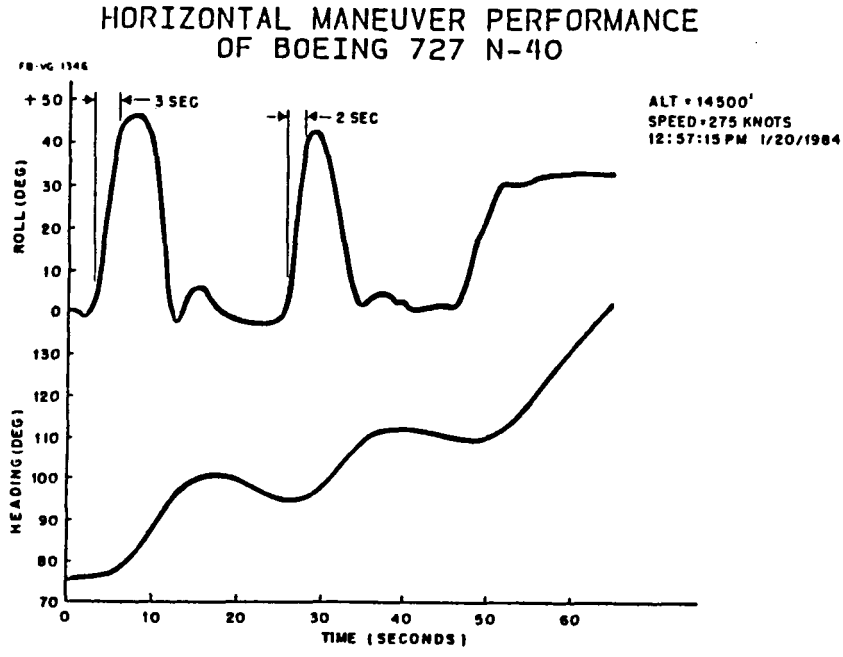

Figure 4.4. Relationship between bank angle and bearing in a typical turning flight [12].

until it reaches a maximum value. The algorithm in Appendix D will work for any arbitrary function that describes the bank angle as a function of time. Figure 4.5 shows four typical escape curves. The velocity is 287 knots and the numerical calculation was done in millisecond steps. The four curves are 6 sec to 45°, 10 sec to 45°, 6 sec to 30°, and 10 sec to 30°. For example, 6 sec to 45° means that it takes 6 seconds to roll to a bank angle of 45° (linearly) and keeps at 45°.

F. ELEVATION ANGLE AND BEARING CALCULATION

Since the escape curve was discussed in Section E, the next step is to calculate the exact elevation angle and bearing of the intruder relative to the TCAS-fixed coordinate system. Appendix E shows a detailed procedure to calculate the elevation and azimuth angles in the TCAS-fixed coordinate system.

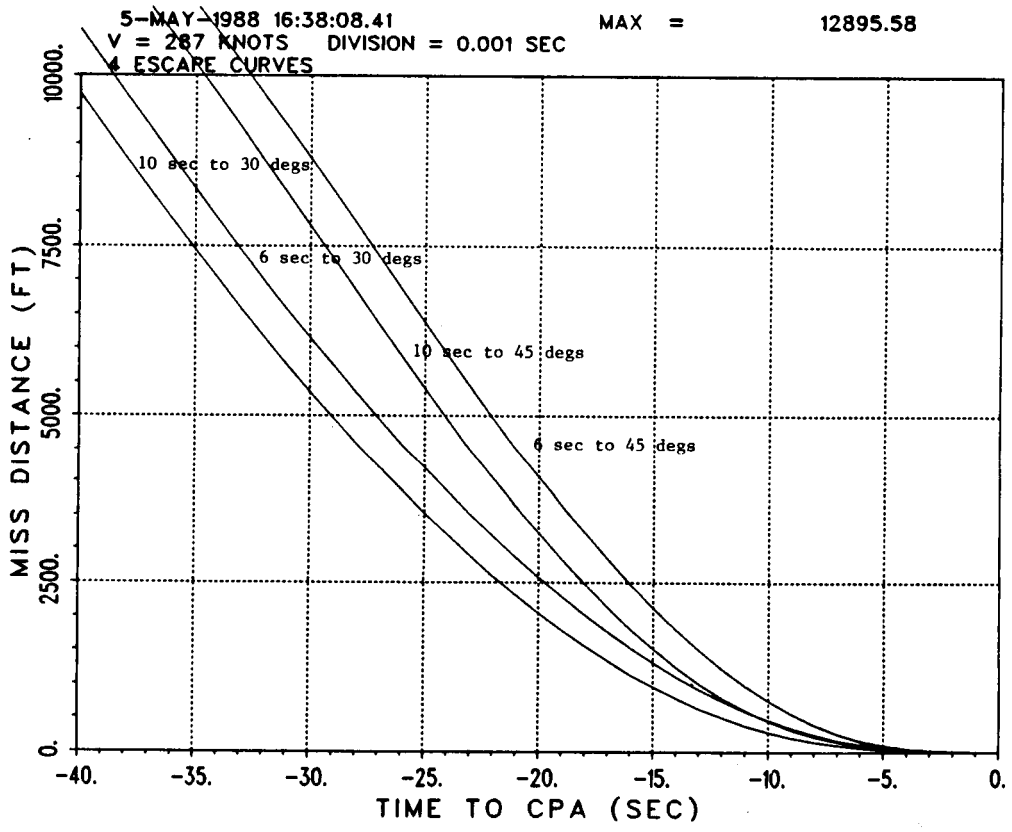

Figure 4.5. Four typical escape curves.

Figure 4.6 shows the definitions of the elevation and azimuth angles. Actually, θ=90° - elevation angle is more useful in this simulation than the elevation angle. From Appendix E, where the calculations of the theta and azimuth angles are discussed, θ is given by

$$\theta = \cos^{-1}\left(\frac{y\cdot\sin\theta_B + z\cdot\cos\theta_B}{\sqrt{x^2 + y^2 + z^2}}\right) \tag{4.3}$$

where (x,y,z) is the target position relative to the airplane-fixed coordinate system and θ_B is the bank angle. When θ_B=0, one finds that

$$\theta = \cos^{-1}\frac{z}{\sqrt{x^2 + y^2 + z^2}} \tag{4.4}$$

as defined originally. Furthermore, the azimuth angle, ϕ, can be expressed as follows:

$$\phi = \tan^{-1}\left(\frac{y\cdot\cos\theta_B - z\cdot\sin\theta_B}{x}\right) \quad . \tag{4.5}$$

When θ_B=0, (4.5) reduces to

$$\phi = \tan^{-1}\frac{y}{x} \quad . \tag{4.6}$$

All the calculations of the TCAS system are done in the TCAS-fixed coordinate system; however, all the results of the simulation are displayed in the airplane-fixed coordinate system. Thus, Appendix E also discusses the transformation between the TCAS-fixed and airplane-fixed coordinates.

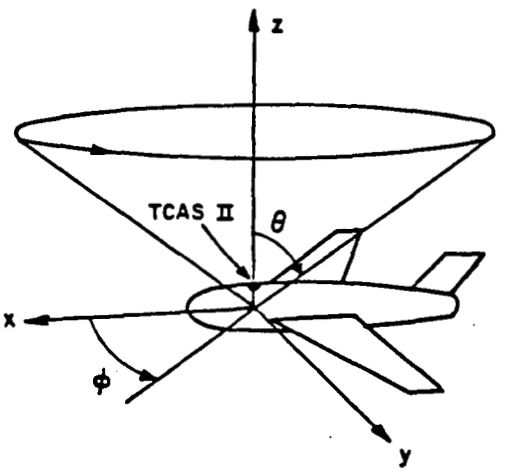

Elevation angle = 90-θ
Azimuth angle = ϕ

Figure 4.6. Definition of elevation and azimuth angles [4].

G. DEGRADATION OF THE PERFORMANCE OF THE TCAS-III SYSTEM

As mentioned in the introduction of this chapter, the performance of the TCAS system is negatively affected by various sources of error which are carefully discussed in [4], [11]. In this simulation the sources of error are divided into two parts. The first is the error due to structural scattering which is described by the scattering error curves and the second source of error is given by a Gaussian noise generator of zero mean and a standard deviation which is given in this section.

Recall that in the encounter it is assumed that both airplanes are flying in straight lines, at a constant altitude and speed with respect to the earth-fixed coordinate system. Once the exact position of the

intruder is determined in the airplane-fixed coordinate system (range, elevation angle, and bearing), the error curves are added to the exact bearing to simulate the errors due to structural scattering. If desired, one can also add the output of the noise generator to the bearing information to simulate the random errors induced by thermal noise, hardware-related errors, etc. Note that the bearing obtained after the two sources of error are added is referred to as the detected bearing. This is discussed in more detail in [4].

The standard deviation of the noise generator is given by [4]

$$\sigma_B = \left\{1.13^2 \left(.97^2 + \frac{(.35 + .64)^2}{S/N}\right) + .14^2\right\}^{1/2} \tag{4.7}$$

where

$$S/N = 10^{(SN_o/10 - 2\cdot\text{Log}\,(R/R_o))} \tag{4.8}$$

If the transponder power is 27 dBW, SN_o is 26.4 dB at R_o=20 NMI (nautical miles) [11]. Equation (4.7) then becomes

$$\sigma_B = (1.22 + R^2 \times 3.67 \times 10^{-3})^{1/2} . \tag{4.9}$$

where R is in nautical miles (NMI).

It is easy to see that when R is small, σ_B is nearly a constant; however, when R is large, σ_B is a function of distance. Appendix F discusses the computer program used to generate random numbers with a normal distribution.

Once the detected bearing of the intruder in the TCAS-fixed coordinate system is obtained, and because the range and height of the intruder in the airplane-coordinate is known from the communication of the two aircraft, the detected position of the intruder in the airplane-fixed coordinate system can be calculated as shown in Appendix E.

H. α-β FILTER

The function of the alpha-beta filter is to accept samples of the intruder's position and to filter this data so that the resulting output samples are the smoothed estimates of the present position and velocity of the intruder.

According to [9], the values of α=0.25 and β=0.066, were selected for the alpha-beta filter in the TCAS system. When the target's speed is between 100 ft./sec and 1000 ft./sec, and its acceleration is below 16 ft./sec^2, and the update rate of the detected data is 1 second, they are optimum choices.

There are two separate α-β filters for the x and y coordinates. Each filter is defined by the following set of difference equations [4]:

$$\bar{X}_x = X_{pk} + \alpha(X_k - X_{pk}) \tag{4.10}$$

$$\bar{\dot{X}}_k = \bar{\dot{X}}_{k-1} + \frac{\beta}{T}(X_k - X_{pk}) \tag{4.11}$$

and

$$X_{p(k+1)} = \bar{X}_k + T \cdot \bar{\dot{X}}_k \tag{4.12}$$

where

T : sampling time period

X_k: detected position of the K^{th} measurement

$\bar{X}_k$: smooth estimation of the K^{th} position

$\bar{\dot{X}}_k$: smooth estimation of the K^{th} velocity, and

X_{pk}: predicted value.

Because the desired outputs are $\bar{X}_k$ and $\bar{\dot{X}}_k$, Equations (4.10)-(4.12) can be simplified as follows:

$$\bar{X}_k = (1-\alpha)(\bar{X}_{k-1} + T\cdot\bar{\dot{X}}_{k-1}) + \alpha X_k \qquad (4.13)$$

and

$$\bar{\dot{X}}_k = (1-\beta)\,\bar{\dot{X}}_{k-1} + \frac{\beta}{T}\,(X_k - \bar{X}_{k-1}) \qquad (4.14)$$

Since these are recursive equations, $\bar{X}_o = X_o$ and $\bar{\dot{X}}_o = \dot{X}_o$ are chosen as the initial values, where X_o and $\dot{X}_o$ are the x- or y-components of the initial position and velocity, respectively, of the intruder in the airplane-fixed coordinate system.

I. CALCULATION OF PARAMETERS

Some parameters can be deduced from the basic information of the relative path of the intruder. From these parameters, one can better understand the performance of the TCAS system. Also, two important curves, the horizontal miss distance curve and the threshold envelope,

which are used to predict a collision, can be obtained from these parameters.

In order to predict a collision there are four basic parameters that need to be calculated; namely, time to CPA (closest point of horizontal approach), miss distance (in the x-y plane), bearing rate in the x-y plane and threshold. Additional parameters are explained in more detail in Reference [10]. The horizontal miss distance at CPA between an intruder and the TCAS-equipped aircraft is the predicted closest point of approach as shown in Figure 4.7. When this miss distance is small, the two airplanes will be dangerously close if they are flying at about the same altitude. This parameter is valid when the relative path of the intruder is a straight line. From [4,10], one finds that

$$m_k = \frac{\bar{X}_k \cdot \bar{\dot{Y}}_k - \bar{Y}_k \cdot \bar{\dot{X}}_k}{V_k} \qquad \text{and} \qquad V_k = \sqrt{\bar{\dot{X}}_k^2 + \bar{\dot{Y}}_k^2} \tag{4.15}$$

where

m_k: miss distance at the k^{th} time index

$\bar{\dot{X}}_k$, $\bar{\dot{Y}}_k$: smoothed estimation of the relative velocities in the x,y directions at the k^{th} time index, and

$\bar{X}_k$, $\bar{Y}_k$: smoothed estimation of the relative positions at the k^{th} time index.

Another important parameter is the bearing rate, $\dot{B}$, the change of the bearing per second. The sign of $\dot{B}$ indicates the direction of the change of the target's bearing, where positive $\dot{B}$ indicates counter clockwise rotation and negative $\dot{B}$ indicates clockwise rotation. The bearing rate at the k^{th} time index is given by [4]

$$\dot{B}_k = \frac{\bar{X}_k \dot{\bar{Y}}_k - \bar{Y}_k \dot{\bar{X}}_k}{\bar{X}_k^2 + \bar{Y}_k^2} \quad . \tag{4.16}$$

Therefore, m_k can be rewritten as

$$m_k = \frac{\bar{X}_k^2 + \bar{Y}_k^2}{V_k} \cdot \dot{B}_k \quad . \tag{4.17}$$

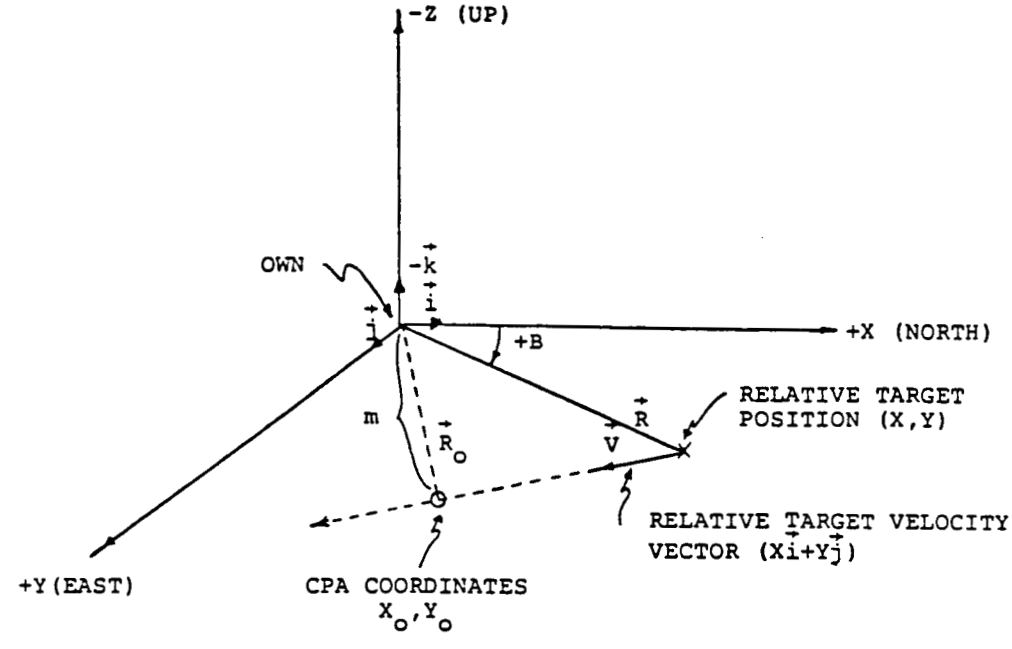

Figure 4.7. Horizontal projection of target relative to own [10].

Time to CPA (τ_k) is used to estimate how long it will take for the target to reach the closest point of approach. It can be written as

$$\tau_k = \frac{\sqrt{\bar{X}_k^2 + \bar{Y}_k^2}}{\bar{V}_k} \quad . \tag{4.18}$$

From (4.15), the miss distance error can be approximately expressed by

$$\delta m_k = \sqrt{\bar{\dot{X}}_k^2 + \bar{\dot{Y}}_k^2}\ \tau_k^2\ \delta\dot{B}_k \tag{4.19}$$

where $\delta\dot{B}_k$ is the error in estimating the bearing rate. Equation (4.19) is valid as long as the estimates $\bar{\dot{X}}_k$ and $\bar{\dot{Y}}_k$ are accurate.

Equation (4.19) is a very important equation because it indicates that the error in estimating the horizontal miss distance is directly proportional to the error in estimating the bearing rate. According to [11], if the target's horizontal miss distance is at least three times the one-sigma uncertainty in miss distance, then a mid-air collision is virtually assured. Thus, the horizontal threshold T_{hk} is given by

$$T_{hk} = 3\ \sigma_{mk} + 1000 \quad \text{(ft)} \tag{4.20}$$

where σ_{mk} is the standard deviation of the miss distance error at the k^{th} index time, and 1000 is an added safety factor. It follows from (4.19) that

$$T_{hk} = 3\ \sqrt{\bar{\dot{X}}_k^2 + \bar{\dot{Y}}_k^2}\ \tau_k^2\ \sigma_{\dot{B}k} + 1000 \quad \text{(ft)} \tag{4.21}$$

where $\sigma_{\dot{B}k}$ is the standard deviation of the bearing rate error at the k^{th} index time. The standard deviation $\sigma_{\dot{B}k}$ is given by [4,10]

$$\sigma_{\dot{B}k} = (5.88 \times 10^{-3} + 3.67 \times 10^{-3} R_k^2)^{1/2} \qquad (4.22)$$

where R_k is the range at the k^{th} index time. Another threshold that needs to be considered is the vertical threshold. In this report, it is assumed that if the relative altitude of the intruder in the airplane-fixed coordinate system is less than 200 ft., then there is a danger of collision.

J. EXAMPLE

Figure 4.8 depicts a flow chart of the data processing done by a TCAS III system of a typical encounter with an intruder. A ground radar, which is much more accurate than the TCAS system, also tracks the encounter to evaluate the performance of the TCAS array. Figure 4.9(a) shows the path of the intruder in the airplane-fixed coordinate system. Figures 4.9(b), 4.9(c) and 4.9(d) show the errors in calculating the bearing, bearing rate and horizontal miss-distance, respectively, as a function of time. The encounter angle is 90° in the earth-fixed coordinate system and the speeds (also in the earth-fixed coordinate) of the TCAS-equipped and intruder airplanes are 288.44 knots (in the x-direction) and 180 knots (in the y-direction), respectively. The starting position of the intruder is X_o=3.205 NMI (19,486 ft) and Y_o=-2 NMI (-12160 ft); while, its relative altitude is +300 ft. and its

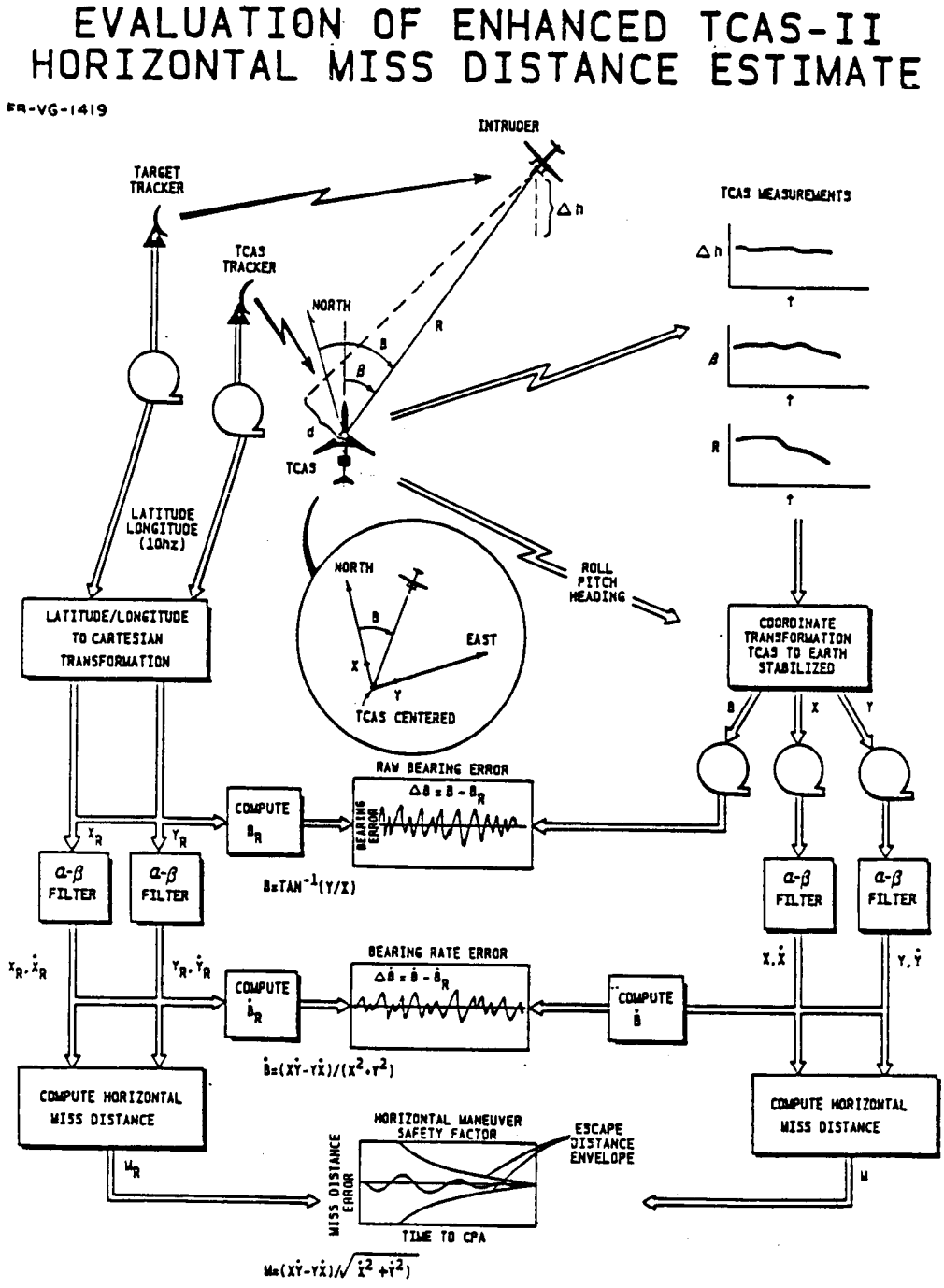

Figure 4.8. Flow chart of encounter tracked by a ground radar and the TCAS III system [14].

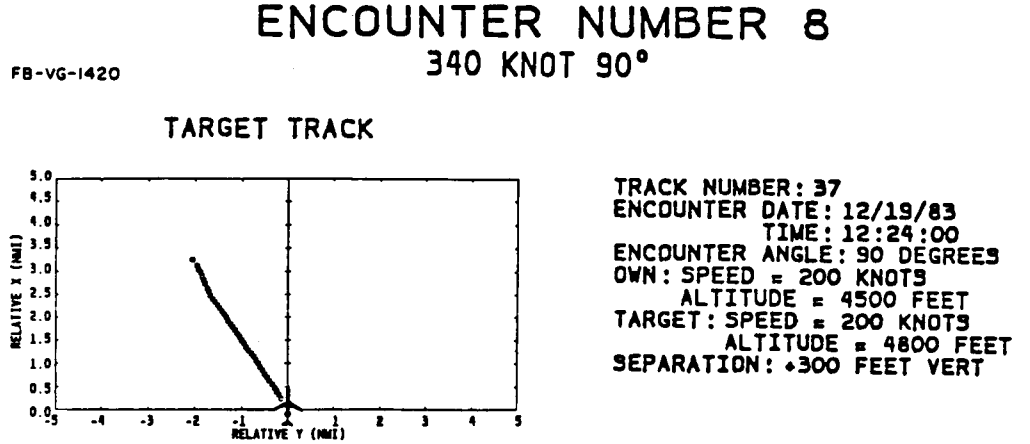

(a) Encounter

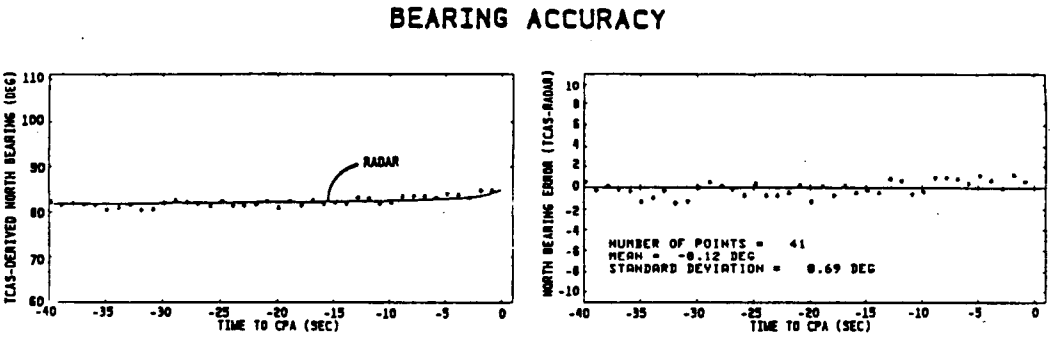

(b) Bearing

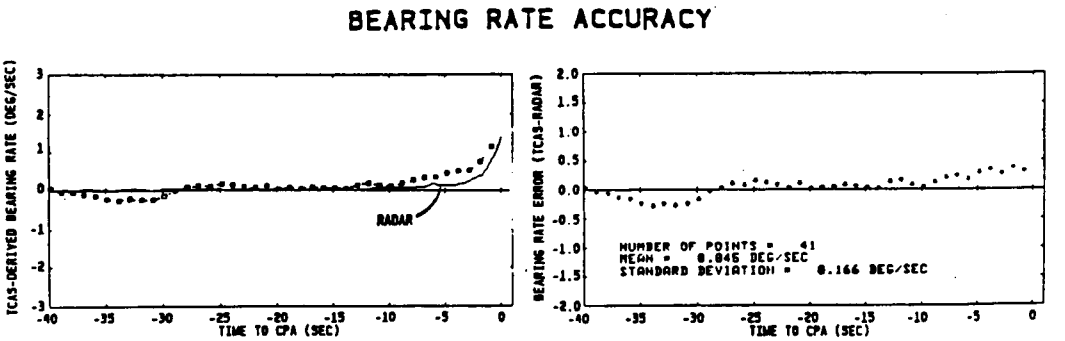

(c) Bearing rate

Figure 4.9. Real encounter example [12].

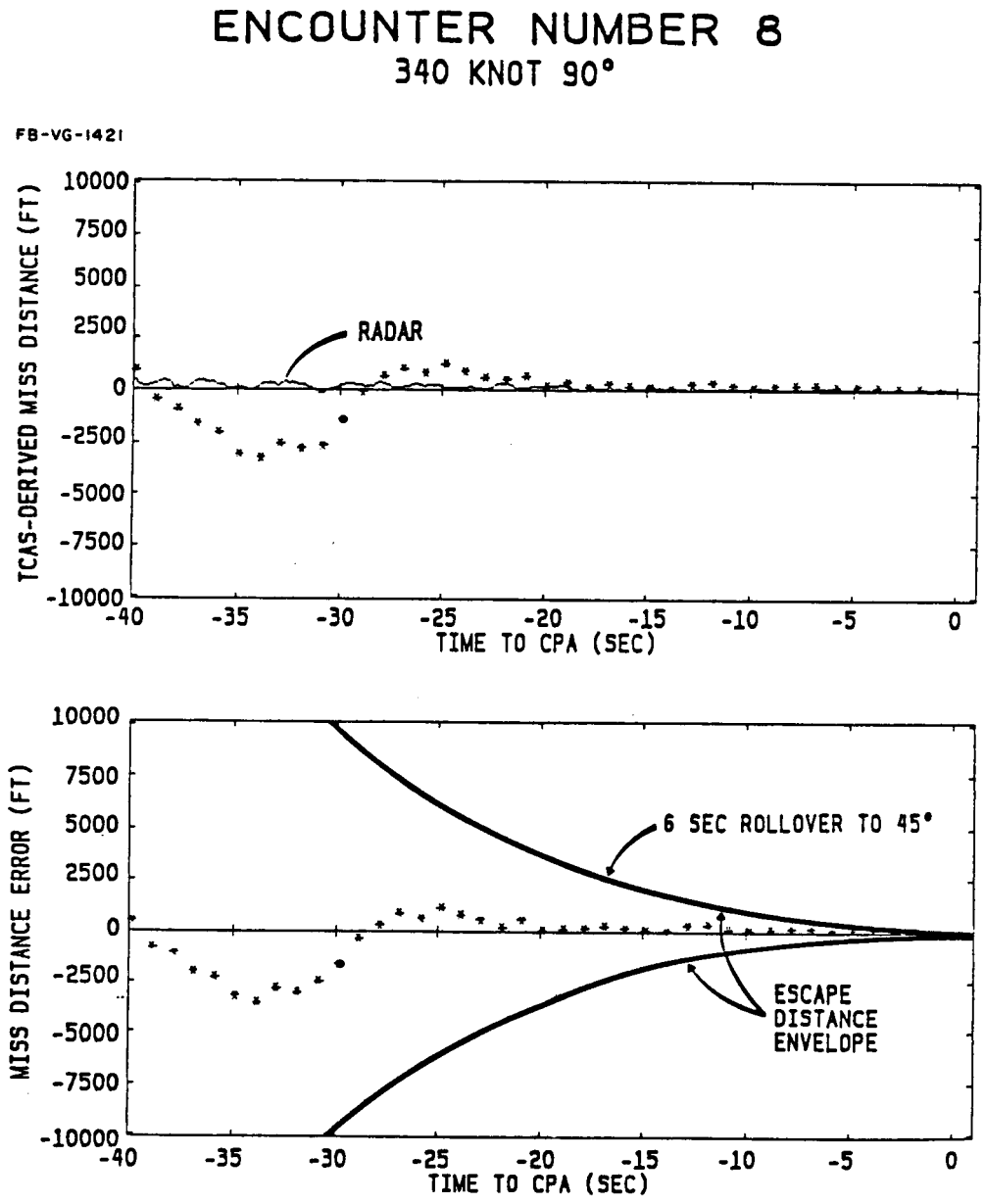

(d) Miss-distance

Figure 4.9. Continued.

relative speed is 340 knots. This means that the time to CPA is 40 seconds.

Figure 4.10 shows the encounter in the earth-fixed coordinate system starting at 40 seconds to CPA. The solid line is the path of the TCAS-equipped aircraft and the dashed line is the path of the target. Figure 4.11 depicts the simulation of this encounter in the airplane-fixed coordinate system without random noise. The solid line is the exact path while the dot-dashed line, which overlaps the solid line and is difficult to identify here, is the detected path. The outside envelope is the horizontal threshold envelope and the cross marks indicate the miss distance curve. Since the miss distance curve falls inside the threshold envelope, according to the TCAS system, there is a potential danger of collision. Of course, the vertical separation has to be checked to decide if there is danger of mid-air collision. The threshold envelope is generated by moving normally (on both sides) to the detected path of the intruder the threshold distance given in (4.21). Likewise, the miss-distance curve is generated by moving normally to the intruder's detected path the miss distance given in (4.17). Note that in contrast to the simulation discussed in [4], in this encounter the Boeing 727 airplane has a top- and bottom-mounted antenna. The top antenna is used when the elevation angle is zero or greater than zero; whereas, the bottom antenna is used for negative angles of elevation.

As shown in Figure 4.2, one can choose to add or not to add random noise. If this noise is not added, the results then reflect the performance of the system with errors due to structural scattering only.

If the noise is added, then the other sources of error, which were already discussed, can be taken into account. Thus, Figure 4.12 is the simulation of the encounter with random noise added. Note that the detected position of the intruder is not affected very much and still overlaps the exact path. However, the miss-distance curve is greatly distorted when the intruder is far from the TCAS-equipped airplane. In Figure 4.12 the miss-distance curve is outside the threshold envelope when the range is 20,000 ft. For purposes of illustration, the miss-distance curve is displayed with circles if it is outside the threshold curve, and with cross-marks if it is inside the threshold envelope. The large distortion of the miss-distance curve can be explained by noting that the noise generator has a standard deviation which is proportional to the range R (see Equation (4.9)). The result in Figure 4.12 is very important because it illustrates the fact that the time at which a decision is made as to whether there is a danger of collision or not should be studied very carefully. The accuracy of the predicted miss-distance increases as the separation between the two airplanes decreases. However, a decision has to be made when there is enough time to execute an escape curve. For example, if a decision would have been made at 20,000 ft. (in Figure 4.12), it would have been concluded that there was not a danger of collision; whereas, if a decision is made at 10,000 ft., the conclusion would have been that there is a danger of collision, but there is the danger that not enough time is left to follow an escape curve.

To evaluate the performance of the TCAS system, it is convenient to plot some parameters as a function of time. Figure 4.13 shows the plots

of some important parameters without random noise. The solid line indicates the real data and the dashed line indicates the detected data. The performance of the TCAS III is pretty good in this situation; i.e., when only structural scattering is taken into account. Figure 4.13(g) shows the plot of the angle theta, defined in Figure 4.6, as a function of time. Since it is always less than or equal to 90°, only the top-mounted antenna was used in this particular encounter.

A more realistic model of the TCAS system is obtained if the output of the noise generator is also taken into account. Figure 4.14(a) shows the output of the noise generator discussed in the previous section. Figures 4.14(b) - 4.14(g) show the same parameters calculated in Figure 4.13; however, noise is taken into account in Figure 4.14. The effect of the random noise can be clearly evident in these results.

According to Figure 4.12 there is a potential danger of collision. Obviously, no decision can be made until the vertical separation of the two airplanes is also evaluated. In the encounter being considered here, the vertical separation is 300 ft. For purposes of illustration, it will be assumed that there is a danger of collision and it is determined that an escape path must be followed by the TCAS-equipped airplane.

Figure 4.15 is the plot in the earth-fixed coordinate when the TCAS III-equipped aircraft takes a turn whose bank angle changes to 45° in 6 seconds. Figure 4.16 is the simulation of this encounter in the airplane-fixed coordinate system when the TCAS-equipped airplane starts the escape curve at 40 seconds to CPA. The top- and bottom-mounted arrays are used in this case. To show the effect of the bottom antenna,

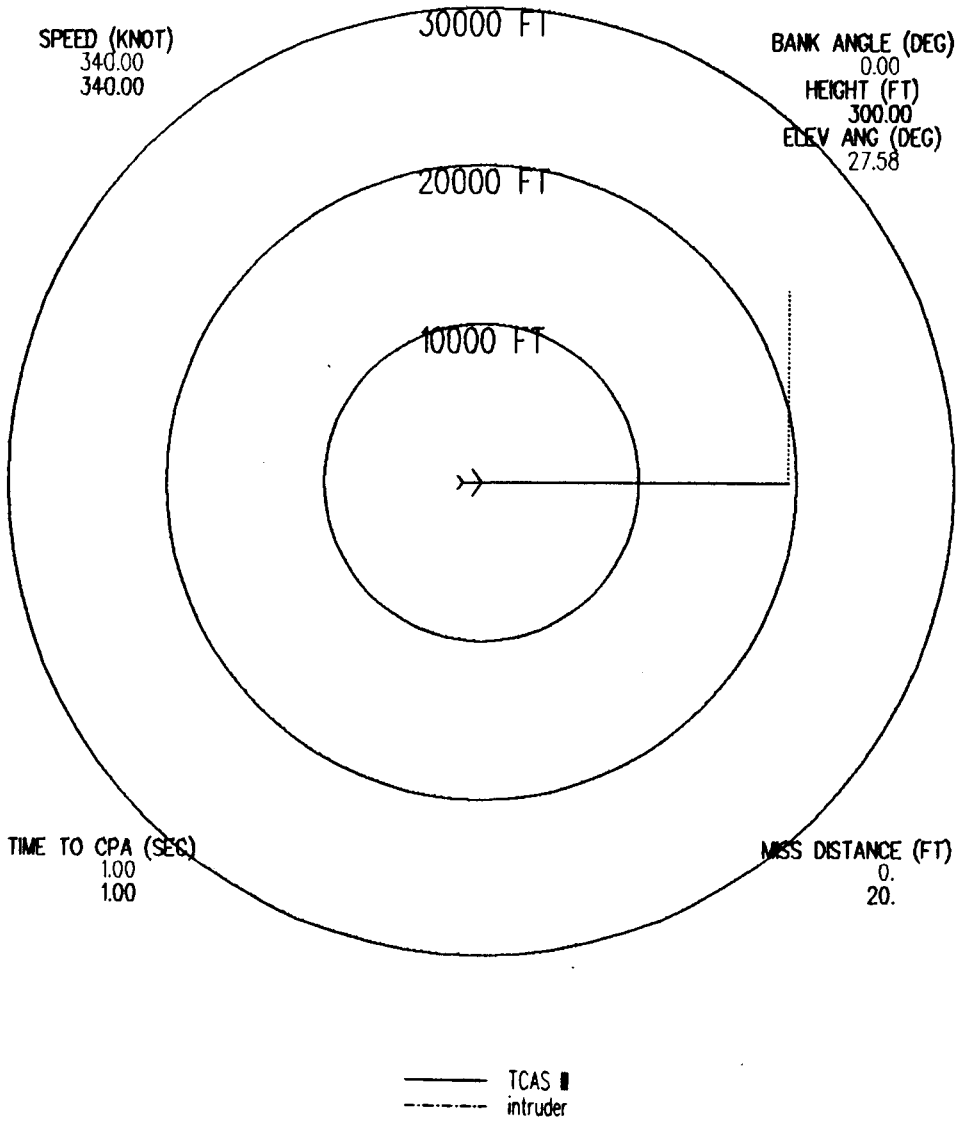

Figure 4.10. The encounter in the earth-fixed coordinate system.

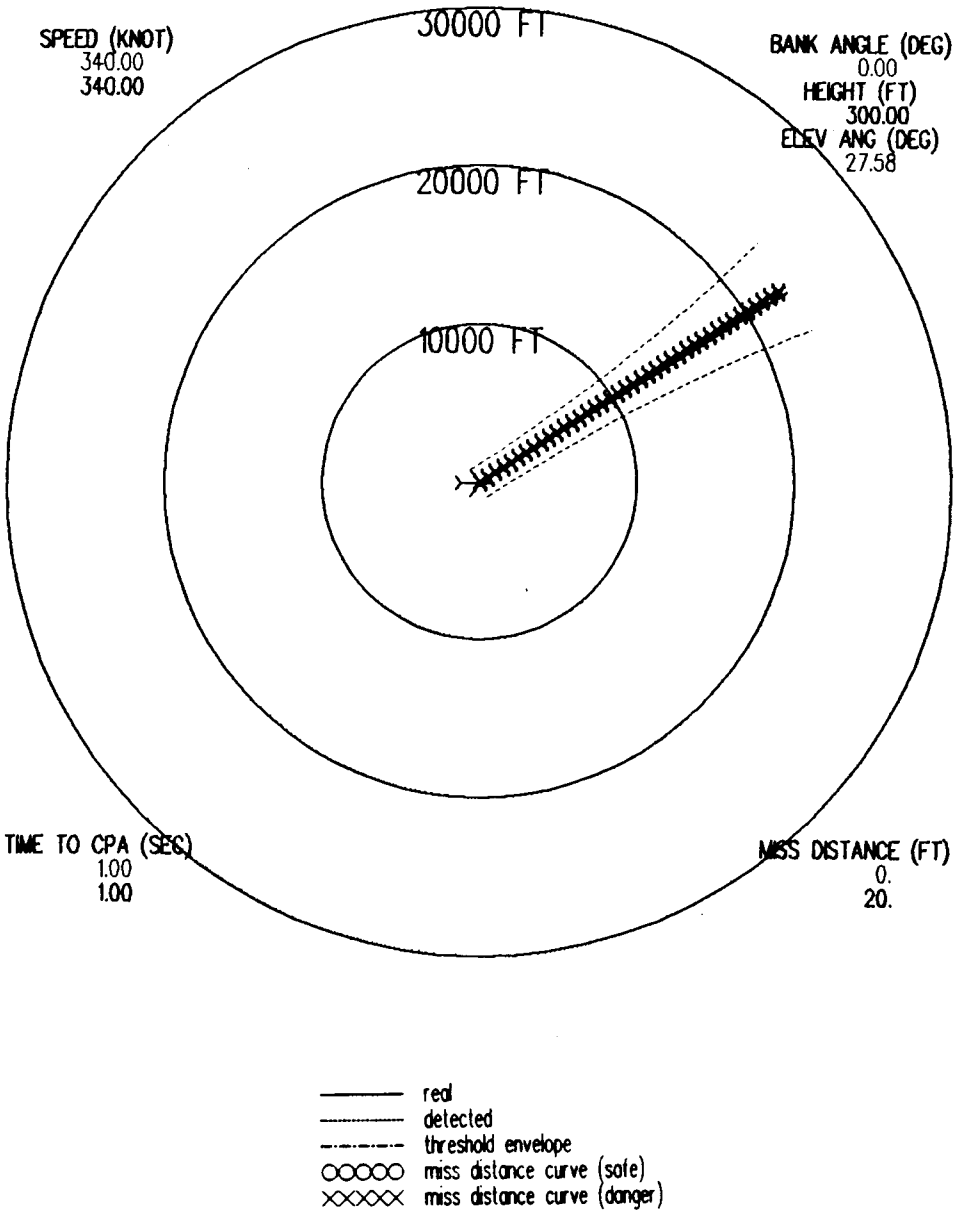

Figure 4.11. The encounter in the airplane-fixed coordinate system without random noise.

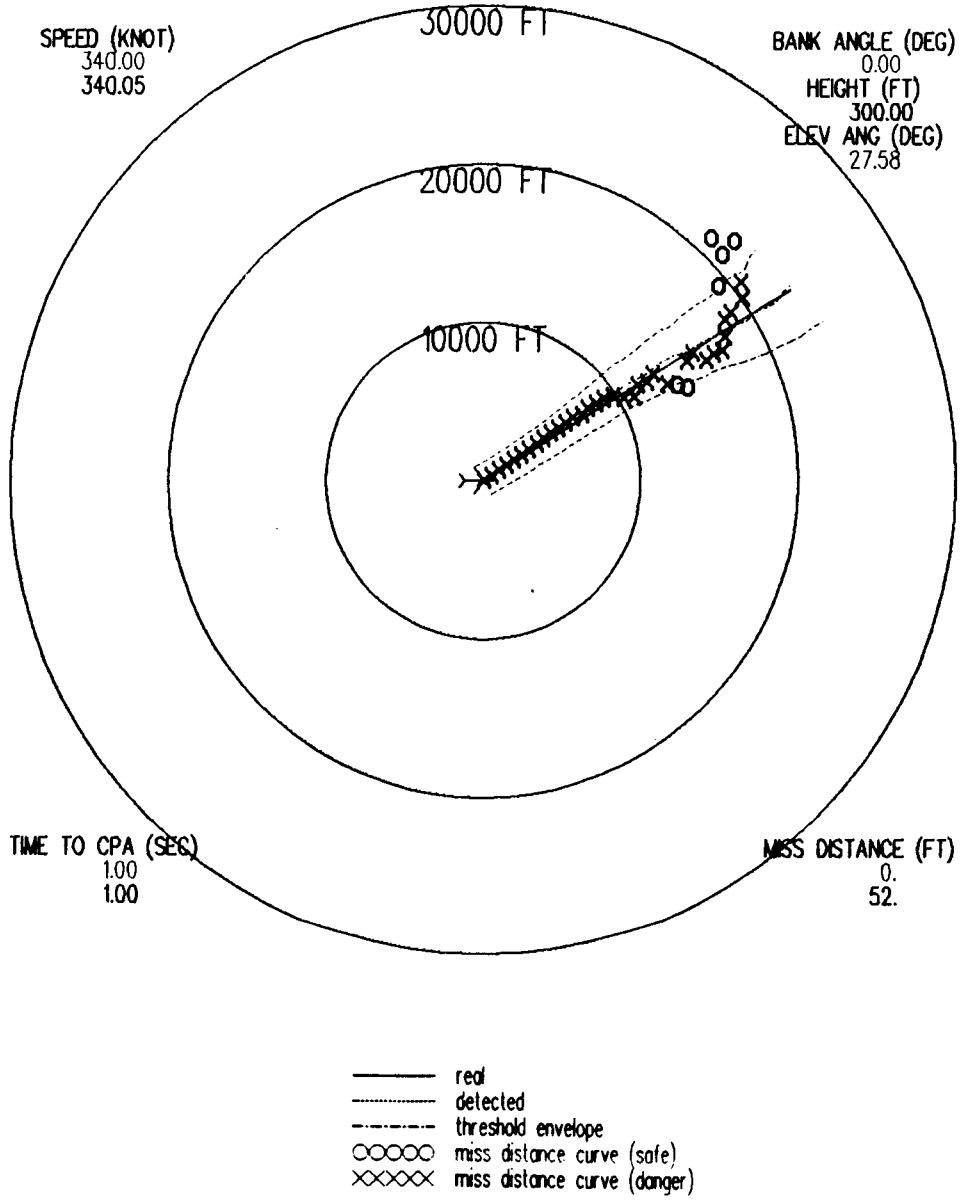

Figure 4.12. Simulation of encounter in airplane-fixed coordinate system with random noise added.

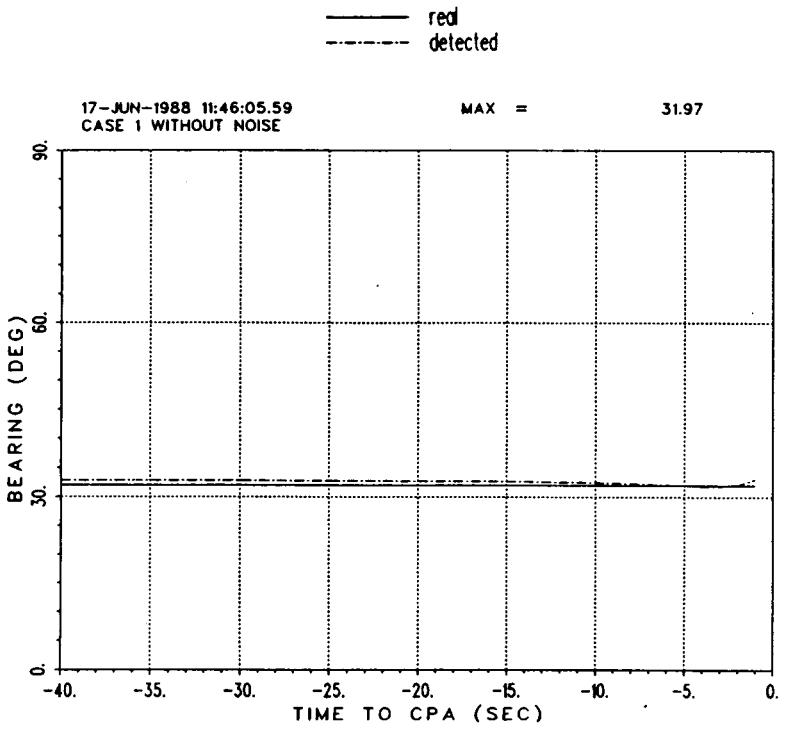

(a) Bearing

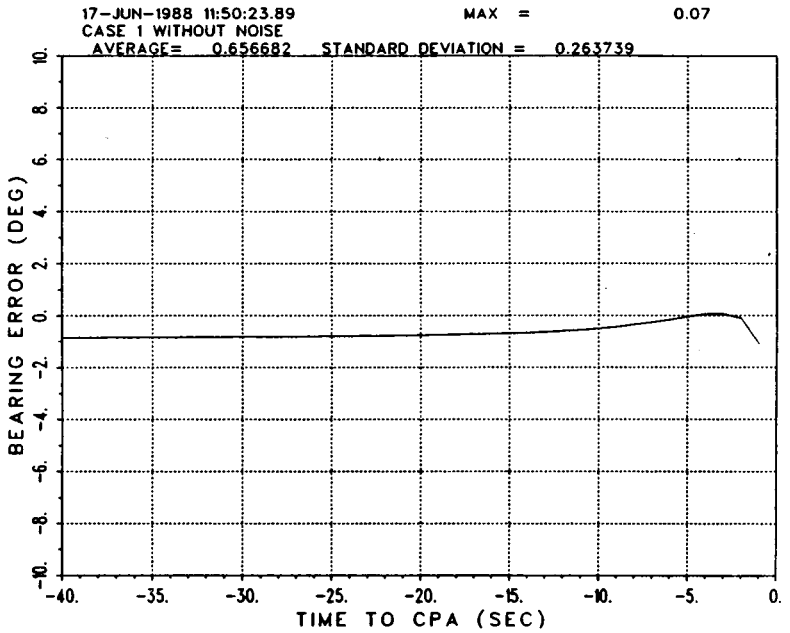

(b) Bearing error

Figure 4.13. The plots of some parameters as a function of time without random noise.

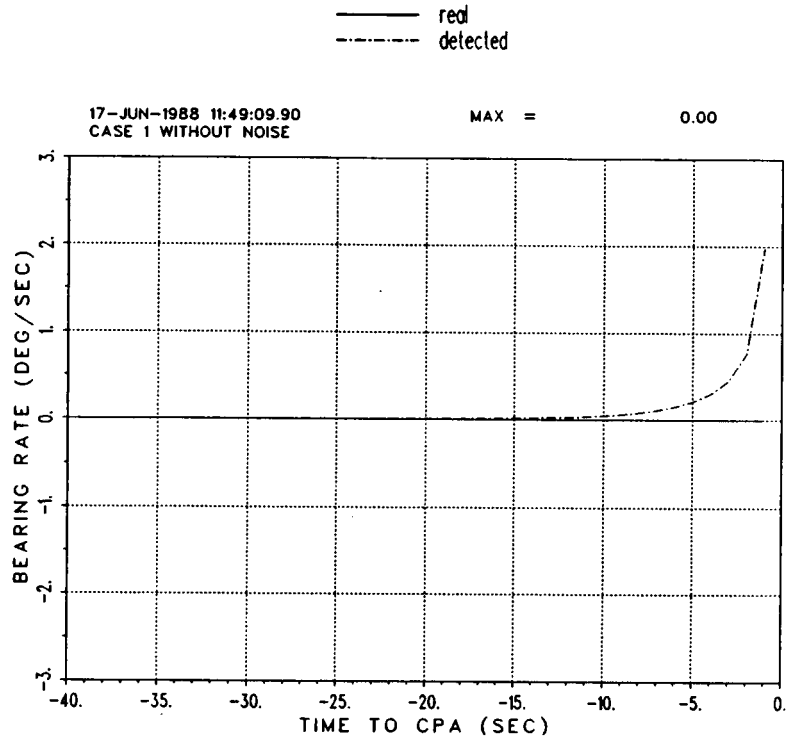

(c) Bearing rate

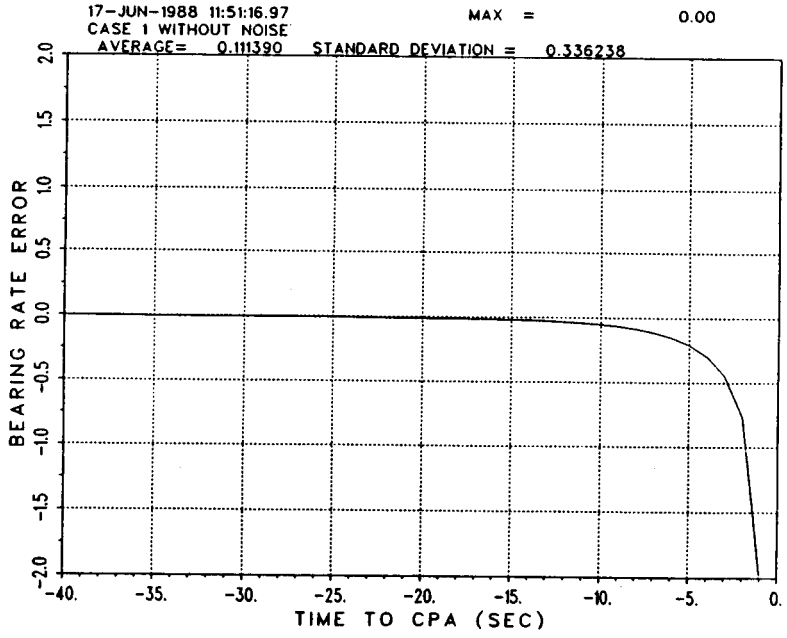

(d) Bearing rate error

Figure 4.13. Continued.

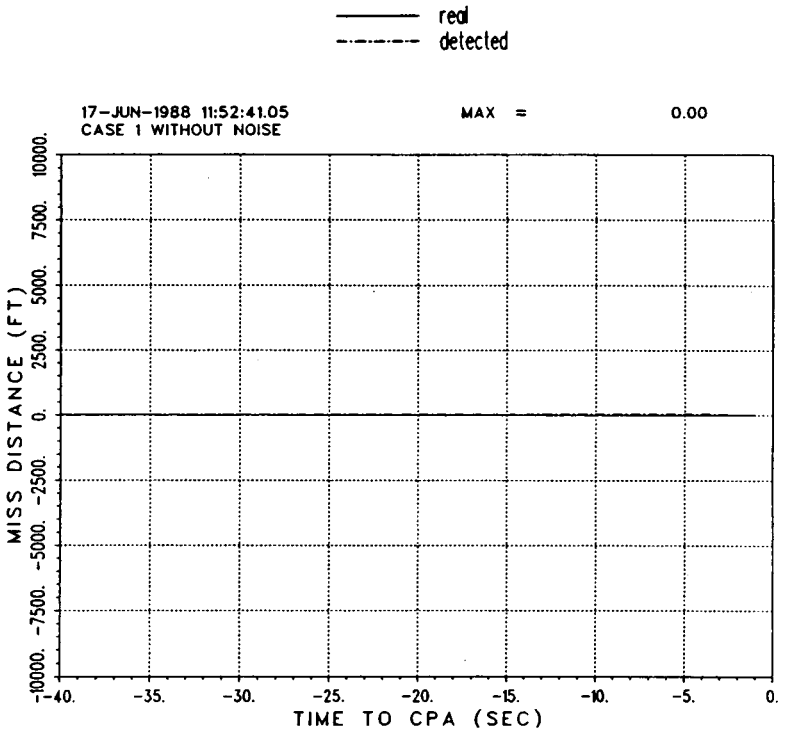

(e) Miss-distance

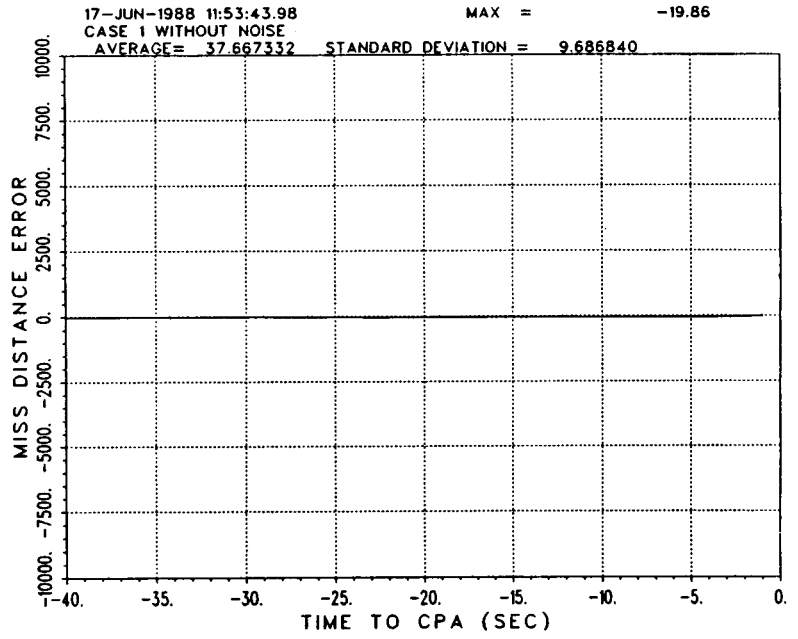

(f) Miss-distance error

Figure 4.13. Continued.

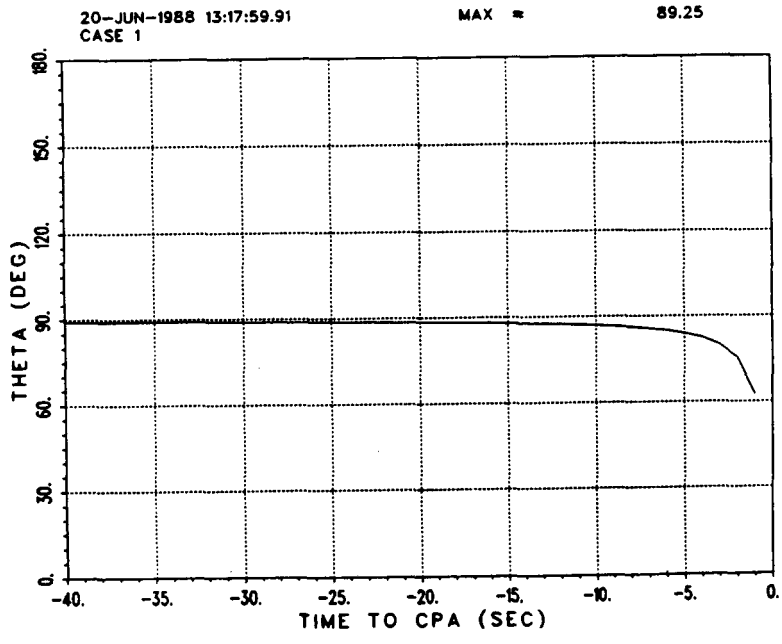

(g) Theta

Figure 4.13. Continued.

Figure 4.17 shows the same encounter where only the top-mounted antenna is used. Figure 4.18 clearly illustrates that using the top- and bottom-mounted antennas gives better results than just the top or bottom antenna alone.

Another case is considered in Figure 4.19 where the TCAS-equipped aircraft turns in the opposite direction, i.e., its bank angle changes to -45° in 6 seconds. Figure 4.20 is the simulation for this case.

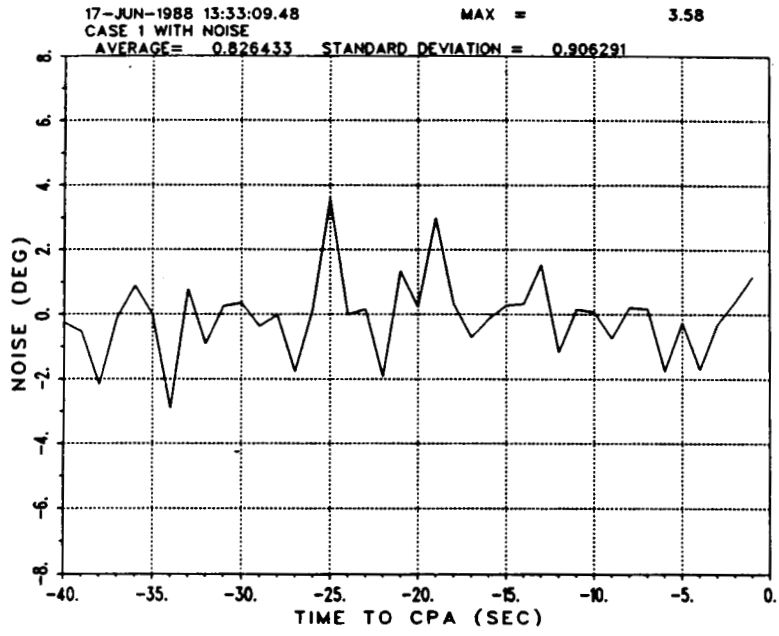

(a) Error added

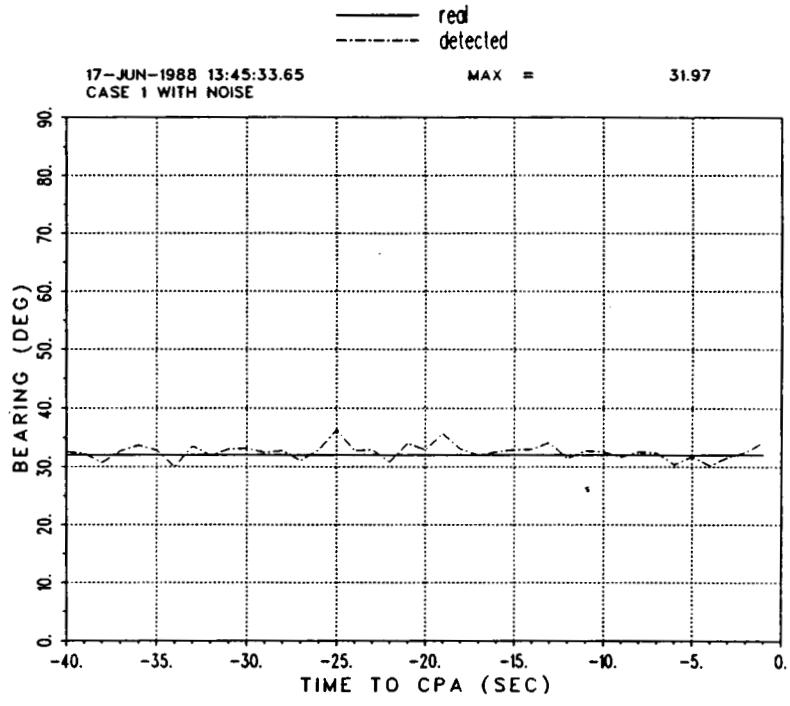

(b) Bearing

Figure 4.14. The plots of some parameters as a function of time with random noise added.

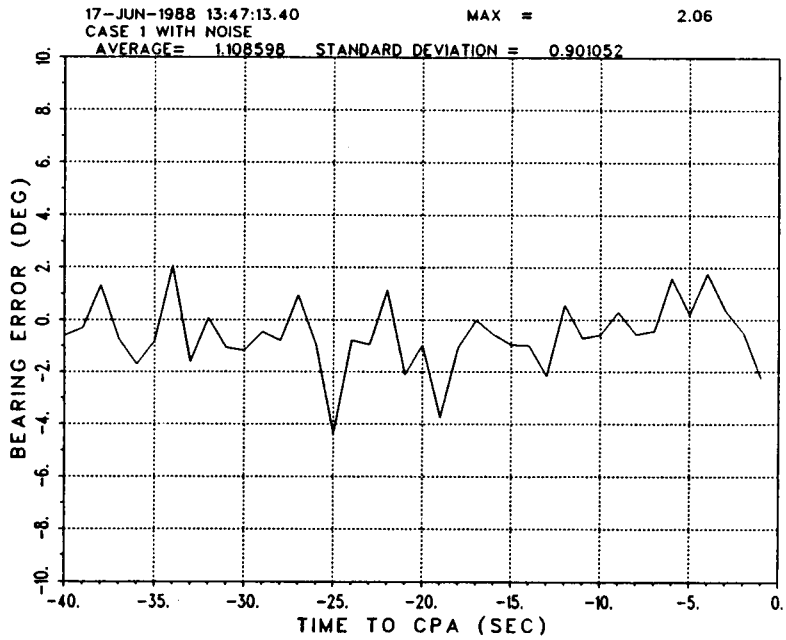

(c) Bearing error

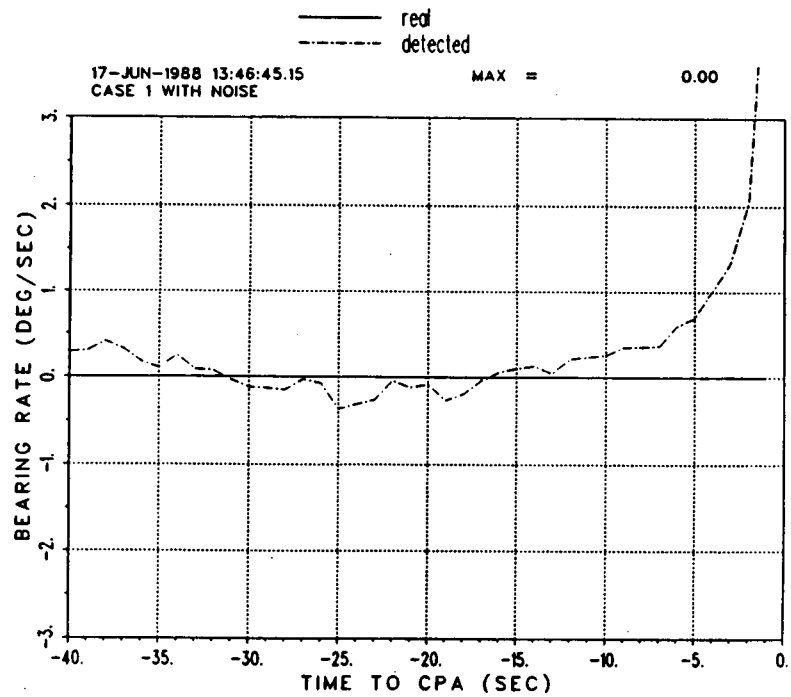

(d) Bearing rate

Figure 4.14. Continued.

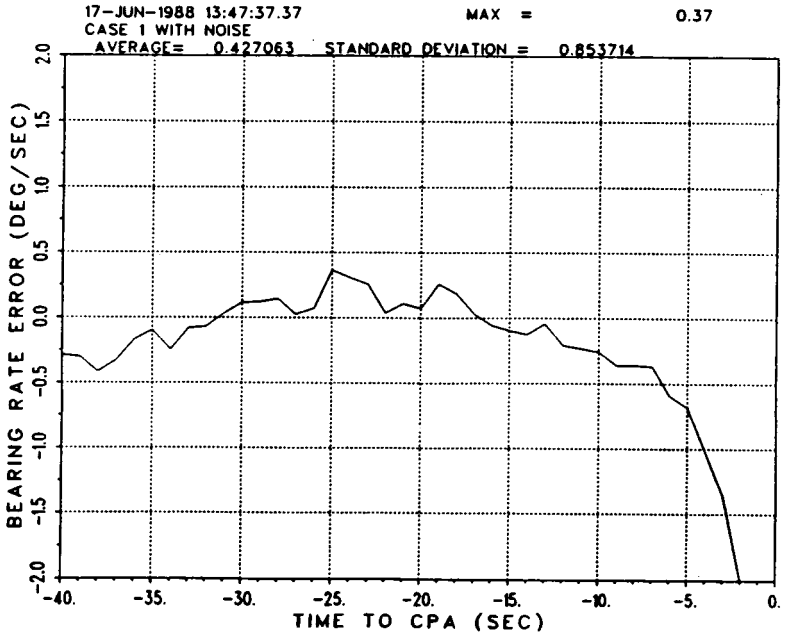

(e) Bearing rate error

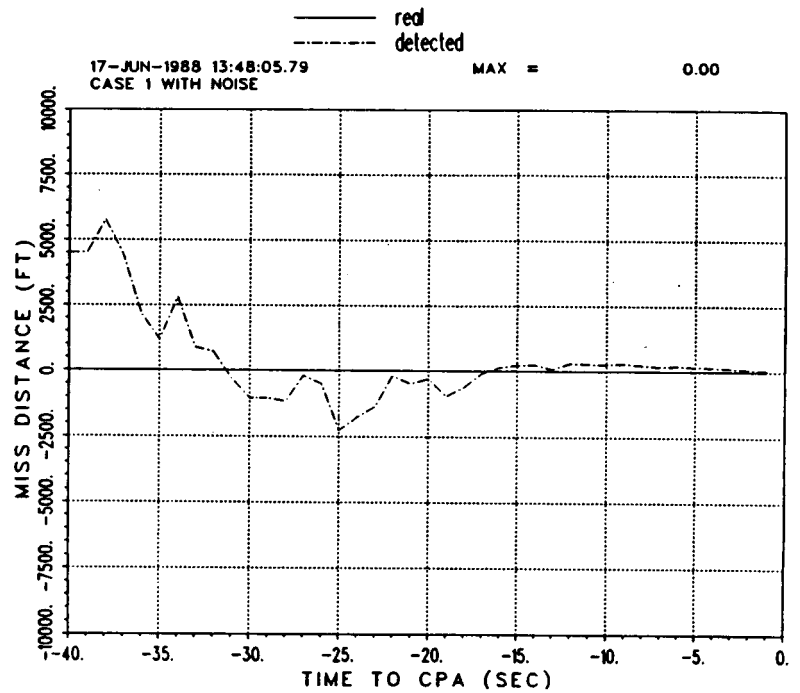

(f) Miss distance

Figure 4.14. Continued.

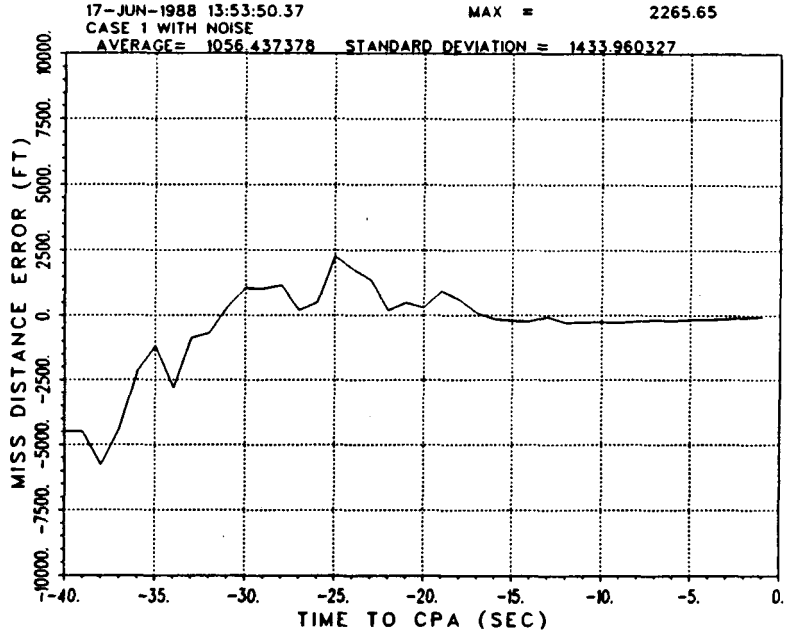

(g) Miss distance error

Figure 4.14. Continued.

Comparing this result with the previous one, the two escape curves are really effective because either one can be selected to avoid the collision.

Figures 4.21 and 4.22 are the plots for another case where the TCAS-equipped airplane takes a turn whose bank angle changes to 30° in 10 seconds, which is not as sharp as the previous escape curve considered in Figure 4.15 or 4.19. Figures 4.23 and 4.24 are the plots where the TCAS-equipped airplane takes a turn in the opposite direction (10 seconds to -30°). Both cases are with random noise.

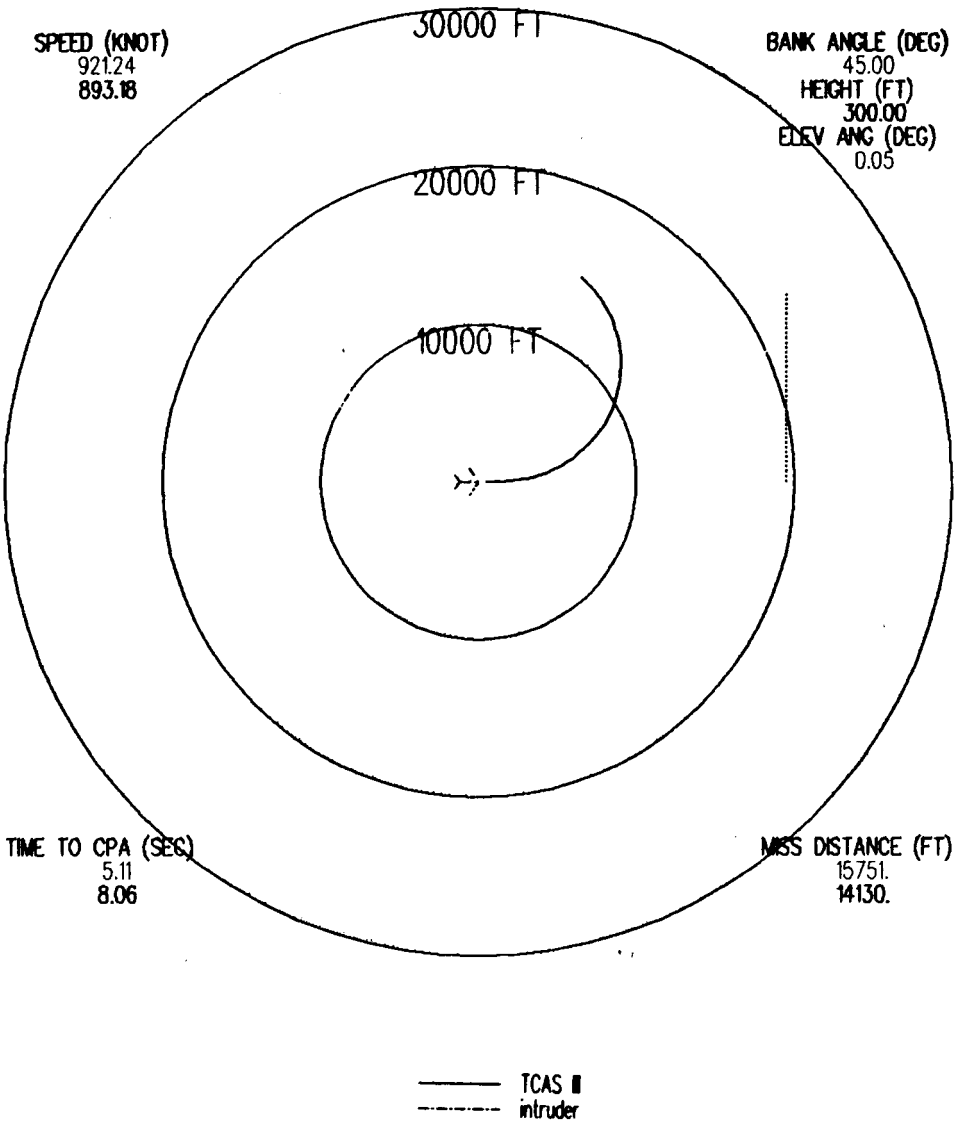

Figure 4.15. The plot in the earth-fixed coordinate system when the TCAS III takes an escape curve with 6 sec to 45°.

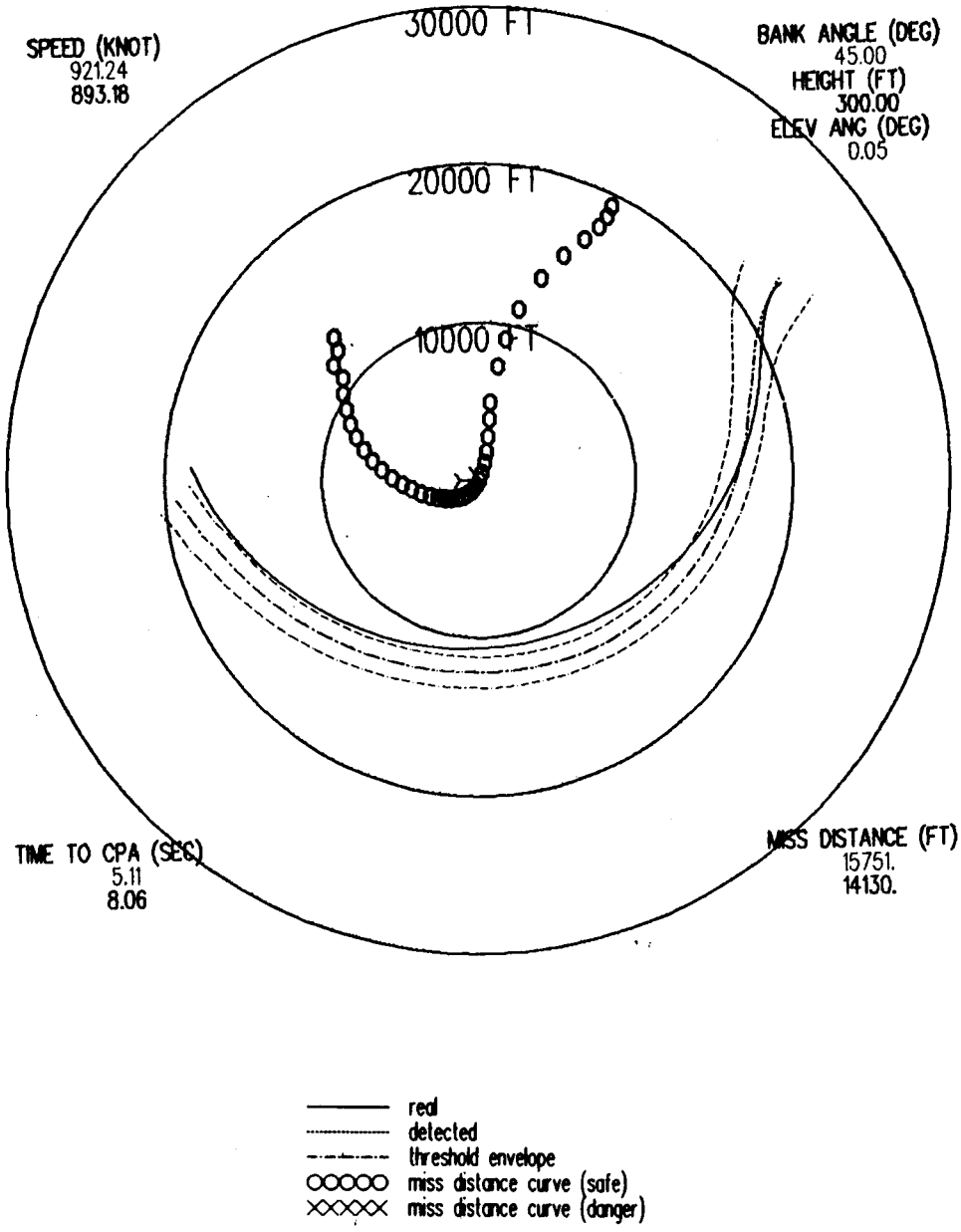

Figure 4.16. Simulation of encounter without random noise in the airplane-fixed coordinate system when the TCAS-equipped airplane takes an escape curve of 6 sec to 45°.

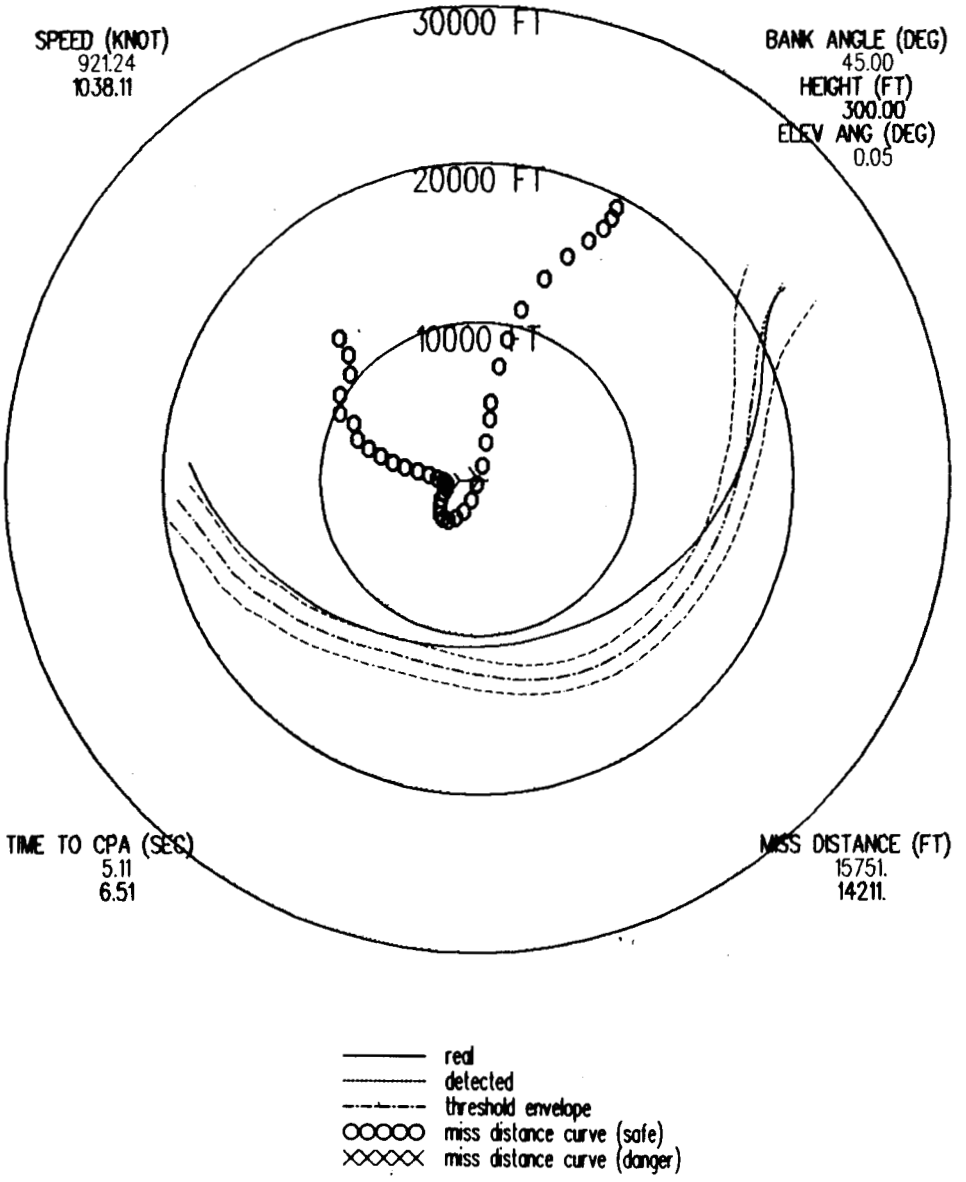

Figure 4.17. Same case as Figure 4.16 but with the top antenna only.

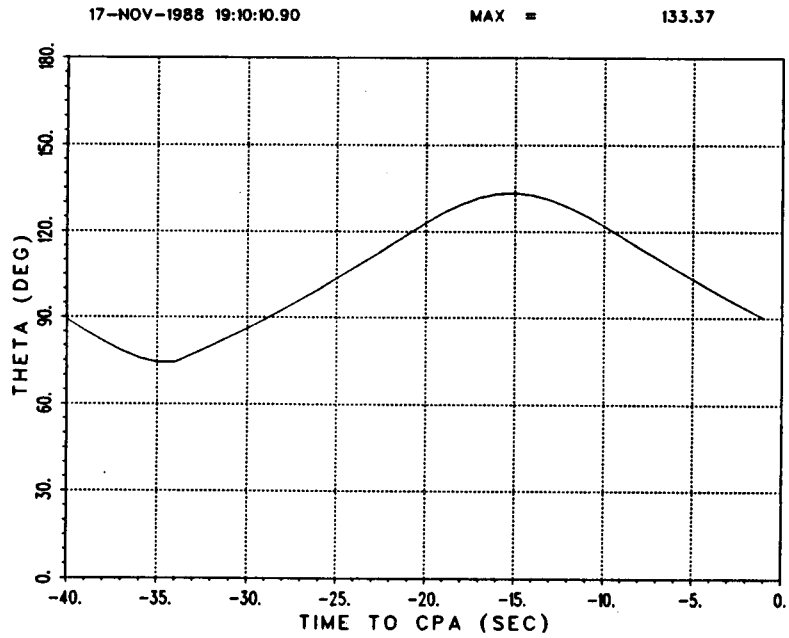

(a) Theta

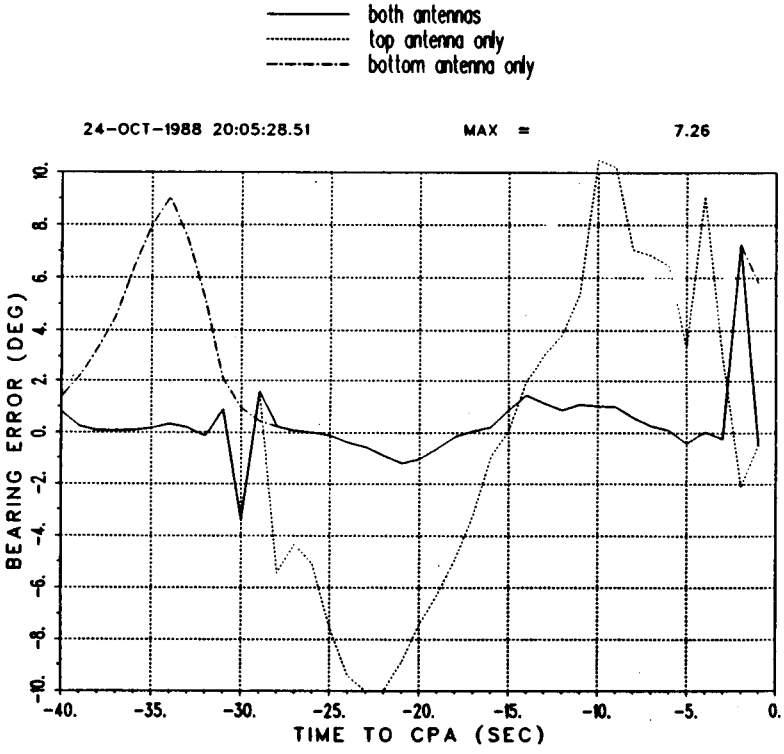

(b) Bearing Error

Figure 4.18. Comparison of error curves for a top-mounted, bottom-mounted and top- and bottom-mounted TCAS array.

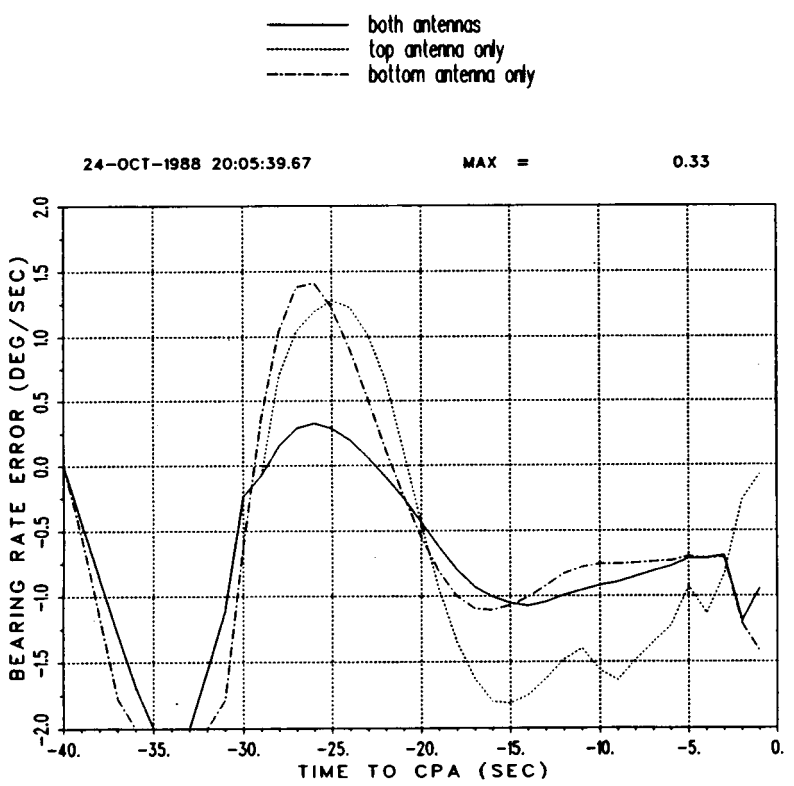

(c) Bearing Rate Error

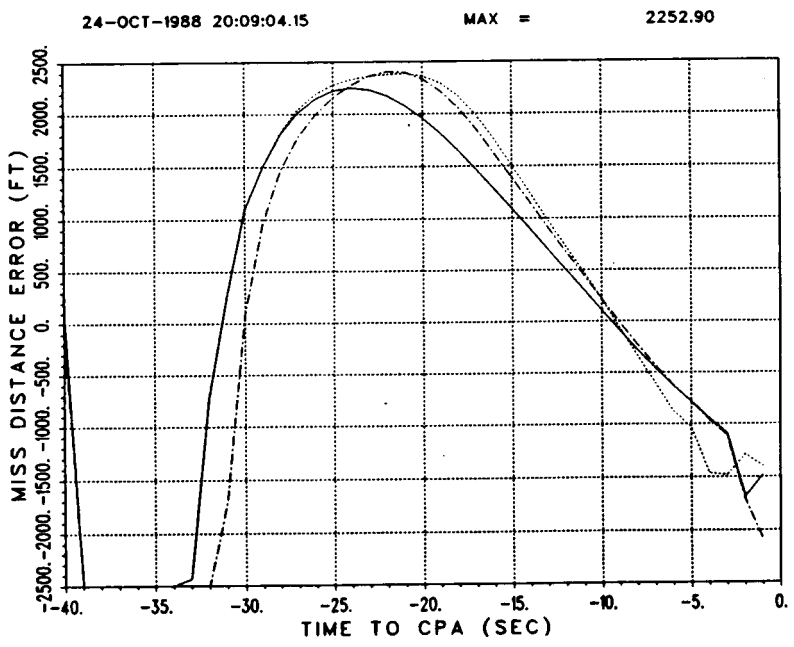

(d) Miss Distance Error

Figure 4.18. Continued.

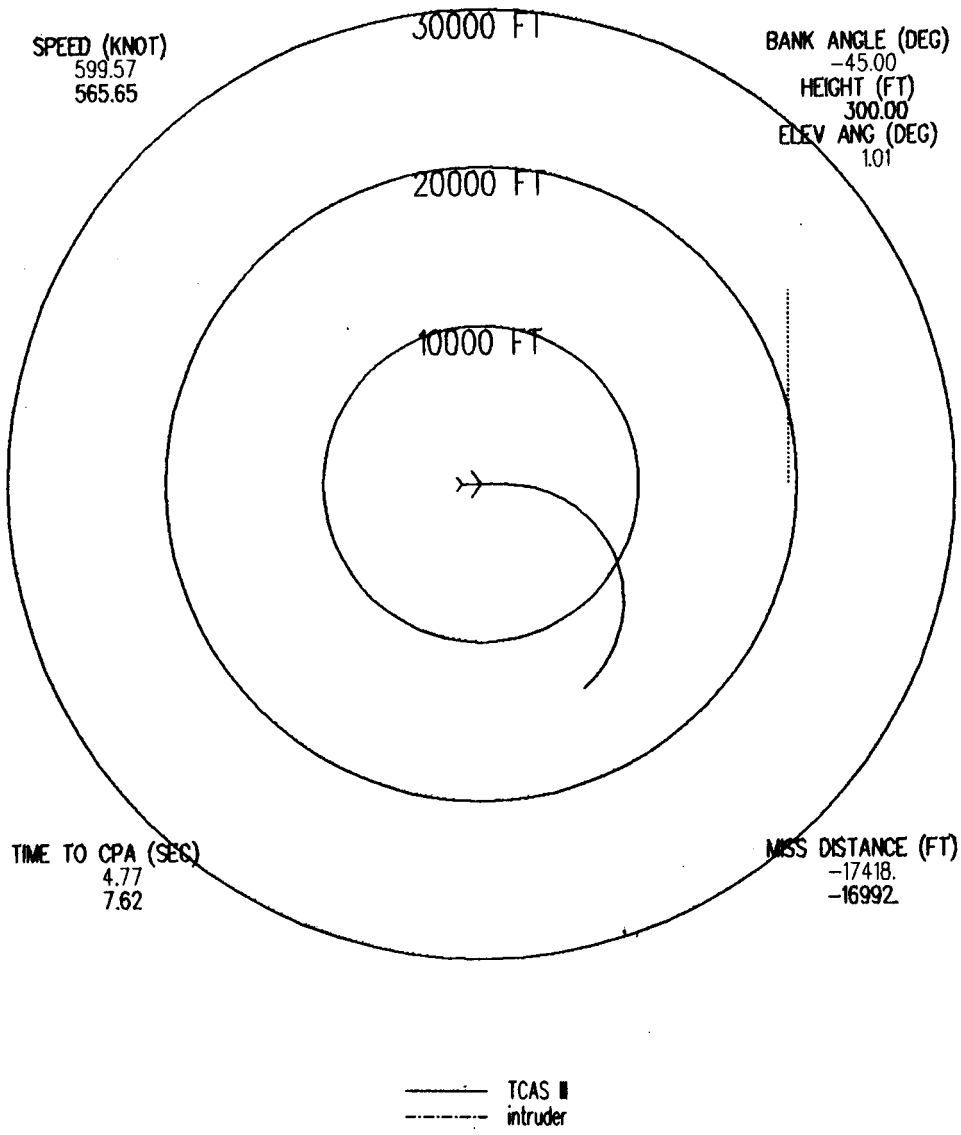

Figure 4.19. Encounter in the earth-fixed coordinate system when the TCAS III-equipped airplane takes an escape curve of 6 sec to -45°.

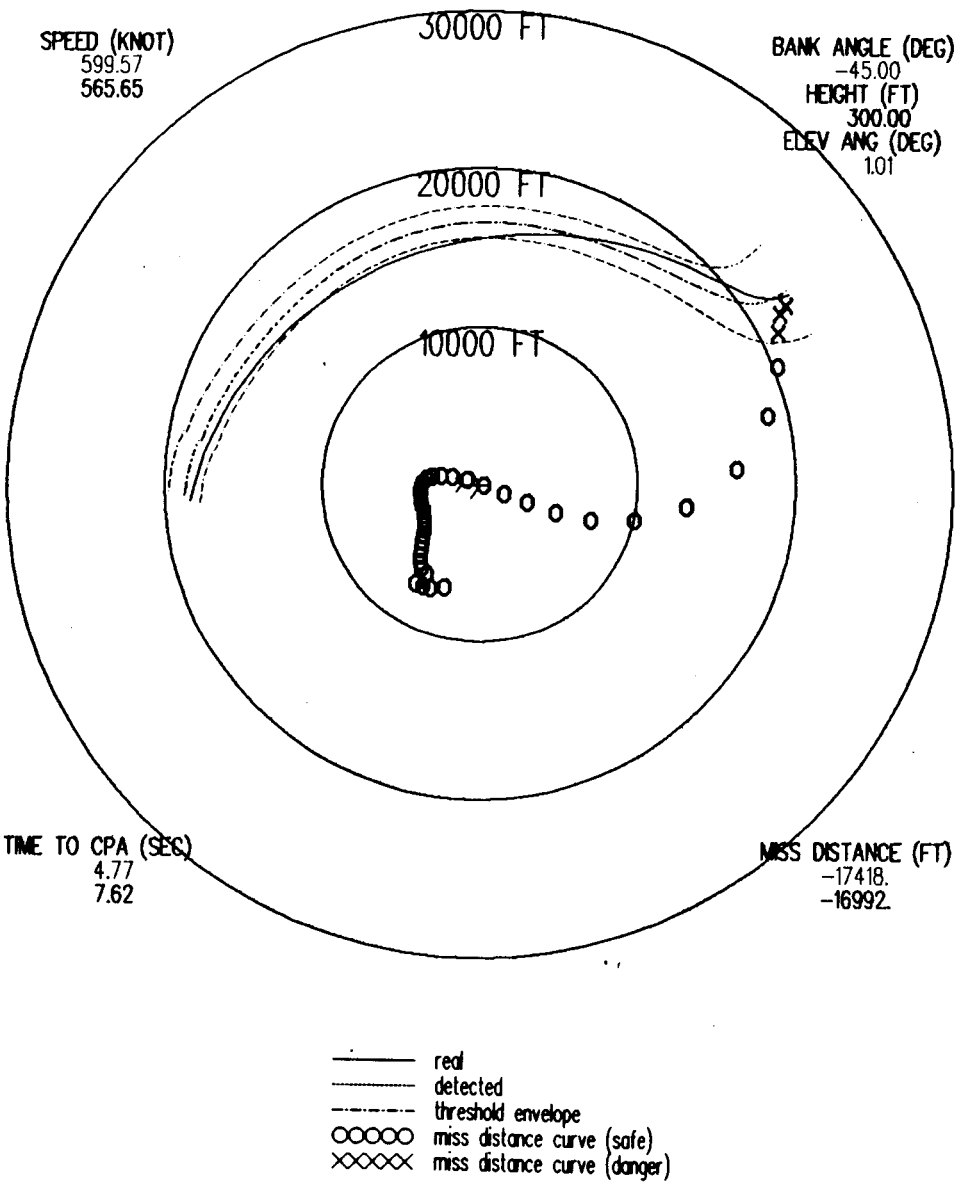

Figure 4.20. Simulation of encounter of Figure 4.19 in the airplane-fixed coordinate system without random noise.

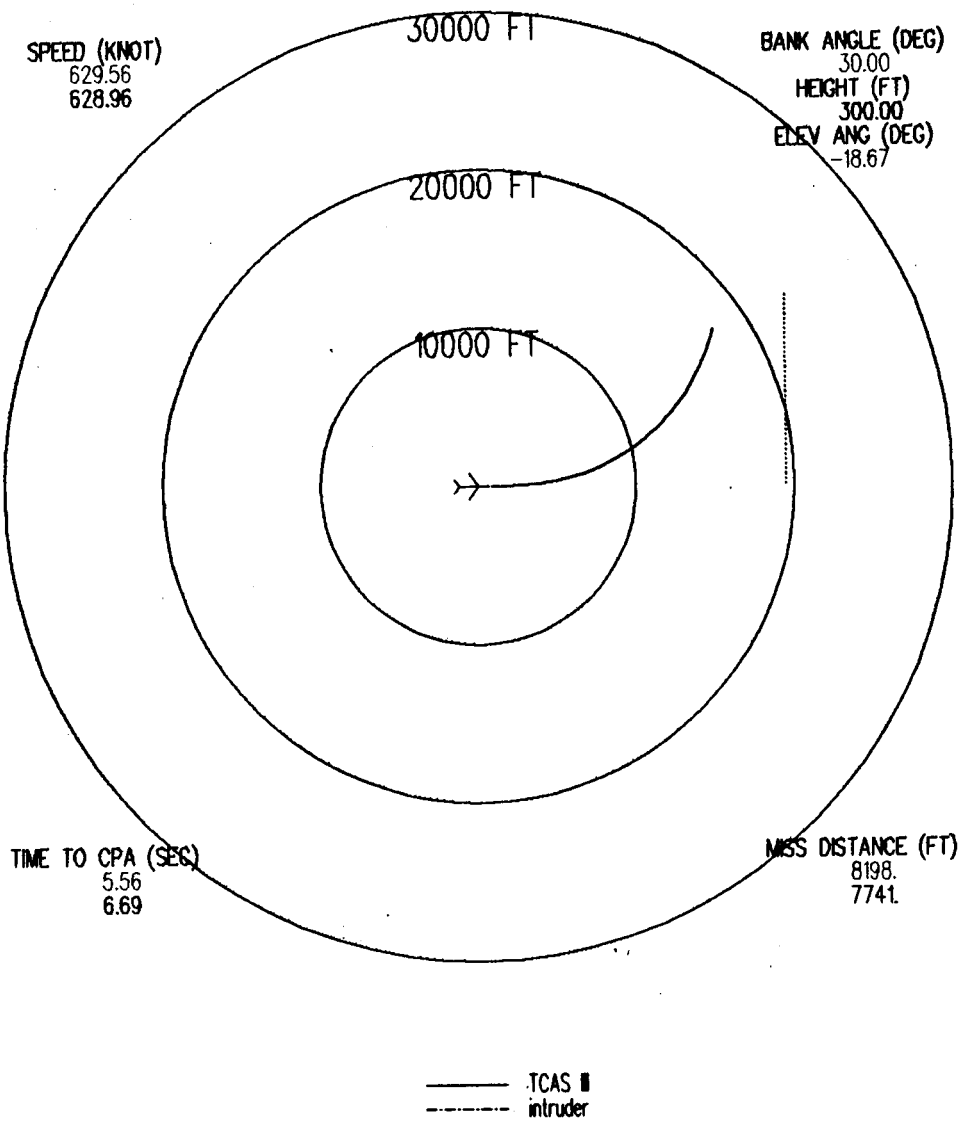

Figure 4.21. Encounter in the earth-fixed coordinate system when the TCAS III-equipped airplane takes an escape curve of 10 sec to 30°.

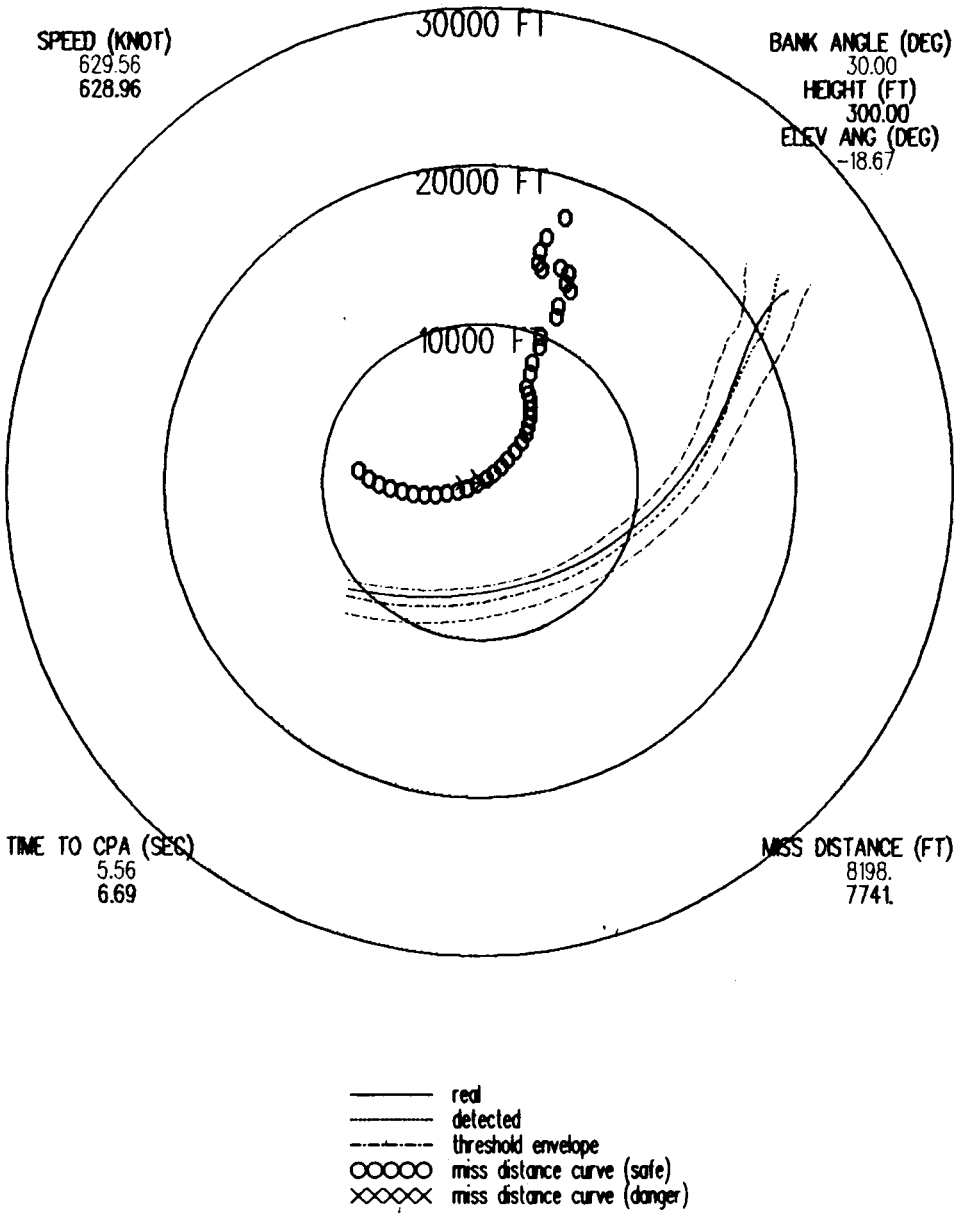

Figure 4.22. Simulation of encounter of Figure 4.21 in the airplane-fixed coordinate system with random noise added.

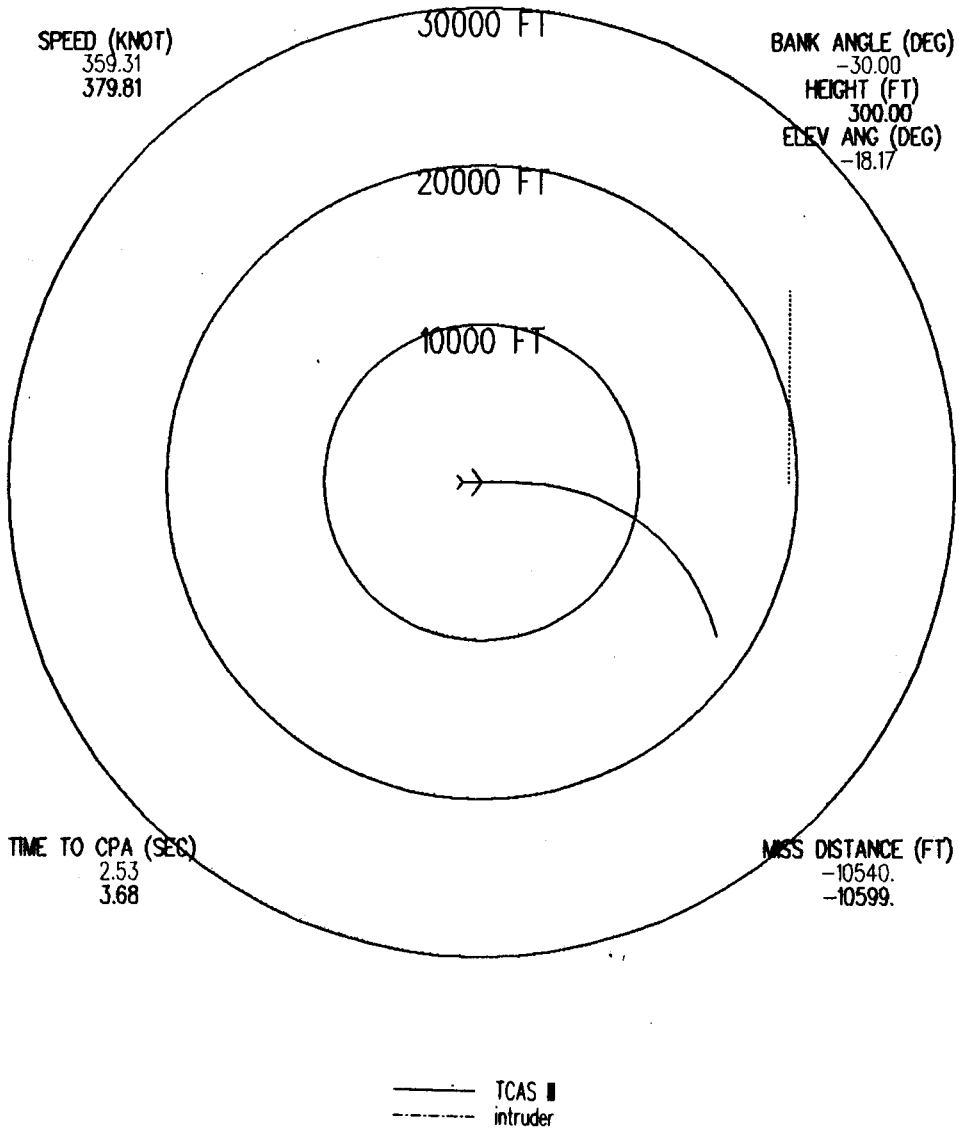

Figure 4.23. Encounter in the earth-fixed coordinate system when the TCAS III-equipped airplane takes an escape curve of 10 sec to -30°.

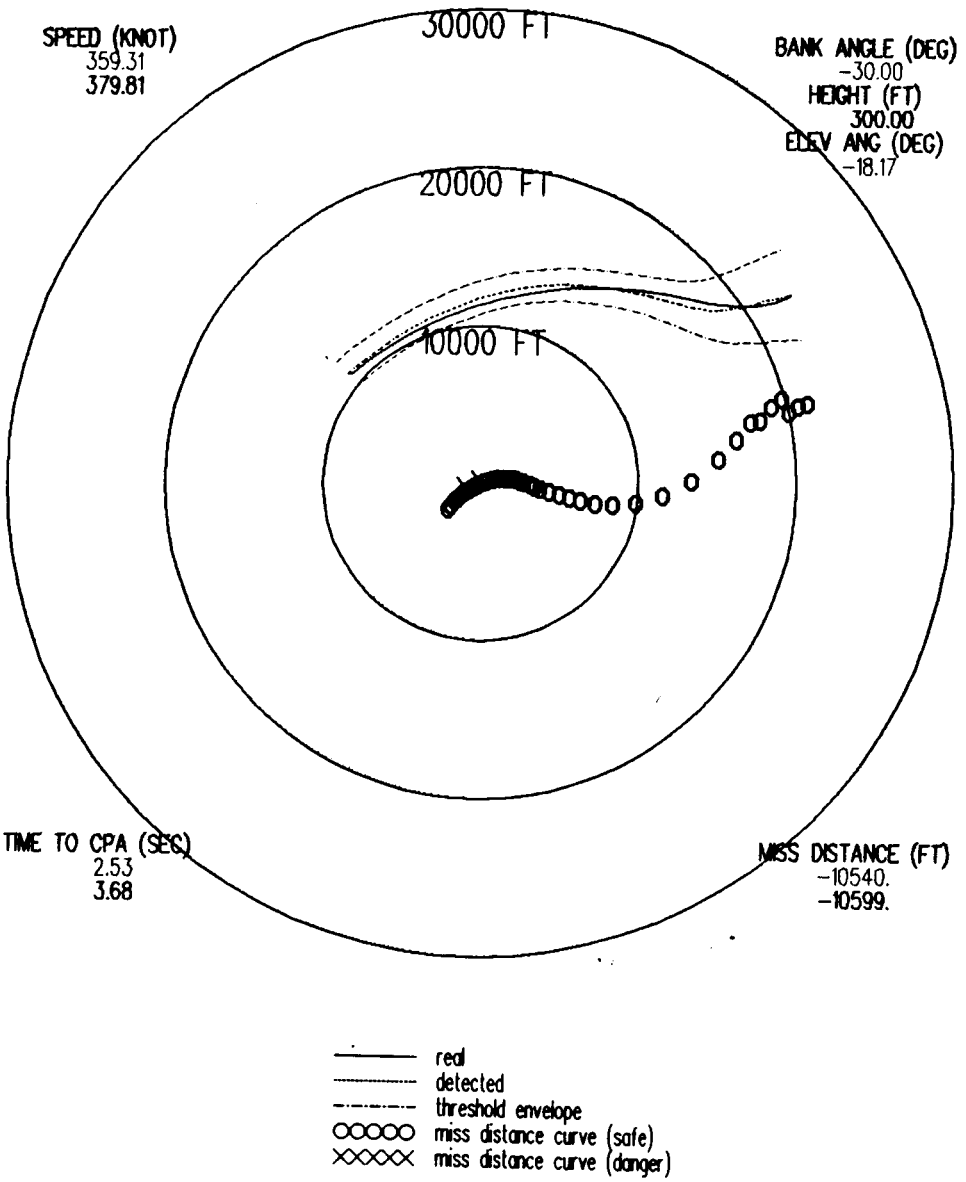

Figure 4.24. Simulation of encounter of Figure 4.23 in the airplane-fixed coordinate system with random noise added.

CHAPTER V

CONCLUSIONS

The purpose of this study is to develop a procedure to simulate and estimate the performance of the Enhanced TCAS II system mounted on the Boeing 727. It is worth mentioning that the procedure proposed here applies to any other arrays mounted on the fuselage of any type of aircraft.

There are three major steps that are followed to develop this simulation. In the first step, two new computer models of the TCAS III array elements (top-loaded monopoles) are developed with the help of a moment method code [6,7]. These two models are better and more realistic than the old two-monopole model [1]. The radiation pattern of these two models (four- and nine-element models) are compared with measured data to verify the analysis. Once the element models are obtained, the next step is to build the complete model for the TCAS array which means that the phase center of the actual array elements have to be determined. Due to the lack of measured data, a moment method code was used for this purpose. Note that in previous studies [4], it was assumed that the phase center of each element of the actual array was located at the actual element position. As shown by the moment method analysis, this assumption was not correct. Note that the phase centers of the two new models (four- and nine-element) had to be determined also.

The second important step is to build a computer model of the aircraft, in this case a Boeing 727. This airplane model was used in the Aircraft Code to calculate the radiation patterns of the TCAS array elements. The element radiation patterns were then properly combined to obtain the array patterns; i.e., sum and difference beams. Three different array models were used; namely, the new two-monopole, four-monopole and nine-monopole models. The difference between the old two-monopole and the new two-monopole array models was the assumed phase center of the actual array elements. In the new two-monopole model, the phase center of the TCAS array elements was obtained with the moment method code. The sum and difference beams were then used to obtain the monopulse curves and then the scattering error curves. The scattering error curves are useful because they can be used to predict the overall performance of the TCAS system. They can also be used to search for the optimum position of the TCAS array on the fuselage of the airplane under study.

It turns out that in the region $-90° < \phi < 90°$, all the models discussed here generate similar scattering error curves. However, in the other regions there were discrepancies between the various error curves. The old and new two-monopole models predicted large errors in these regions. The results of the four- and nine-monopole models were considered more accurate; however, the region of greatest interest is $-90° < \phi < 90°$; which means that the two-monopole model could still be used.

The last step was to utilize all the data and algorithms developed here and in [9-16] to construct an algorithm that simulates the tracking of an intruder by a Boeing 727 equipped with top and bottom

TCAS antenna arrays. Although a similar algorithm has been developed in [4] for a Boeing 737, the major improvement in the present algorithm is the inclusion of accurate escape curves, which take into account the roll of the aircraft as it changes bearing. Furthermore, the new algorithm can switch between the top and bottom arrays to evaluate the performance of each one. This new algorithm is very useful in evaluating the performance of the TCAS arrays.

There are still some areas of future research associated with this general topic discussed here. The weights of the TCAS array elements, which are used to generate the sum and difference beams, were obtained for a flat array. They may have to be adjusted in the computer models so that the measured and calculated sum and difference beams are in better agreement. Another area of research is to investigate whether other antennas in the vicinity of the TCAS array, especially those antennas operating at frequencies close to the TCAS array frequency of operation affect the overall performance of the TCAS system.

APPENDIX A

SOME INPUT DATA FOR THE CASES IN CHAPTER II

Tables A.1, A.2 and A.3 are input data of the ESP III Code [6,7]. Table A.1 simulates the transponder (see Figure 2.2) of the TCAS III on a flat infinite ground plane to find its input impedance. Table A.2 simulates the array-element of the TCAS III array (small monopole of Figure 2.2) on a flat infinite ground plane to also find its impedance. Table A.3 simulates the whole TCAS III antenna array on an infinite ground plane to calculate the induced current on each monopole and its radiation pattern.

Tables A.4 through A.6 are input data for the Aircraft Code [2]. Table A.4 shows a Boeing 727 with the top-mounted off-centered TCAS III system using the new two-monopole model for each element. Tables A.5 and A.6 show the four-monopole model and the nine-monopole model, respectively. For detailed information, please refer Chapter II.

Table A.1

Transponder Model

```
1,2,1,1,0,1,4,6,18,1,1,0
0,1,3,60.
1,1,3,80.
0,1,3,0.,90.,0.
0,1,3,90.
1060.,57.,1.9812E-3
2
8,0.25,0,3,0
3.3388E-2,1.383E-2,1.905E-2
1.383E-2,3.3388E-2,1.905E-2
-1.383E-2,3.3388E-2,1.905E-2
-3.3388E-2,1.383E-2,1.905E-2
-3.3388E-2,-1.383E-2,1.905E-2
-1.383E-2,-3.3388E-2,1.905E-2
1.383E-2,-3.3388E-2,1.905E-2
3.3388E-2,-1.383E-2,1.905E-2
8,0.25,0,3,0
3.3388E-2,1.383E-2,-1.905E-2
1.383E-2,3.3388E-2,-1.905E-2
-1.383E-2,3.3388E-2,-1.905E-2
-3.3388E-2,1.383E-2,-1.905E-2
-3.3388E-2,-1.383E-2,-1.905E-2
-1.383E-2,-3.3388E-2,-1.905E-2
1.383E-2,-3.3388E-2,-1.905E-2
3.3388E-2,-1.383E-2,-1.905E-2
0,0
2,3,2,1,0,0
0.,0.,1.905E-2
0.,0.,0.
0.,0.,-1.905E-2
1,2
2,3
1,1,(1.0,0.),(0.,0.)
1,0,1,(0.,0.),(0.,0.),0.117
2,1,2,(0.,0.),(0.,0.),0.117
```

Table A.2

Monopole Model

```
1,2,1,1,0,1,4,6,18,1,1,0
0,1,3,60.
1,1,3,80.
0,1,3,0.,90.,0.
0,1,3,90.
1060.,57.,1.9812E-3
2
8,0.25,0,3,0
2.2506000E-02,9.3219997E-03,1.905E-2
9.3219997E-03,2.2506000E-02,1.905E-2
-9.3219997E-03,2.2506000E-02,1.905E-2
-2.2506000E-02,9.3219997E-03,1.905E-2
-2.2506000E-02,-9.3219997E-03,1.905E-2
-9.3219997E-03,-2.2506000E-02,1.905E-2
9.3219997E-03,-2.2506000E-02,1.905E-2
2.2506000E-02,-9.3219997E-03,1.905E-2
8,0.25,0,3,0
2.2506000E-02,9.3219997E-03,-1.905E-2
9.3219997E-03,2.2506000E-02,-1.905E-2
-9.3219997E-03,2.2506000E-02,-1.905E-2
-2.2506000E-02,9.3219997E-03,-1.905E-2
-2.2506000E-02,-9.3219997E-03,-1.905E-2
-9.3219997E-03,-2.2506000E-02,-1.905E-2
9.3219997E-03,-2.2506000E-02,-1.905E-2
2.2506000E-02,-9.3219997E-03,-1.905E-2
0,0
2,3,2,1,0,0
0.,0.,1.905E-2
0.,0.,0.
0.,0.,-1.905E-2
1,2
2,3
2,0,(1.0,0.),(0.,0.)
1,0,1,(0.,0.),(0.,0.),0.079
2,1,2,(0.,0.),(0.,0.),0.079
```

Table A.3

Complete TCAS III Model

```
1,2,1,1,1,1,4,6,18,1,1,0
0,1,3,60.
1,1,3,80.
0,1,3,0.,90.,0.
0,1,3,90.
1060.,57.,1.9812E-3
18
8,0.25,0,3,0
3.3388E-2,1.383E-2,1.905E-2
1.383E-2,3.3388E-2,1.905E-2
-1.383E-2,3.3388E-2,1.905E-2
-3.3388E-2,1.383E-2,1.905E-2
-3.3388E-2,-1.383E-2,1.905E-2
-1.383E-2,-3.3388E-2,1.905E-2
1.383E-2,-3.3388E-2,1.905E-2
3.3388E-2,-1.383E-2,1.905E-2
8,0.25,0,3,0
3.3388E-2,1.383E-2,-1.905E-2
1.383E-2,3.3388E-2,-1.905E-2
-1.383E-2,3.3388E-2,-1.905E-2
-3.3388E-2,1.383E-2,-1.905E-2
-3.3388E-2,-1.383E-2,-1.905E-2
-1.383E-2,-3.3388E-2,-1.905E-2
1.383E-2,-3.3388E-2,-1.905E-2
3.3388E-2,-1.383E-2,-1.905E-2
8,0.25,0,3,0
-7.1786687E-02,0.1036147,1.905E-2
-8.4970683E-02,0.1167987,1.905E-2
-0.1036147,0.1167987,1.905E-2
-0.1167987,0.1036147,1.905E-2
-0.1167987,8.4970683E-02,1.905E-2
-0.1036147,7.1786687E-02,1.905E-2
-8.4970683E-02,7.1786687E-02,1.905E-2
-7.1786687E-02,8.4970683E-02,1.905E-2
8,0.25,0,3,0
-7.1786687E-02,0.1036147,-1.905E-2
-8.4970683E-02,0.1167987,-1.905E-2
-0.1036147,0.1167987,-1.905E-2
-0.1167987,0.1036147,-1.905E-2
-0.1167987,8.4970683E-02,-1.905E-2
-0.1036147,7.1786687E-02,-1.905E-2
-8.4970683E-02,7.1786687E-02,-1.905E-2
-7.1786687E-02,8.4970683E-02,-1.905E-2
8,0.25,0,3,0
-0.1108440,9.3219997E-03,1.905E-2
-0.1240280,2.2506000E-02,1.905E-2
```

Table A.3 -- Continued

```
-0.1426720,2.2506000E-02,1.905E-2
-0.1558560,9.3219997E-03,1.905E-2
-0.1558560,-9.3219997E-03,1.905E-2
-0.1426720,-2.2506000E-02,1.905E-2
-0.1240280,-2.2506000E-02,1.905E-2
-0.1108440,-9.3219997E-03,1.905E-2
8,0.25,0,3,0
-0.1108440,9.3219997E-03,-1.905E-2
-0.1240280,2.2506000E-02,-1.905E-2
-0.1426720,2.2506000E-02,-1.905E-2
-0.1558560,9.3219997E-03,-1.905E-2
-0.1558560,-9.3219997E-03,-1.905E-2
-0.1426720,-2.2506000E-02,-1.905E-2
-0.1240280,-2.2506000E-02,-1.905E-2
-0.1108440,-9.3219997E-03,-1.905E-2
8,0.25,0,3,0
-7.1786687E-02,-8.4970683E-02,1.905E-2
-8.4970683E-02,-7.1786687E-02,1.905E-2
-0.1036147,-7.1786687E-02,1.905E-2
-0.1167987,-8.4970683E-02,1.905E-2
-0.1167987,-0.1036147,1.905E-2
-0.1036147,-0.1167987,1.905E-2
-8.4970683E-02,-0.1167987,1.905E-2
-7.1786687E-02,-0.1036147,1.905E-2
8,0.25,0,3,0
-7.1786687E-02,-8.4970683E-02,-1.905E-2
-8.4970683E-02,-7.1786687E-02,-1.905E-2
-0.1036147,-7.1786687E-02,-1.905E-2
-0.1167987,-8.4970683E-02,-1.905E-2
-0.1167987,-0.1036147,-1.905E-2
-0.1036147,-0.1167987,-1.905E-2
-8.4970683E-02,-0.1167987,-1.905E-2
-7.1786687E-02,-0.1036147,-1.905E-2
8,0.25,0,3,0
2.2506000E-02,-0.1240280,1.905E-2
9.3219997E-03,-0.1108440,1.905E-2
-9.3219997E-03,-0.1108440,1.905E-2
-2.2506000E-02,-0.1240280,1.905E-2
-2.2506000E-02,-0.1426720,1.905E-2
-9.3219997E-03,-0.1558560,1.905E-2
9.3219997E-03,-0.1558560,1.905E-2
2.2506000E-02,-0.1426720,1.905E-2
8,0.25,0,3,0
2.2506000E-02,-0.1240280,-1.905E-2
9.3219997E-03,-0.1108440,-1.905E-2
-9.3219997E-03,-0.1108440,-1.905E-2
-2.2506000E-02,-0.1240280,-1.905E-2
-2.2506000E-02,-0.1426720,-1.905E-2
-9.3219997E-03,-0.1558560,-1.905E-2
9.3219997E-03,-0.1558560,-1.905E-2
```

Table A.3 -- Continued

```
2.2506000E-02,-0.1426720,-1.905E-2
8,0.25,0,3,0
0.1167987,-8.4970683E-02,1.905E-2
0.1036147,-7.1786687E-02,1.905E-2
8.4970683E-02,-7.1786687E-02,1.905E-2
7.1786687E-02,-8.4970683E-02,1.905E-2
7.1786687E-02,-0.1036147,1.905E-2
8.4970683E-02,-0.1167987,1.905E-2
0.1036147,-0.1167987,1.905E-2
0.1167987,-0.1036147,1.905E-2
8,0.25,0,3,0
0.1167987,-8.4970683E-02,-1.905E-2
0.1036147,-7.1786687E-02,-1.905E-2
8.4970683E-02,-7.1786687E-02,-1.905E-2
7.1786687E-02,-8.4970683E-02,-1.905E-2
7.1786687E-02,-0.1036147,-1.905E-2
8.4970683E-02,-0.1167987,-1.905E-2
0.1036147,-0.1167987,-1.905E-2
0.1167987,-0.1036147,-1.905E-2
8,0.25,0,3,0
0.1558560,9.3219997E-03,1.905E-2
0.1426720,2.2506000E-02,1.905E-2
0.1240280,2.2506000E-02,1.905E-2
0.1108440,9.3219997E-03,1.905E-2
0.1108440,-9.3219997E-03,1.905E-2
0.1240280,-2.2506000E-02,1.905E-2
0.1426720,-2.2506000E-02,1.905E-2
0.1558560,-9.3219997E-03,1.905E-2
8,0.25,0,3,0
0.1558560,9.3219997E-03,-1.905E-2
0.1426720,2.2506000E-02,-1.905E-2
0.1240280,2.2506000E-02,-1.905E-2
0.1108440,9.3219997E-03,-1.905E-2
0.1108440,-9.3219997E-03,-1.905E-2
0.1240280,-2.2506000E-02,-1.905E-2
0.1426720,-2.2506000E-02,-1.905E-2
0.1558560,-9.3219997E-03,-1.905E-2
8,0.25,0,3,0
0.1167987,0.1036147,1.905E-2
0.1036147,0.1167987,1.905E-2
8.4970683E-02,0.1167987,1.905E-2
7.1786687E-02,0.1036147,1.905E-2
7.1786687E-02,8.4970683E-02,1.905E-2
8.4970683E-02,7.1786687E-02,1.905E-2
0.1036147,7.1786687E-02,1.905E-2
0.1167987,8.4970683E-02,1.905E-2
8,0.25,0,3,0
0.1167987,0.1036147,-1.905E-2
0.1036147,0.1167987,-1.905E-2
8.4970683E-02,0.1167987,-1.905E-2
```

Table A.3 -- Continued

```
7.1786687E-02,0.1036147,-1.905E-2
7.1786687E-02,8.4970683E-02,-1.905E-2
8.4970683E-02,7.1786687E-02,-1.905E-2
0.1036147,7.1786687E-02,-1.905E-2
0.1167987,8.4970683E-02,-1.905E-2
8,0.25,0,3,0
2.2506000E-02,0.1426720,1.905E-2
9.3219997E-03,0.1558560,1.905E-2
-9.3219997E-03,0.1558560,1.905E-2
-2.2506000E-02,0.1426720,1.905E-2
-2.2506000E-02,0.1240280,1.905E-2
-9.3219997E-03,0.1108440,1.905E-2
9.3219997E-03,0.1108440,1.905E-2
2.2506000E-02,0.1240280,1.905E-2
8,0.25,0,3,0
2.2506000E-02,0.1426720,-1.905E-2
9.3219997E-03,0.1558560,-1.905E-2
-9.3219997E-03,0.1558560,-1.905E-2
-2.2506000E-02,0.1426720,-1.905E-2
-2.2506000E-02,0.1240280,-1.905E-2
-9.3219997E-03,0.1108440,-1.905E-2
9.3219997E-03,0.1108440,-1.905E-2
2.2506000E-02,0.1240280,-1.905E-2
0,0
18,27,18,9,0,0
0.,0.,1.905E-2
0.,0.,0.
0.,0.,-1.905E-2
-9.429E-2,9.429E-2,1.905E-2
-9.429E-2,9.429E-2,0.
-9.429E-2,9.429E-2,-1.905E-2
-0.13335,0.,1.905E-2
-0.13335,0.,0.
-0.13335,0.,-1.905E-2
-9.429E-2,-9.429E-2,1.905E-2
-9.429E-2,-9.429E-2,0.
-9.429E-2,-9.429E-2,-1.905E-2
0.,-0.13335,1.905E-2
0.,-0.13335,0.
0.,-0.13335,-1.905E-2
9.429E-2,-9.429E-2,1.905E-2
9.429E-2,-9.429E-2,0.
9.429E-2,-9.429E-2,-1.905E-2
0.13335,0.,1.905E-2
0.13335,0.,0.
0.13335,0.,-1.905E-2
9.429E-2,9.429E-2,1.905E-2
9.429E-2,9.429E-2,0.
9.429E-2,9.429E-2,-1.905E-2
0.,0.13335,1.905E-2
```

Table A.3 -- Continued

```
0.,0.13335,0.
0.,0.13335,-1.905E-2
1,2
2,3
4,5
5,6
7,8
8,9
10,11
11,12
13,14
14,15
16,17
17,18
19,20
20,21
22,23
23,24
25,26
26,27
1,1,(0.,0.),(23.906,-159.389)
3,1,(0.,0.),(20.208,-142.638)
5,1,(0.,0.),(20.208,-142.638)
7,1,(0.,0.),(20.208,-142.638)
9,1,(0.,0.),(20.208,-142.638)
11,1,(0.,0.),(20.208,-142.638)
13,1,(0.,0.),(20.208,-142.638)
15,1,(0.,0.),(20.208,-142.638)
17,1,(2.,0.),(20.208,-142.638)
1,0,1,(0.,0.),(0.,0.),0.117
2,1,2,(0.,0.),(0.,0.),0.117
3,0,3,(0.,0.),(0.,0.),0.079
4,1,4,(0.,0.),(0.,0.),0.079
5,0,5,(0.,0.),(0.,0.),0.079
6,1,6,(0.,0.),(0.,0.),0.079
7,0,7,(0.,0.),(0.,0.),0.079
8,1,8,(0.,0.),(0.,0.),0.079
9,0,9,(0.,0.),(0.,0.),0.079
10,1,10,(0.,0.),(0.,0.),0.079
11,0,11,(0.,0.),(0.,0.),0.079
12,1,12,(0.,0.),(0.,0.),0.079
13,0,13,(0.,0.),(0.,0.),0.079
14,1,14,(0.,0.),(0.,0.),0.079
15,0,15,(0.,0.),(0.,0.),0.079
16,1,16,(0.,0.),(0.,0.),0.079
17,0,17,(0.,0.),(0.,0.),0.079
18,1,18,(0.,0.),(0.,0.),0.079
```

Table A.4

Boeing 727 Model with Top-Mounted Off-Centered TCAS III (Two-Monopole Model)

```
UN:INCHES
3
FQ:1.06 GHZ
1,1.06,1.
FG:
74.,74.,1064.,330.
T
0.,0.,50.
PD:
90.,0.,80.
0,360,1
T,1000000.
BO:
T
PP:POLAR PLOT IN DB
F
1,2.,3
PG:LEFT WING
6,T
-48.4,78.,249.
-48.4,277.,411.
-48.4,625.,636.
-48.4,652.,750.
-48.4,250.,587.
-48.4,76.,558.
PG:RIGHT WING
6,T
-48.4,-76.,558.
-48.4,-250.,587.
-48.4,-652.,750.
-48.4,-625.,636.
-48.4,-277.,411.
-48.4,-78.,249.
PG:RIGHT VERTICAL STABILIZER
4,T
40.6,0.,719.
227.6,0.,996.
227.6,-15.,1257.
40.6,-15.,980.
PG:LEFT VERTICAL STABILIZER
4,T
40.6,15.,980.
227.6,15.,1257.
227.6,0.,996.
40.6,0.,719.
```

Table A.4 -- Continued

```
PG:LEFT HORIZONTAL STABILIZER
4,F
214.6,14.,1188.
214.6,210.,1243.
214.6,210.,1172.
214.6,14.,1016.
PG:RIGHT HORIZONTAL STABILIZER
4,F
214.6,-14.,1016.
214.6,-210.,1172.
214.6,-210.,1243.
214.6,-14.,1188.
PG:CENTER ENGINE FRONT
4,T
50.6,22.,652.5
120.6,22.,652.5
120.6,-22.,652.5
50.6,-22.,652.5
PG:CENTER ENGINE LEFT
4,T
45.6,22.,710.
120.6,22.,815.
120.6,22.,652.5
50.6,22.,652.5
PG: CENTER ENGINE RIGHT
4,T
50.6,-22.,652.5
120.6,-22.,652.5
120.6,-22.,815.
45.6,-22.,710.
PG:RIGHT ENGINE TOP
4,F
38.6,-80.,646.
38.6,-80.,837.
38.6,-140.,837.
38.6,-140.,646.
PG:RIGHT ENGINE FRONT
4,F
38.6,-80.,646.
38.6,-140.,646.
-24.4,-140.,646.
-24.4,-80.,646.
PG:RIGHT ENGINE SIDE
4,F
38.6,-80.,646.
-24.4,-80.,646.
-24.4,-80.,837.
38.6,-80.,837.
PG:RIGHT PYLON
4,T
```

Table A.4 - Continued

```
-11.9,-60.,854.
-11.9,-81.,827.
-11.9,-81.,682.
-11.9,-65.,682.
PG:LEFT PYLON
4,T
-11.9,65.,682.
-11.9,81.,682.
-11.9,81.,827.
-11.9,60.,854.
PG:LEFT ENGINE TOP
4,F
38.6,80.,646.
38.6,140.,646.
38.6,140.,837.
38.6,80.,837.
PG:LEFT ENGINE FRONT
4,F
38.6,80.,646.
-24.4,80.,646.
-24.4,140.,646.
38.6,140.,646.
PG:LEFT ENGINE SIDE
4,F
38.6,80.,646.
38.6,80.,837.
-24.4,80.,837.
-24.4,80.,646.
SG:ELEMENT 1
-0.47,45.856
2
1.14,-45.
0.,0.,0.,2.78,3
1.,-45.
1.64,135.
0.,0.,0.,2.78,3
0.698,45.
EX:
SG:ELEMENT 2
0.86,50.
2
1.14,0.
0.,0.,0.,2.78,3
1.,-45.
1.64,180.
0.,0.,0.,2.78,3
0.698,45.
EX:
SG:ELEMENT 3
-0.47,54.144
```

Table A.4 - Continued

```
2
1.14,45.
0.,0.,0.,2.78,3
1.,-45.
1.64,225.
0.,0.,0.,2.78,3
0.698,45.
EX:
SG:ELEMENT 4
-3.683,55.86
2
1.14,90.
0.,0.,0.,2.78,3
1.,-45.
1.64,270.
0.,0.,0.,2.78,3
0.698,45.
EX:
SG:ELEMENT 5
-6.895,54.144
2
1.14,135.
0.,0.,0.,2.78,3
1.,-45.
1.64,-45.
0.,0.,0.,2.78,3
0.698,45.
EX:
SG:ELEMENT 6
-8.224,50.
2
1.14,180.
0.,0.,0.,2.78,3
1.,-45.
1.64,0.
0.,0.,0.,2.78,3
0.698,45.
EX:
SG:ELEMENT 7
-6.886,45.856
2
1.14,225.
0.,0.,0.,2.78,3
1.,-45.
1.64,45.
0.,0.,0.,2.78,3
0.698,45.
EX:
SG:ELEMENT 8
-3.681,44.14
```

Table A.4 - Continued

```
2
1.14,270.
0.,0.,0.,2.78,3
1.,-45.
1.64,90.
0.,0.,0.,2.78,3
0.698,45.
EX:
```

Table A.5

Boeing 727 Model with Top-Mounted Off-Centered TCAS III (Four-Monopole Model)

```
UN:INCHES
3
FQ:1.06 GHZ
1,1.06,1.
FG:
74.,74.,1064.,330.
T
0.,0.,50.
PD:
90.,0.,80.
0,360,1
T,1000000.
BO:
T
PP:POLAR PLOT IN DB
F
1,2.,3
PG:LEFT WING
6,T
-48.4,78.,249.
-48.4,277.,411.
-48.4,625.,636.
-48.4,652.,750.
-48.4,250.,587.
-48.4,76.,558.
PG:RIGHT WING
6,T
-48.4,-76.,558.
-48.4,-250.,587.
-48.4,-652.,750.
-48.4,-625.,636.
-48.4,-277.,411.
-48.4,-78.,249.
PG:RIGHT VERTICAL STABILIZER
4,T
40.6,0.,719.
227.6,0.,996.
227.6,-15.,1257.
40.6,-15.,980.
PG:LEFT VERTICAL STABILIZER
4,T
40.6,15.,980.
227.6,15.,1257.
227.6,0.,996.
40.6,0.,719.
```

Table A.5 - Continued

```
PG:LEFT HORIZONTAL STABILIZER
4,F
214.6,14.,1188.
214.6,210.,1243.
214.6,210.,1172.
214.6,14.,1016.
PG:RIGHT HORIZONTAL STABILIZER
4,F
214.6,-14.,1016.
214.6,-210.,1172.
214.6,-210.,1243.
214.6,-14.,1188.
PG:CENTER ENGINE FRONT
4,T
50.6,22.,652.5
120.6,22.,652.5
120.6,-22.,652.5
50.6,-22.,652.5
PG:CENTER ENGINE LEFT
4,T
45.6,22.,710.
120.6,22.,815.
120.6,22.,652.5
50.6,22.,652.5
PG: CENTER ENGINE RIGHT
4,T
50.6,-22.,652.5
120.6,-22.,652.5
120.6,-22.,815.
45.6,-22.,710.
PG:RIGHT ENGINE TOP
4,F
38.6,-80.,646.
38.6,-80.,837.
38.6,-140.,837.
38.6,-140.,646.
PG:RIGHT ENGINE FRONT
4,F
38.6,-80.,646.
38.6,-140.,646.
-24.4,-140.,646.
-24.4,-80.,646.
PG:RIGHT ENGINE SIDE
4,F
38.6,-80.,646.
-24.4,-80.,646.
-24.4,-80.,837.
38.6,-80.,837.
PG:RIGHT PYLON
4,T
```

Table A.5 - Continued

```
-11.9,-60.,854.
-11.9,-81.,827.
-11.9,-81.,682.
-11.9,-65.,682.
PG:LEFT PYLON
4,T
-11.9,65.,682.
-11.9,81.,682.
-11.9,81.,827.
-11.9,60.,854.
PG:LEFT ENGINE TOP
4,F
38.6,80.,646.
38.6,140.,646.
38.6,140.,837.
38.6,80.,837.
PG:LEFT ENGINE FRONT
4,F
38.6,80.,646.
-24.4,80.,646.
-24.4,140.,646.
38.6,140.,646.
PG:LEFT ENGINE SIDE
4,F
38.6,80.,646.
38.6,80.,837.
-24.4,80.,837.
-24.4,80.,646.
SG:ELEMENT 1 INDUCED CURRENT MODEL ON 727
-3.885,50.262
4
0.,0.
0.,0.,0.,2.78,3
0.3564,102.
5.25,0.
0.,0.,0.,2.78,3
0.4169,103.
5.25,270.
0.,0.,0.,2.78,3
0.4422,101.
5.25,-45.
0.,0.,0.,2.78,3
0.812,-19.
EX:
SG:ELEMENT 2 INDUCED CURRENT MODEL ON 727
-3.969,50.
4
0.,0.
0.,0.,0.,2.78,3
0.3564,102.
```

Table A.5 - Continued

```
5.25,45.
0.,0.,0.,2.78,3
0.4169,103.
5.25,-45.
0.,0.,0.,2.78,3
0.4422,101.
5.25,0.
0.,0.,0.,2.78,3
0.812,-19.
EX:
SG:ELEMENT 3 INDUCED CURRENT MODEL ON 727
-3.88,49.738
4
0.,0.
0.,0.,0.,2.78,3
0.3564,102.
5.25,90.
0.,0.,0.,2.78,3
0.4169,103.
5.25,0.
0.,0.,0.,2.78,3
0.4422,101.
5.25,45.
0.,0.,0.,2.78,3
0.812,-19.
EX:
SG:ELEMENT 4 INDUCED CURRENT MODEL ON 727
-3.682,49.63
4
0.,0.
0.,0.,0.,2.78,3
0.3564,102.
5.25,135.
0.,0.,0.,2.78,3
0.4169,103.
5.25,45.
0.,0.,0.,2.78,3
0.4422,101.
5.25,90.
0.,0.,0.,2.78,3
0.812,-19.
EX:
SG:ELEMENT 5 INDUCED CURRENT MODEL ON 727
-3.479,49.738
4
0.,0.
0.,0.,0.,2.78,3
0.3564,102.
5.25,180.
0.,0.,0.,2.78,3
```

Table A.5 - Continued

```
0.4169,103.
5.25,90.
0.,0.,0.,2.78,3
0.4422,101.
5.25,135.
0.,0.,0.,2.78,3
0.812,-19.
EX:
SG:ELEMENT 6 INDUCED CURRENT MODEL ON 727
-3.395,50.
4
0.,0.
0.,0.,0.,2.78,3
0.3564,102.
5.25,225.
0.,0.,0.,2.78,3
0.4169,103.
5.25,135.
0.,0.,0.,2.78,3
0.4422,101.
5.25,180.
0.,0.,0.,2.78,3
0.812,-19.
EX:
SG:ELEMENT 7 INDUCED CURRENT MODEL ON 727
-3.479,50.262
4
0.,0.
0.,0.,0.,2.78,3
0.3564,102.
5.25,270.
0.,0.,0.,2.78,3
0.4169,103.
5.25,180.
0.,0.,0.,2.78,3
0.4422,101.
5.25,225.
0.,0.,0.,2.78,3
0.812,-19.
EX:
SG:ELEMENT 8 INDUCED CURRENT MODEL ON 727
-3.682,50.37
4
0.,0.
0.,0.,0.,2.78,3
0.3564,102.
5.25,-45.
0.,0.,0.,2.78,3
0.4169,103.
5.25,225.
```

Table A.5 - Continued

```
0.,0.,0.,2.78,3
0.4422,101.
5.25,270.
0.,0.,0.,2.78,3
0.812,-19.
EX:
```

Table A.6

Boeing 727 Model with Top-Mounted Off-Centered TCAS II (Nine-Monopole Model)

```
UN:INCHES
3
FQ:1.06 GHZ
1,1.06,1.
FG:BOEING 727
74.,74.,1064.,330.
T
0.,0.,50.
PD:
90.,0.,80.
0,360,1
T,1000000.
BO:
T
PP:POLAR PLOT IN DB
F
1,2.,3
PG:LEFT WING
6,T
-48.4,78.,249.
-48.4,277.,411.
-48.4,625.,636.
-48.4,652.,750.
-48.4,250.,587.
-48.4,76.,558.
PG:RIGHT WING
6,T
-48.4,-76.,558.
-48.4,-250.,587.
-48.4,-652.,750.
-48.4,-625.,636.
-48.4,-277.,411.
-48.4,-78.,249.
PG:RIGHT VERTICAL STABILIZER
4,T
40.6,0.,719.
227.6,0.,996.
227.6,-15.,1257.
40.6,-15.,980.
PG:LEFT VERTICAL STABILIZER
4,T
40.6,15.,980.
227.6,15.,1257.
227.6,0.,996.
40.6,0.,719.
```

Table A.6 - Continued

```
PG:LEFT HORIZONTAL STABILIZER
4,F
214.6,14.,1188.
214.6,210.,1243.
214.6,210.,1172.
214.6,14.,1016.
PG:RIGHT HORIZONTAL STABILIZER
4,F
214.6,-14.,1016.
214.6,-210.,1172.
214.6,-210.,1243.
214.6,-14.,1188.
PG:CENTER ENGINE FRONT
4,T
50.6,22.,652.5
120.6,22.,652.5
120.6,-22.,652.5
50.6,-22.,652.5
PG:CENTER ENGINE LEFT
4,T
45.6,22.,710.
120.6,22.,815.
120.6,22.,652.5
50.6,22.,652.5
PG: CENTER ENGINE RIGHT
4,T
50.6,-22.,652.5
120.6,-22.,652.5
120.6,-22.,815.
45.6,-22.,710.
PG:RIGHT ENGINE TOP
4,F
38.6,-80.,646.
38.6,-80.,837.
38.6,-140.,837.
38.6,-140.,646.
PG:RIGHT ENGINE FRONT
4,F
38.6,-80.,646.
38.6,-140.,646.
-24.4,-140.,646.
-24.4,-80.,646.
PG:RIGHT ENGINE SIDE
4,F
38.6,-80.,646.
-24.4,-80.,646.
-24.4,-80.,837.
38.6,-80.,837.
PG:RIGHT PYLON
4,T
```

Table A.6 - Continued

```
-11.9,-60.,854.
-11.9,-81.,827.
-11.9,-81.,682.
-11.9,-65.,682.
PG:LEFT PYLON
4,T
-11.9,65.,682.
-11.9,81.,682.
-11.9,81.,827.
-11.9,60.,854.
PG:LEFT ENGINE TOP
4,F
38.6,80.,646.
38.6,140.,646.
38.6,140.,837.
38.6,80.,837.
PG:LEFT ENGINE FRONT
4,F
38.6,80.,646.
-24.4,80.,646.
-24.4,140.,646.
38.6,140.,646.
PG:LEFT ENGINE SIDE
4,F
38.6,80.,646.
38.6,80.,837.
-24.4,80.,837.
-24.4,80.,646.
SG:ELEMENT 1
-3.682,50.
9
0.,0.
0.,0.,0.,2.78,3
0.198,102.
5.25,0.
0.,0.,0.,2.78,3
0.379,103.
5.25,45.
0.,0.,0.,2.78,3
0.113,-143.
5.25,90.
0.,0.,0.,2.78,3
0.081,-93.
5.25,135.
0.,0.,0.,2.78,3
0.058,-88.
5.25,180.
0.,0.,0.,2.78,3
0.078,-97.
5.25,225.
```

Table A.6 - Continued

```
0.,0.,0.,2.78,3
0.109,-142.
5.25,270.
0.,0.,0.,2.78,3
0.402,101.
5.25,315.
0.,0.,0.,2.78,3
0.812,-19.
EX:
SG:ELEMENT 2
-3.682,50.
9
0.,0.
0.,0.,0.,2.78,3
0.198,102.
5.25,45.
0.,0.,0.,2.78,3
0.379,103.
5.25,90.
0.,0.,0.,2.78,3
0.113,-143.
5.25,135.
0.,0.,0.,2.78,3
0.081,-93.
5.25,180.
0.,0.,0.,2.78,3
0.058,-88.
5.25,225.
0.,0.,0.,2.78,3
0.078,-97.
5.25,270.
0.,0.,0.,2.78,3
0.109,-142.
5.25,315.
0.,0.,0.,2.78,3
0.402,101.
5.25,0.
0.,0.,0.,2.78,3
0.812,-19.
EX:
SG:ELEMENT 3
-3.682,50.
9
0.,0.
0.,0.,0.,2.78,3
0.198,102.
5.25,90.
0.,0.,0.,2.78,3
0.379,103.
5.25,135.
```

Table A.6 - Continued

```
0.,0.,0.,2.78,3
0.113,-143.
5.25,180.
0.,0.,0.,2.78,3
0.081,-93.
5.25,225.
0.,0.,0.,2.78,3
0.058,-88.
5.25,270.
0.,0.,0.,2.78,3
0.078,-97.
5.25,315.
0.,0.,0.,2.78,3
0.109,-142.
5.25,0.
0.,0.,0.,2.78,3
0.402,101.
5.25,45.
0.,0.,0.,2.78,3
0.812,-19.
EX:
SG:ELEMENT 4
-3.682,50.
9
0.,0.
0.,0.,0.,2.78,3
0.198,102.
5.25,135.
0.,0.,0.,2.78,3
0.379,103.
5.25,180.
0.,0.,0.,2.78,3
0.113,-143.
5.25,225.
0.,0.,0.,2.78,3
0.081,-93.
5.25,270.
0.,0.,0.,2.78,3
0.058,-88.
5.25,315.
0.,0.,0.,2.78,3
0.078,-97.
5.25,0.
0.,0.,0.,2.78,3
0.109,-142.
5.25,45.
0.,0.,0.,2.78,3
0.402,101.
5.25,90.
0.,0.,0.,2.78,3
```

Table A.6 - Continued

```
0.812,-19.
EX:
SG:ELEMENT 5
-3.682,50.
9
0.,0.
0.,0.,0.,2.78,3
0.198,102.
5.25,180.
0.,0.,0.,2.78,3
0.379,103.
5.25,225.
0.,0.,0.,2.78,3
0.113,-143.
5.25,270.
0.,0.,0.,2.78,3
0.081,-93.
5.25,315.
0.,0.,0.,2.78,3
0.058,-88.
5.25,0.
0.,0.,0.,2.78,3
0.078,-97.
5.25,45.
0.,0.,0.,2.78,3
0.109,-142.
5.25,90.
0.,0.,0.,2.78,3
0.402,101.
5.25,135.
0.,0.,0.,2.78,3
0.812,-19.
EX:
SG:ELEMENT 6
-3.682,50.
9
0.,0.
0.,0.,0.,2.78,3
0.198,102.
5.25,225.
0.,0.,0.,2.78,3
0.379,103.
5.25,270.
0.,0.,0.,2.78,3
0.113,-143.
5.25,315.
0.,0.,0.,2.78,3
0.081,-93.
5.25,0.
0.,0.,0.,2.78,3
```

Table A.6 - Continued

```
0.058,-88.
5.25,45.
0.,0.,0.,2.78,3
0.078,-97.
5.25,90.
0.,0.,0.,2.78,3
0.109,-142.
5.25,135.
0.,0.,0.,2.78,3
0.402,101.
5.25,180.
0.,0.,0.,2.78,3
0.812,-19.
EX:
SG:ELEMENT 7
-3.682,50.
9
0.,0.
0.,0.,0.,2.78,3
0.198,102.
5.25,270.
0.,0.,0.,2.78,3
0.379,103.
5.25,315.
0.,0.,0.,2.78,3
0.113,-143.
5.25,0.
0.,0.,0.,2.78,3
0.081,-93.
5.25,45.
0.,0.,0.,2.78,3
0.058,-88.
5.25,90.
0.,0.,0.,2.78,3
0.078,-97.
5.25,135.
0.,0.,0.,2.78,3
0.109,-142.
5.25,180.
0.,0.,0.,2.78,3
0.402,101.
5.25,225.
0.,0.,0.,2.78,3
0.812,-19.
EX:
SG:ELEMENT 8
-3.682,50.
9
0.,0.
0.,0.,0.,2.78,3
```

Table A.6 - Continued

```
0.198,102.
5.25,-45.
0.,0.,0.,2.78,3
0.379,103.
5.25,0.
0.,0.,0.,2.78,3
0.113,-143.
5.25,45.
0.,0.,0.,2.78,3
0.081,-93.
5.25,90.
0.,0.,0.,2.78,3
0.058,-88.
5.25,135.
0.,0.,0.,2.78,3
0.078,-97.
5.25,180.
0.,0.,0.,2.78,3
0.109,-142.
5.25,225.
0.,0.,0.,2.78,3
0.402,101.
5.25,270.
0.,0.,0.,2.78,3
0.812,-19.
EX:
```

APPENDIX B

SCATTERING ERROR CURVES

The basic concepts of the scattering error curves are discussed in [3] and [4]. The scattering error curve indicates the errors of the TCAS III system due to the scattering and diffraction by the irregular structure of the aircraft. These curves help to investigate the performance of the TCAS III system.

The first topic discussed here is how to generate scattering error curves. Figure B.1 is a simple flow chart to generate the error curves. The first step is to get a lookup monopulse curve as shown in Figure B.2. First, the TCAS III system is mounted on the fuselage of an aircraft without any plates, and then the Aircraft Code is executed to obtain the radiation patterns. These patterns are referred to as the lookup table and are used to calibrate the system. Then, another program combines these radiation patterns to obtain pairs of sum and difference patterns in 64 different directions. Monopulse curves can then be generated from each pair of sum and difference patterns. According to the research of [3], these lookup monopulse curves do not change significantly when the elevation angle is changed. Also, because in most cases the elevation angles of the target appear in the vicinity of 10°, the lookup monopulse curves are generated for an elevation angle of 10° only.

Following the same procedures, another group of the monopulse curves, where the TCAS III is mounted on the same fuselage with all

plates included, is generated for various elevation angles. As shown in Figure B.2, the lookup monopulse curve is very smooth but the monopulse curve generated with the complete model of the airplane is distorted by the scattering and diffraction of those plates.

Now there are two monopulse curves for each direction of the 64 different bearings; one is error-free and another contains errors. Figure B.2 also shows the process followed to generate the error curve from these two monopulse curves [4]. For example, if the transponder receives a value of 4 dB corresponding to a bearing of 1° off boresight, the lookup monopulse curve indicates the real target's bearing of 7° off boresight. Thus, the error in detecting the target's bearing is 6°. By computing the error for each bearing at a specific elevation angle, an error curve is obtained. Figures 3.5 and 3.6 show some typical examples. The resolution of the bearing in the error curves is 1 degree.

Figure B.3 shows the convention of error curves. It should always be kept in mind that $\phi_{error} = \phi_{detected} - \phi_{real}$. In this convention, if the TCAS is put on the center line of the aircraft, its error curve should be asymmetric because of the symmetric structure of the airplane. Figure 3.8 shows some examples of this situation.

There are two statistical values appearing in each error curve graph. One is the average error and the other is the standard deviation. Because the error curve is asymmetric in most cases, the average value will be close to zero and therefore it is not meaningful. Thus, the standard deviation is more meaningful when the performance of the TCAS system is evaluated.

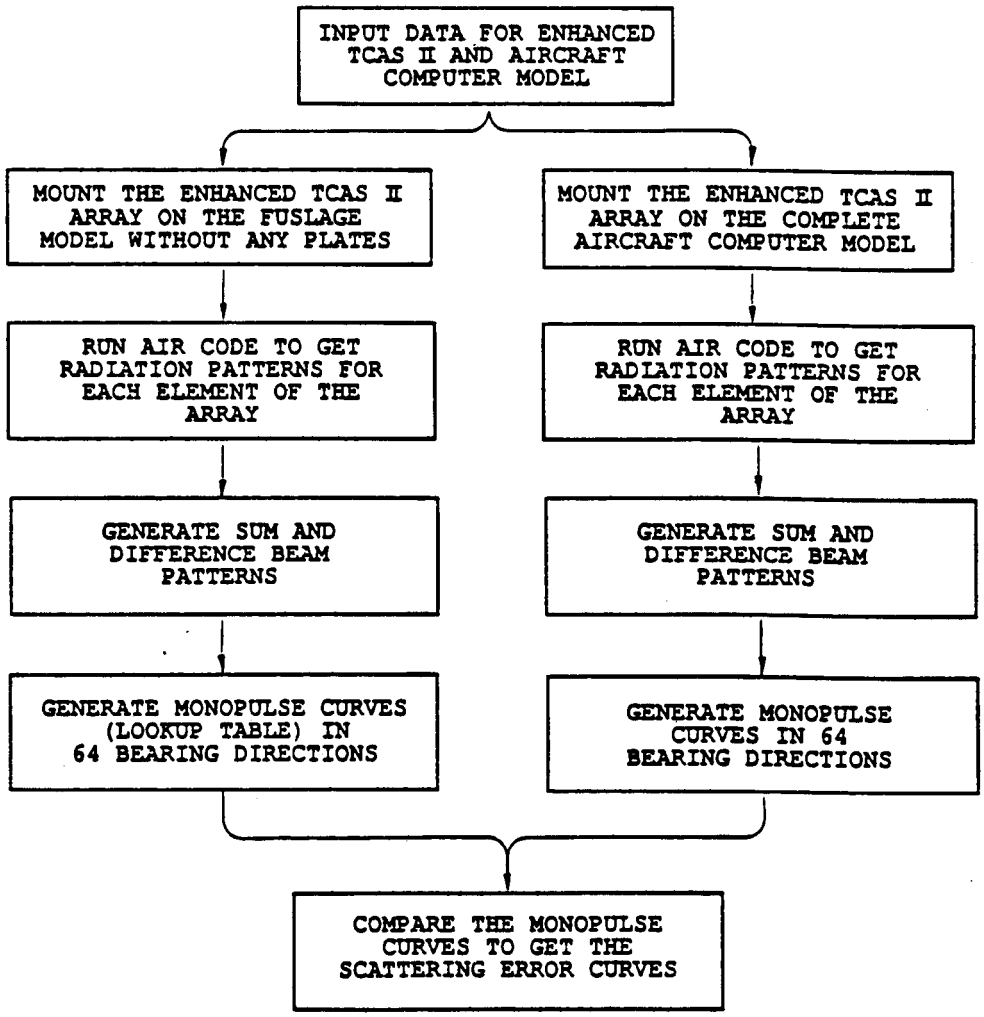

Figure B.1. Flow chart to generate a scattering error curve.

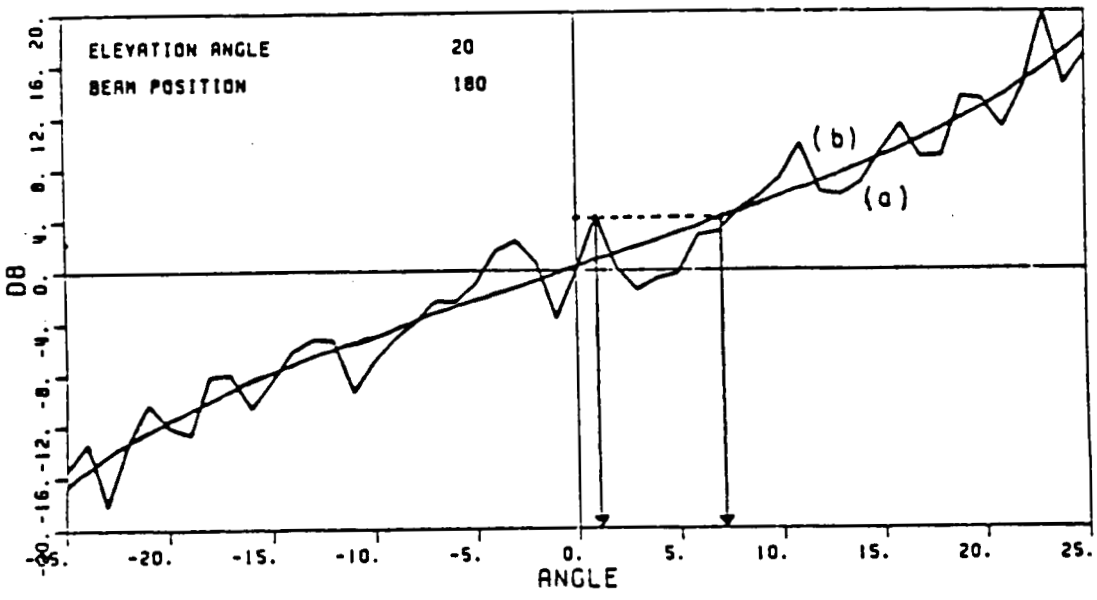

Figure B.2. Procedure followed to generate the error curve from received and lookup monopulse curves [4].

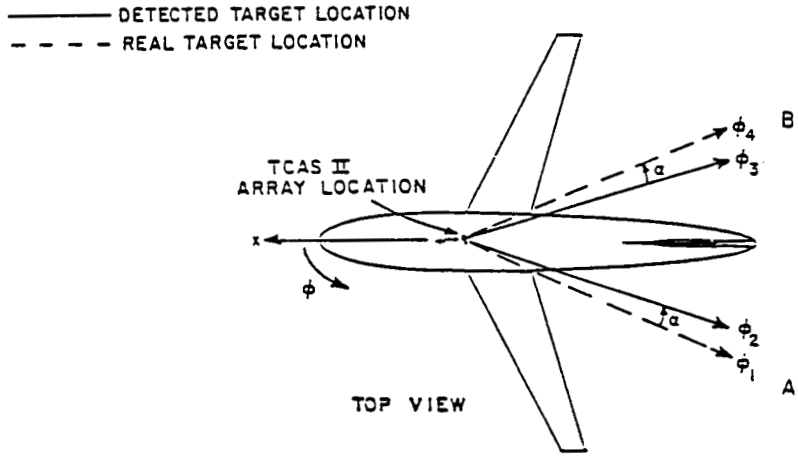

When the target is at A, the bearing error is $\phi_2-\phi_1=\alpha$.
When the target is B, the bearing error is $\phi_3-\phi_4=-\alpha$.

Figure B.3. The convention used to generate the scattering error curve [4].

APPENDIX C

CALCULATION OF RELATIVE POSITION AND VELOCITY

This appendix discusses the transformation between the earth-fixed coordinate system and the airplane-fixed coordinate system. The main differences between these two coordinates are that the former has a fixed origin and fixed coordinate vectors $\hat{x},\hat{y},\hat{z}$; but the latter fixes its coordinates on the flying TCAS array with dynamic coordinate vectors $\hat{x}_r,\hat{y}_r,\hat{z}_r$, which are explained in detail in Section B of Chapter IV.

Assume that

$$\vec{G}(t) = g_x(t)\hat{x} + g_y(t)\hat{y} + g_z(t)\hat{z} \ , \qquad (C.1)$$

$$\vec{F}(t) = f_x(t)\hat{x} + f_y(t)\hat{y} + f_z(t)\hat{z} \ , \qquad (C.2)$$

then

$$\vec{R}(t) = \vec{F}(t) - \vec{G}(t) \ , \qquad (C.3)$$

where $\vec{G}$ is the position of the TCAS-equipped airplane in the earth-fixed coordinate system, $\vec{F}$ is the position of the target in the earth-fixed coordinate system, and $\vec{R}$ is the relative position of the target.

Since $\hat{x}_r$ is the forward direction of the TCAS-equipped airplane,

$$\hat{x}_r = \frac{\vec{V}_G}{\left|\vec{V}_G\right|} \tag{C.4}$$

where

$$\vec{V}_G = \vec{G}'(t) = g_x'\hat{x} + g_y'\hat{y} + g_z'\hat{z} \tag{C.5}$$

and

$$\left|\vec{V}_G\right| = \sqrt{(g_x')^2 + (g_y')^2 + (g_z')^2} \tag{C.6}$$

is the speed of the TCAS array in the earth-fixed coordinate system. Since $\hat{z}_r = \hat{z}$, it follows that

$$\hat{y}_r = \hat{z}_r \times \hat{x}_r = \frac{g_x'\,\hat{y} - g_y'\,\hat{x}}{\left|\vec{V}_G\right|} \quad . \tag{C.7}$$

The two aircraft are flying in the x-y plane, which is parallel to the ground, i.e., $g_z' = f_z' = 0$. Of course, if $g_z' \neq 0$ and $f_z' \neq 0$, this algorithm can be extended to this general case. From (C.4) and (C.7), it follows that

$$\hat{x} = \frac{g_x'\,\hat{x}_r - g_y'\,\hat{y}_r}{\left|\vec{V}_G\right|} \quad , \tag{C.8}$$

$$\hat{y} = \frac{g_y'\,\hat{x}_r + g_x'\,\hat{y}_r}{\left|\vec{V}_G\right|} \quad . \tag{C.9}$$

Then

$$\vec{R}(t) = \hat{x}(f_x-g_x) + \hat{y}(f_y-g_y) + \hat{z}(f_z-g_z)$$

$$= \hat{x}_r \cdot \frac{g_x'(f_x-g_x) + g_y'(f_y-g_y)}{|\vec{V}_G|} +$$

$$+ \hat{y}_r \cdot \frac{-g_y'(f_x-g_x) + g_x'(f_y-g_y)}{|\vec{V}_G|} + \hat{z}_r \cdot (f_z-g_z) \ . \quad (C.10)$$

Therefore, if the position and velocity of the two aircraft in the earth-fixed coordinate system are known, the relative path in the airplane-fixed coordinate system can be obtained from the previous equation.

The relative velocity is the derivative of the relative path, namely

$$\vec{R}'(t) = \hat{x}_r \cdot \frac{g_x''(f_x-g_x) + g_x'(f_x'-g_x') + g_y''(f_y-g_y) + g_y'(f_y'-g_y')}{|\vec{V}_G|}$$

$$+ \hat{y}_r \cdot \frac{g_x''(f_y-g_y) + g_x'(f_y'-g_y') - g_y''(f_x-g_x) - g_y'(f_x'-g_x')}{|\vec{V}_G|}$$

(C.11)

If the two aircraft are flying straight, Equations (C.10) and (C.11) can be simplified. If $\hat{x}_r=\hat{x}$ and $\hat{y}_r=\hat{y}$ are chosen initially, then

$$\vec{R}(t) = \hat{x}_r(f_x-g_x) + \hat{y}_r(f_y-g_y) + \hat{z}_r(f_z-g_z) \ , \quad (C.12)$$

$$\vec{R}'(t) = \hat{x}_r(f_x'-V_G) + \hat{y}_r \cdot f_y' \quad (C.13)$$

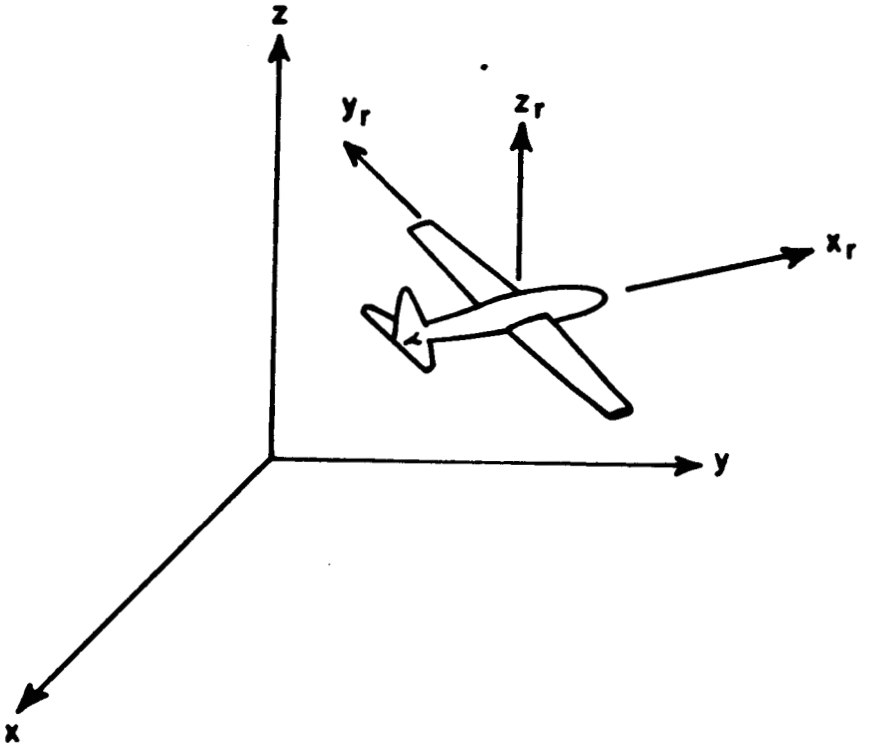

Figure C.1. Earth-fixed coordinate system (x,y,z) and airplane-fixed coordinate system (x_r,y_r,z_r).

APPENDIX D

ALGORITHM OF ESCAPE CURVE CALCULATION

In Chapter IV, Section E, the relationship of the bank angle and normal acceleration is discussed. In this section, the calculation of the contribution of a_n to the motion of the aircraft will be discussed. Also, a numerical algorithm which can be used in the calculation of the escape curve is proposed.

In the earth-fixed coordinate system, the position of the TCAS-equipped airplane is given by

$$\vec{r}(t) = \hat{x}f(t) + \hat{y}g(t) \ . \tag{D.1}$$

Its velocity can be easily calculated, namely

$$\vec{V}(t) = \vec{r}'(t) = \hat{x}f'(t) + \hat{y}g'(t) \tag{D.2}$$

and its acceleration also follows immediately,

$$\vec{A}(t) = \vec{r}''(t) = \hat{x}f''(t) + \hat{y}g''(t) \ . \tag{D.3}$$

The speed, which is the magnitude of its velocity, is given by

$$V = |\vec{V}(t)| = \sqrt{f'(t)^2 + g'(t)^2} \tag{D.4}$$

and the magnitude of its acceleration is

$$A = |\vec{A}(t)| = \sqrt{f''(t)^2 + g''(t)^2} \quad . \tag{D.5}$$

From Figure D.1, the acceleration can be decomposed into two orthogonal parts, tangential acceleration a_t and normal acceleration a_n:

$$\vec{A} = a_t \vec{T} + a_n \vec{N} \tag{D.6}$$

where

$$a_t = \frac{dV}{dt} = \frac{f'(t)\cdot f''(t) + g'(t)\cdot g''(t)}{V} \tag{D.7}$$

and

$$a_n = \sqrt{A^2 - a_t^2} = \frac{|f''(t)g'(t) - g''(t)f'(t)|}{V} \quad . \tag{D.8}$$

For a typical escape curve discussed in Chapter IV, section E, a_t=0 and a_n=gtanϕ, because the aircraft always keeps a constant speed.

If we know the position, velocity and acceleration of an object at time T, how can we calculate its new position, velocity and acceleration at the next time T+ΔT? Equations (D.9) through (D.14) are recursive equations which answer this question, namely

$$X(T+\Delta T) = X(T) + V_X(T)\cdot \Delta T \tag{D.9}$$

$$Y(T+\Delta T) = Y(T) + V_Y(T)\cdot \Delta T \tag{D.10}$$

$$V_X(T+\Delta T) = V_X(T) + A_X(T)\cdot \Delta T \tag{D.11}$$

$$V_Y(T+\Delta T) = V_Y(T) + A_Y(T)\cdot\Delta T \tag{D.12}$$

$$A_X(T) = -\frac{V_Y(T)}{V(T)} \cdot a_n(T) \tag{D.13}$$

$$A_Y(T) = \frac{V_X(T)}{V(T)} \cdot a_n(T) \tag{D.14}$$

where in the earth-fixed coordinate system:

X,Y: positions in x,y coordinates,

V_x,V_y: velocities in x,y directions,

A_x,A_y: acceleration in x,y directions.

Accuracy and cost are the most important factors to be considered in a numerical calculation. Double precision is used here to improve the accuracy. Also, the time period ΔT in the calculation will influence the accuracy and CPU time needed. Figure D.2 is a test for this numerical method. The aircraft maintains a constant speed of 250 knots and a constant bank angle of 45° but with a different ΔT in the two cases. The curves should be circles due to a constant normal acceleration. Also, the accuracy can be verified from the turn radius r from (4.1) and from the figures. From Table D.1, the accuracy of the calculation for 0.01 second period is good enough and it is chosen for our simulation of the escape curves.

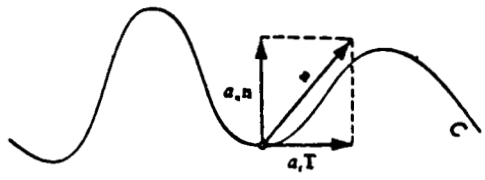

Figure D.1. The decomposition of the acceleration.

Table D.1

Comparison of the Testing

$$\text{Ideal turn radius} = \frac{(250 \text{ knots})}{g * \tan 45^\circ} = 5544.995 \text{ ft}$$

Time division	Turn radius (ft)	Error
0.01 sec	5550.915	0.1%
0.001 sec	5545.105	0.002%

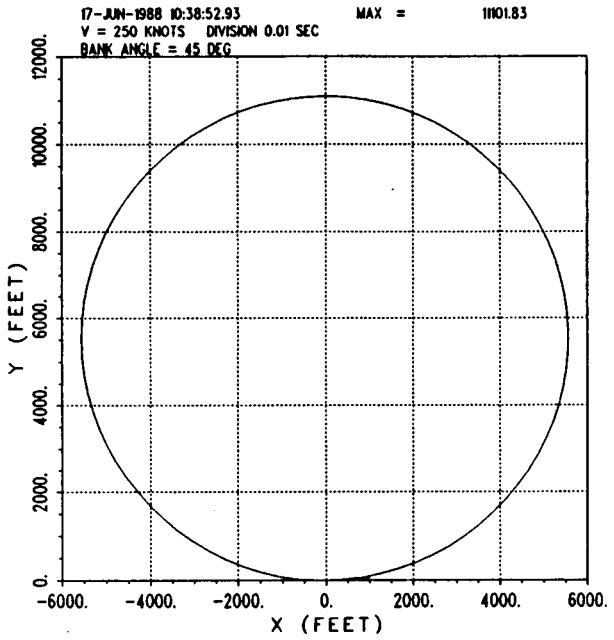

(a) Time period (ΔT) of 0.01 second

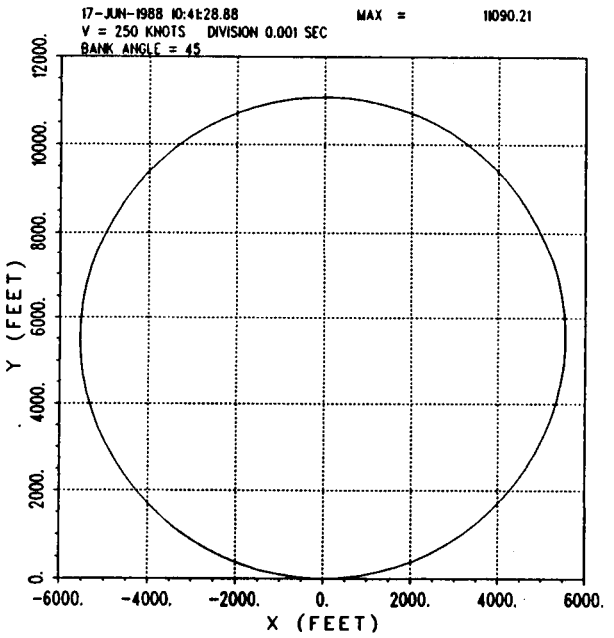

(b) Time period (ΔT) of 0.001 second

Figure D.2. Tests of escape curve algorithm.

APPENDIX E

ROLLING EFFECTS TO ELEVATION ANGLE AND AZIMUTH ANGLE

There are two coordinate systems used in the calculations of the elevation and azimuth angles; namely, the airplane-fixed coordinate system and the TCAS-fixed coordinate system. The only difference between these two coordinate systems is explained in Chapter IV, Section B. Originally, the calculations of the elevation and azimuth angles of the target are very simple in the airplane-fixed coordinate system because it is parallel to the earth-fixed coordinate system and thus the relative path in the airplane-fixed coordinate system can be deduced easily as shown in Appendix C. However, when the TCAS-equipped aircraft turns, the calculations of the elevation and azimuth angles on the TCAS-fixed coordinate system are not simple any more, and it requires a transformation between these two systems, i.e., airplane-fixed and TCAS-fixed coordinate systems.

From Figure E.1, the x'-y' plane can be expressed as:

$$\sin\theta_B \cdot y + \cos\theta_B \cdot z = 0 \quad . \tag{E.1}$$

The elevation angle is the angle between $\vec{r}$ and the x'-y' plane, which is $90°-\theta'$. Furthermore,

$$\theta' = \cos^{-1} \frac{\vec{r}\cdot\vec{n}}{|\vec{r}|}$$

$$= \cos^{-1} \frac{y \sin\theta_B + z\cos\theta_B}{\sqrt{x^2+y^2+z^2}} \quad . \tag{E.2}$$

The transformation between the two systems can be expressed as follows:

$$\begin{bmatrix} x' \\ y' \\ z' \end{bmatrix} = \begin{bmatrix} 1 & 0 & 0 \\ 0 & \cos\theta_B & -\sin\theta_B \\ 0 & \sin\theta_B & \cos\theta_B \end{bmatrix} \begin{bmatrix} x \\ y \\ z \end{bmatrix} \tag{E.3}$$

where (x',y',z') is the target's position in the TCAS-fixed coordinate. The azimuth angle ϕ' in the TCAS-fixed coordinate system is then given by

$$\phi' = \tan^{-1} \frac{y'}{x'}$$

$$= \tan^{-1} \left(\frac{y\cdot\cos\theta_B - z\cdot\sin\theta_B}{x} \right) \quad . \tag{E.4}$$

Then ϕ' and θ' of the TCAS-fixed coordinate system are deduced from the data in the airplane-fixed coordinate system. When the TCAS system obtains a detected bearing ϕ', relative height h and distance R, an inverse transformation is required to find the relative positions in the airplane-fixed coordinate system. Recall that R, h and ϕ' can be written as follows:

$$R = \sqrt{x^2+y^2+z^2} = \sqrt{x'^2+y'^2+z'^2} \tag{E.5}$$

$$h = Z \tag{E.6}$$

$$\phi' = \tan^{-1} \frac{y'}{x'} \tag{E.7}$$

Then from (E.4)

$$\tan\phi' = \frac{y\cos\theta_B - z\sin\theta_B}{x} \quad . \tag{E.8}$$

Finally, let

$$m = \frac{\tan\phi'}{\cos\theta_B} \ , \tag{E.9}$$

$$c = h \cdot \tan\theta_B \ , \tag{E.10}$$

and

$$r^2 = x^2+y^2 = R^2-h^2 \ . \tag{E.11}$$

Solving for (E.5), (E.6) and (E.8), one gets

$$x = \frac{-mc + \sqrt{(m^2+1)r^2-c^2}}{m^2+1} \tag{E.12}$$

and

$$y = mx + C \ . \tag{E.13}$$

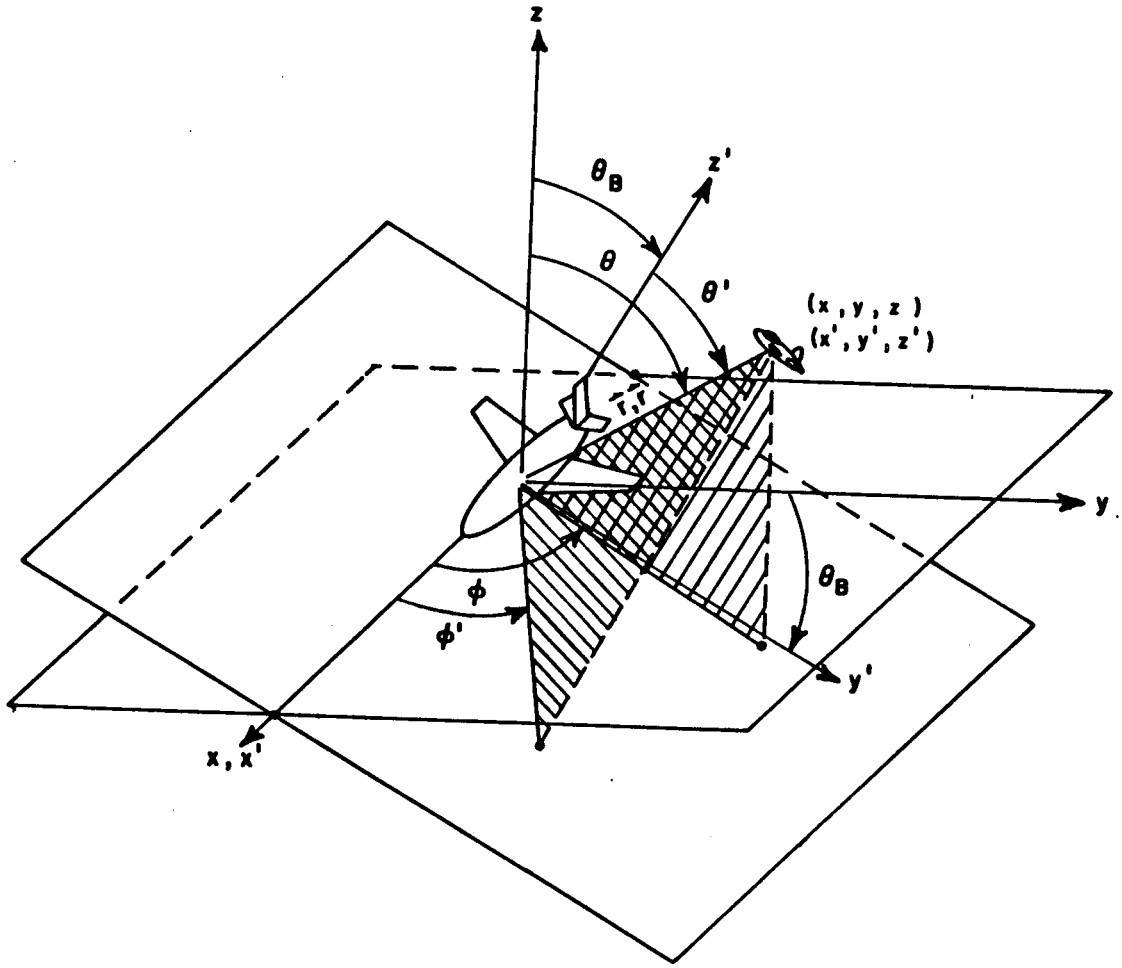

x,y,z : airplane-fixed coordinate system

x′,y′,z′: TCAS-fixed coordinate system

θ_B : bank angle

$\vec{r}$: target position

θ,ϕ : elevation and azimuth angles in the airplane-fixed coordinate system

θ',ϕ' : elevation and azimuth angles in the TCAS-fixed coordinate system

Figure E.1. Airplane-fixed coordinate system and TCAS-fixed coordinate system.

APPENDIX F

GAUSSIAN NOISE GENERATOR

Suppose we want to implement a random noise generator which can generate random numbers with Gaussian distribution $N(\mu,\sigma^2)$, where μ is the mean and σ^2 is the variance. In the FORTRAN language, there is a RAN function, which generates random numbers with a uniform distribution in [0,1). Then the mean value of this distribution is $\frac{1}{2}$; and the variance of this distribution is $\frac{1}{12}$.

From the Central Limit Theorem [20], let $x_1, x_2, \ldots, x_n$ be a sequence of independent random variables with mean value μ_i and variance σ_i^2. Let $x=x_1+\ldots+x_n$, then

$$\lim_{n\to\infty} \frac{x - \sum_{i=1}^{n} \mu_i}{\sqrt{\sum_{i=1}^{n} \sigma_i^2}}$$

will be approximately the normal distribution with mean 0 and variance 1. Furthermore, if X has the normal distribution $N(\mu,\sigma^2)$ and if $Y=ax+b$, then Y has the distribution $N(a\mu+b,a^2\sigma^2)$ [20].

From the above two theorems, the Gaussian distribution can be generated by the combination of uniform distribution as follows:

$$N(\mu,\sigma^2) = \sigma * \frac{\sum_{i=1}^{n} (RAN(x) - \frac{1}{2})}{\sqrt{\frac{n}{12}}} + \mu \quad . \tag{F.1}$$

In our case, $\mu=0$, σ is given by (4.9) and n is chosen as 12 for simplicity; hence, (F.1) becomes

$$N(0,\sigma^2) = \sigma * \sum_{i=1}^{12} (RAN(X) - 0.5). \tag{F.2}$$

This formula is used in our program to simulate the generation of Gaussian noise.

REFERENCES

[1] R.G. Rojas, W.D. Burnside, P. Law, B. Grandchamp, "Simulation of the Enhanced Traffic Alert and Collision Avoidance System (TCAS II)," The Ohio State University ElectroScience Laboratory Technical Report 716199-3, generated under Grant NSG 1498, for NASA, Langley Research Center, Hampton, Virginia, September 1985.

[2] W.D. Burnside, J.J. Kim, B. Grandchamp, R.G. Rojas and P.H. Law, "Airborne Antenna Radiation Pattern Code User's Manual," The Ohio State University ElectroScience Laboratory Technical Report 716199-4, generated under Grant NSG 1498, for NASA, Langley Research Center, Hampton, Virginia, September 1985.

[3] P.H. Law, W.D. Burnside and R.G. Rojas, "A Study of a Collision Avoidance System," The Ohio State University ElectroScience Laboratory Technical Report 716199-8, generated under Grant NSG 1498, for NASA, Langley Research Center, Hampton, Virginia, March 1986.

[4] R.G. Rojas, P. Law and W.D. Burnside, "Simulation of an Enhanced TCAS II System in Operation," The Ohio State University ElectroScience Laboratory Technical Report 716199-9, generated under Grant NSG 1498, for NASA, Langley Research Center, Hampton, Virginia, October 1987.

[5] B.J. Grandchamp, W.D. Burnside, R.G. Rojas, "A Study of the TCAS II Collision Avoidance System Mounted on a Boeing 737 Aircraft," Tech. Rpt. 716199-10, generated under Grant NSG 1498, for NASA, Langley Resarch Center, Hampton, VA, Dec. 1985.

[6] E.H. Newman, "A User's Manual for Electromagnetic Surface Patch (ESP) Code: Version II - Polygonal Plates and Wires," The Ohio State University ElectroScience Laboratory Technical Report 717067-4, generated under Contract N00014-78-C-0049 for Rockwell International Corporation, Los Angeles, California, May 1985.

[7] E.H. Newman and R.L. Dilsavor, "A User's Manual for Electromagnetic Surface Patch Code: ESP Version III," The Ohio State University ElectroScience Laboratory Technical Report 716148-19, generated under Grant NSG 1613, for NASA, Langley Research Center, Hampton, Virginia, May 1987.

[8] H.H. Hurt, Jr., "Aerodynamics for Naval Aviators," U.S. Navy, January 1985.

[9] A.I. Sinsky, "Alpha-Beta Tracking Errors for Orbiting Targets," Report No. BCD-TN-81-033, Bendix Communications Division, June 1981.

[10] A.I. Sinsky, "Miss Distance Prediction Algorithm," Report No. BCD-TN-84-004, Bendix Communications Division, July 1982.

[11] A.I. Sinsky and R.J. Tier, "System Angle Accuracy Prediction," Report BCD-TN-82-035, Bendix Communications Division, July 1982.

[12] "Enhanced TCAS II," Bimonthly Review, Bendix Communications Division, February 1984.

[13] "Enhanced TCAS II System Summary," Report No. BCD-TR-098, Bendix Communications Division, February 1984.

[14] A.I. Sinsky, J.E. Reed and J. Fee, "Enhanced TCAS II Tracking Accuracy," AIAA/IEEE Digital Avionics Systems Conference Paper 84-2738-cp, December 1984.

[15] A.I. Sinsky, "Circular Array Design Equations," Special Technical Report 119, Advanced Development Group, Bendix Communications Division, January 1985.

[16] "Flush Mounted/Adaptive Antenna Arrays," Bendix Communications Division, December 1982.

[17] "Our Burdened Skies," IEEE Spectrum, Vol. 23, No. 11, pp. 33 - 82, November 1986.

[18] C.A. Balanis, Antenna Theory, Harper & Row Publishers, Inc., 1982.

[19] Carl B. Jezierski, personal communication, June 1987.

[20] Paul L. Meyer, Introductory Probability and Statistical Applications, Addison-Wesley Publishing Company, Inc., 1970.

50272-101

REPORT DOCUMENTATION PAGE	1. REPORT NO.	2.	3. Recipient's Accession No.

4. Title and Subtitle
Improved Computer Simulation of the
TCAS III Circular Array Mounted on an Aircraft

5. Report Date
March 1989

6.

7. Author(s)
R.G. Rojas, Y.C. Chen, W.D. Burnside

8. Performing Org. Rept. No.
716199-12

9. Performing Organization Name and Address
The Ohio State University
ElectroScience Laboratory
1320 Kinnear Road
Columbus, OH 43212

10. Project/Task/Work Unit No.

11. Contract(C) or Grant(G) No.
(C)
(G) NSG 1498

12. Sponsoring Organization Name and Address
National Aeronautics and Space Administration Center
Langley Research Center
Hampton, VA 23665

13. Report Type/Period Covered
Technical

14.

15. Supplementary Notes

16. Abstract (Limit: 200 words)

The Traffic advisory and Collision Avoidance System (TCAS) is being developed by the Federal Aviation Administration (FAA) to assist aircraft pilots in mid-air collision avoidance. This report concentrates on the computer simulation of the enhanced TCAS II systems mounted on a Boeing 727. First, the moment method is used to obtain an accurate model for the enhanced TCAS II antenna array. Then, the OSU Aircraft Code is used to generate theoretical radiation patterns of this model mounted on a simulated Boeing 727 model. Scattering error curves obtained from these patterns can be used to evaluate the performance of this system in determining the angular position of another aircraft with respect to the TCAS-equipped aircraft. Finally, the tracking of another aircraft is simulated when the TCAS-equipped aircraft follows a prescribed escape curve. In short, the computer models developed in this report have generality, completeness and yield reasonable results.

17. Document Analysis a. Descriptors

b. Identifiers/Open-Ended Terms

c. COSATI Field/Group

18. Availability Statement	19. Security Class (This Report) Unclassified	21. No. of Pages 181
	20. Security Class (This Page) Unclassified	22. Price

(See ANSI-Z39.18) *See Instructions on Reverse* OPTIONAL FORM 272 (4-77)
Department of Commerce